8-2018

INVESTIGATING THE ROLES OF TAP63 AND TAP73 IN CUTANEOUS SQUAMOUS CELL CARCINOMA AND LUNG ADENOCARCINOMA

Andrew J. Davis

INVESTIGATING THE ROLES OF TAP63 AND TAP73 IN CUTANEOUS SQUAMOUS CELL CARCINOMA AND LUNG ADENOCARCINOMA

by

Andrew John Davis, B.S.

APPROVED:

_____
Elsa R. Flores, Ph.D.
Advisory Professor

_____
Rebecca Berdeaux, Ph.D.

_____
Nancy A. Jenkins, Ph.D.

_____
Lei Li, Ph.D.

_____
Kenneth Y. Tsai, M.D., Ph.D.

APPROVED:

_____
Dean, The University of Texas
MD Anderson Cancer Center UTHealth Graduate School of Biomedical Sciences

INVESTIGATING THE ROLES OF TAP63 AND TAP73 IN CUTANEOUS SQUAMOUS CELL CARCINOMA AND LUNG ADENOCARCINOMA.

A
DISSERTATION
Presented to the Faculty of

The University of Texas
MD Anderson Cancer Center UTHealth
Graduate School of Biomedical Sciences

in Partial Fulfillment
of the Requirements
for the Degree of

DOCTOR OF PHILOSOPHY

by

Andrew John Davis, B.S.

Houston, Texas

August, 2018

DEDICATION

To Amber, Lucy, and my parents, for their unending love and support,

and their ever-needed encouragement.

ACKNOWLEDGEMENTS

My thesis research would not be possible without the encouragement, support and guidance of my mentor, colleagues, family and friends. I am grateful for all that they have done and continue to do for me. It is difficult to truly and effectively express the feelings of gratitude that I have for everyone who has helped me along the way. Nevertheless, I would like to preface my thesis by saying thank you to everyone who has helped me reach this milestone.

I would like to begin by thanking my Ph.D. mentor, Dr. Elsa R. Flores, first and foremost, for giving me the opportunity to join her laboratory and her research team. I am truly thankful for her guidance and support, and for preparing me for a future in science. I appreciate the knowledge and critical, yet honest feedback that she has shared with me during my Ph.D. training. She has provided helpful advice on how to be a great scientist, and has impressed upon me the importance of our research. Above all, she taught me to aim high and to maintain the utmost standards for myself.

I would also like to thank my advisory committee members, including Dr. Rebecca Berdeaux, Dr. Lei Li, Dr. Nancy Jenkins, and Dr. Kenneth Y. Tsai. They have been incredibly supportive of my research, as well as my career development. I am thankful for their critical, yet reliably useful comments and advice, which have helped guide me through my thesis research.

I would also like to express my gratitude to all of my current and former colleagues from the Flores lab. The deep scientific discussions, as well as the critical feedback and advice they provided were invaluable to my success. I would further

like to thank them for being great friends, who provided plenty of encouragement and support over the past few years. I have learned so much from the more senior members, including Xiaohua, Deepa, Avinash, Marco, Ramon, Young Jin, and Marlese. I would also like to thank Ngoc, Payal, and Sarah, with whom I joined the Flores lab. It is remarkable how much we have accomplished and how far we have progressed since we joined the lab. Moreoever, much of the work described in my thesis would not have been possible without significant contributions from my colleagues, including Rahul, Maksym, Jason, Ioannis, and Hayley. Thank you for all of your help pushing our research forward.

In addition, I would like to thank all of my friends back in Connecticut, including Brett, Dale, Garrett, Ivan, Jason, and Marky. It's wild to think about how long we've been friends, and all of the crazy things we have done. Even after moving across the country, each of you has remained in my life and have been incredibly supportive of Amber and me over the years. Thank you for teaching me what it means to be a wonderful friend.

Last but not least, I would like to acknowledge the most important people in my life--my family. None of this would have been possible without the love and support, first and foremost, from my parents. They have instilled in me the importance of education, not only as a means to achieve financial success but something to be valued for its own sake. I appreciate the steps they took to foster my interests in all areas related to science and biology. Most importantly, I appreciate the love and support they have provided me.

I would like to thank my brother, Jim, and my sister, Beth for being strong role models, and for always being there for me when I needed help. I would also like to acknowledge my late cousin, Kyle. His battle with cancer had a lasting impact on me and truly inspired me to dedicate my life to cancer research.

And finally, I want like to thank my beautiful wife Amber, and my daughter Lucy. Amber is an incredible woman who has stood by me and loved me unconditionally for all of the years we have been together. She has made unbelievable sacrifices for me so I could pursue my degree, including relocating to Texas from the northeast, only to move to Florida a short while later. I would not have been able to make it to this point without her. Most importantly, she's the amazing mother of the most important person in my life--my beautiful, precocious little daughter, Lucy. Amber, I love you, and I hope you know that I appreciate everything that you do for me.

Lucy, you are an amazing little girl who motivates me to be better in every way imaginable.

INVESTIGATING THE ROLES OF TAP63 AND TAP73 IN CUTANEOUS SQUAMOUS CELL CARCINOMA AND LUNG ADENOCARCINOMA.

Andrew John Davis, B.S.

Advisory Professor: Elsa R. Flores, Ph.D.

TP63 and TP73 (which encode p63 and p73, respectively) are highly conserved transcription factors with important roles in development and tissue homeostasis. Similar to their homolog, p53, both p63 and p73 have been shown to mediate tumor suppression in multiple tissue types. Interestingly, however, both genes are expressed as multiple isoforms, which appear to have different and, in many cases, antagonistic functions. Through the use of isoform-specific null alleles of p63 and p73 our lab and others have shown that the full-length N-terminal isoforms of p63 *and* p73 (referred to as TAp63 and TAp73, respectively) exhibit distinct functions in development, metabolism and tumor suppression. My thesis research focuses on understanding the conserved functions of TAp63 and TAp73 in tumorigenesis. To do so, I have utilized multiple model systems to investigate the contributions of TAp63 and TAp73 in the development and progression of cutaneous squamous cell carcinoma (cuSCC) and lung adenocarcinoma (LUAC). I have found that TAp63-null (*TAp63*$^{-/-}$) mice exhibit increased susceptibility to UVR-induced cuSCC. To identify TAp63-regulated transcriptional programs relevant to the pathophysiology cuSCC, we performed RNA sequencing of cuSCC and normal tissues from wild-type (*WT*) and *TAp63*$^{-/-}$ mice. My data revealed significant perturbations in global miRNA and mRNA expression in TAp63-deficient tumors, which resembled similar transcriptional changes in human cuSCC, including the downregulation of miR-30c-2* and miR-

497. Proteomic profiling of cuSCC cell lines and subsequent validation experiments led to the discovery of novel direct targets of miR-497 and miR-30c-2*. The most relevant of these proteins exhibited pro-oncogenic functions, including roles in cell cycle and mitotic progression. My data establishes TAp63 as an essential regulator of miRNA expression during skin carcinogenesis and reveals a previously undescribed network of miRNAs and mRNAs, which include viable, yet previously unexplored targets for therapeutic intervention. Along with TAp63-mediated tumor suppression in the skin, I have also developed a novel TAp73 conditional knockout mouse, which includes a conditional fluorescent reporter (*TAp73*^{fltd}) that allows us to follow the deletion event at the cellular level. Using this model we have found that the loss of TAp73 accelerates the initiation and progression of oncogenic Kras-driven LUAC. Our data suggests that TAp73 may be necessary for anti-tumor immune responses. In addition, we have found that the loss of TAp73 promotes migration and invasion in human LUAC cell lines. These studies suggest that TAp73 can suppress tumor development and progression through both cell-autonomous and non-cell-autonomous mechanisms. Together, the studies described in this dissertation provide insights into the genetic and epigenetic mechanisms that contribute to cuSCC and LUAC development, which may, in turn, inform future biomarker and drug discovery studies.

TABLE OF CONTENTS

LIST OF FIGURES

CHAPTER 1:

CHAPTER 3:

LIST OF TABLES

LIST OF APPENDICES

CHAPTER 1: INTRODUCTION

Chapter 1: INTRODUCTION

1.1. The p53/p63/p73 family of transcription factors

1.1.1. An overview

This dissertation is comprised of two related projects focused on understanding the conserved functions of TAp63 and TAp73 in tumorigenesis. To do so, I have utilized multiple model systems to investigate the contributions of each of these genes to the development and progression of cutaneous squamous cell carcinoma (cuSCC) and lung adenocarcinoma (LUAC). These model systems include genetically engineered mouse models (GEMMs), human cancer cell lines, and orthotopic tumor models. Using these model systems I have uncovered tumor suppressive functions for TAp63 and TAp73 in cuSCC and LUAC, respectively. Molecular and biochemical assays were employed to probe the specific mechanisms through which these genes mediate tumor suppression, in both mice and humans. Through these studies I have uncovered and described multiple conserved functions for TAp63 and TAp73 in the pathogenesis of human cancer. Ultimately, the insights we have made may inform future biomarker studies and the design of targeted therapies for cuSCC and LUAC.

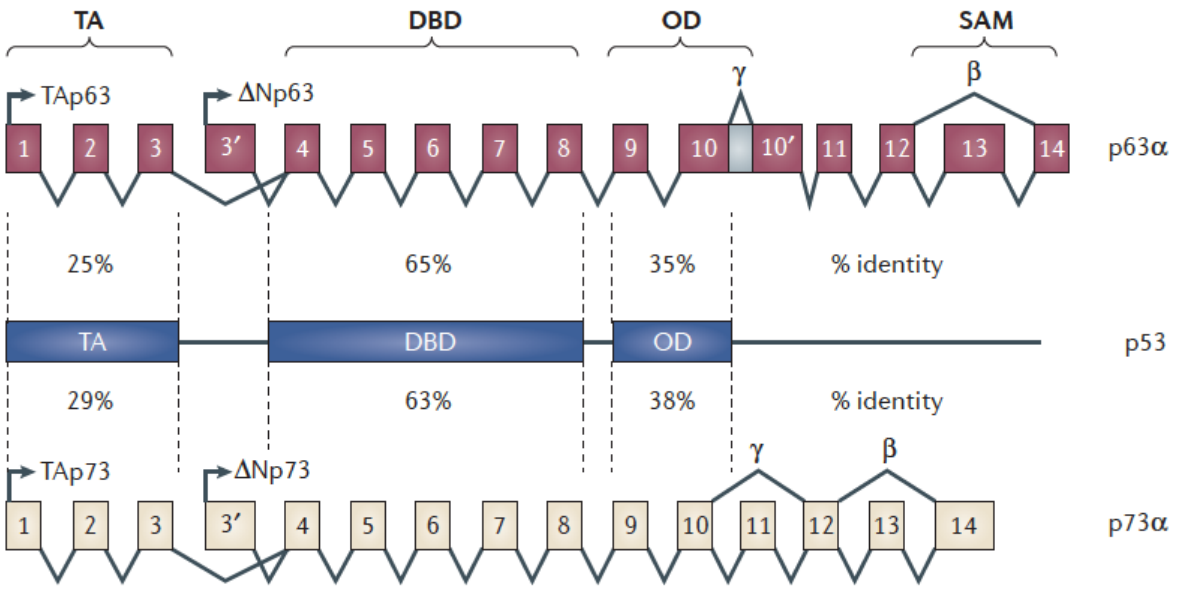

Figure 1: p53, p63 and p73 are homologous transcription factors that are expressed as complex isoforms. The exonic structure of p63 (maroon) and p73 (tan), with approximate sequence homology to p53. Importantly, p63 and p73 are expressed as multiple, complex isoforms, due to the presence of 2 alternative promoters and alternative splicing at the 3' end of both genes. This in turn results in the expression of at least 2 sub-classes of p63 and p73 isoforms, which are typically referred to as TAp63/ΔNp63 and TAp73/ΔNp73 respectively.

(This figure is reproduced from Su X, Chakravarti D, Flores ER. p63 steps into the limelight: crucial roles in the suppression of tumorigenesis and metastasis. Nat Rev Cancer. 2013; 13(2):136-43 (1), with permission from Copyright Clearance Center)

1.1.2. Isoform-specific functions of p63 and p73

In recent years, significant progress has been made in understanding the roles of the *TP63* and *TP73* genes in tumor suppression and normal development. Both have been shown to regulate a number of genes involved in apoptosis, cell cycle regulation (2, 3), DNA repair (4, 5), metabolism (6-9), immunity (10, 11), cellular adhesion (12, 13), stemness (14), and cellular differentiation (15-18).

Interestingly, early studies suggested that *TP63* and *TP73* could be tumor promoting, as they were frequently amplified or overexpressed in certain tumor types (19, 20). These seemingly contradictory observations were explained by the expression of multiple *TP63* and *TP73* transcript isoforms, which have been shown to exhibit distinct, as well as antagonistic functions (21, 22). Full-length isoforms expressed from the 5' promoter contain an N-terminal transactivation domain (referred to as TAp63 and TAp73), and are thus structurally and functionally similar to p53 (Figure 1) (1, 21, 23). In fact, studies have shown that the presence of this domain allows TAp63 and TAp73 to similarly regulate many of the canonical p53 target genes (4, 6, 21, 24). In contrast, the isoforms that are expressed from the downstream 3' promoter lack the N-terminal transactivation domain (referred to as ΔNp63 and ΔNp73), and are thus unable to transcriptionally activate canonical p53 target genes (3, 21, 25, 26). Interestingly, however, there is growing evidence that ΔN isoforms can activate transcription (27, 28). In fact, our laboratory has demonstrated that the α, β, and γ isoforms of ΔNp63 can transactivate DGCR8 expression, whereas TAp63 isoforms have no effect on DGCR8 expression (29). Nevertheless, multiple studies have shown that ΔNp63 and ΔNp73 isoforms can

antagonize the transcriptional activities of p53, TAp63, and TAp73 and can thus function as oncogenes when overexpressed (6, 30, 31). For example, ΔNp63 has been shown to bind and repress the transcription of well-characterized tumor suppressors, including $p21^{WAF1/Cip1}$ and 14-3-3σ (32). Accordingly, we have explored the possibility of targeting and inhibiting ΔNp63 and ΔNp73 as therapeutic strategies for the treatment of human cancers (6, 33, 34).

Taken together, research of p63 and p73 has revealed several important functions for each gene in normal development and human diseases, including cancer. While these observations have been complicated by the presence of multiple isoforms of each gene, significant progress has been made in elucidating the various roles each isoform plays in different cellular and physiological contexts.

1.2. p63 isoforms in epithelial development and tumor suppression

1.2.1. Epithelial development and homeostasis

The skin is the largest organ system in the body, and consists of the dermis, basement membrane, and epidermis. Together, the skin provides protection from external physical damage, infection from microbes, and prevents fluid loss and dehydration. The epidermis contains a number of different appendages including hair follicles (HFs), sweat glands (SWGs), sebaceous glands (SGs), and nails (35). While hair follicles mediate thermal regulation, they also function as anchors for arrector pili muscles, blood vessels, and sensory neurons (36).

During early development in mice the surface of the ectoderm is lined by a single-layered epithelium, which is characterized by the expression of cytokeratin 18

(K18) (37). Thickening and stratification of the epidermis begins on embryonic day E9.5, and this event is accompanied by de novo expression of cytokeratin 5 (K5) and 14 (K14). The spinous and granular layers form around E15.5, each of which is characterized by the expression of the differentiation markers cytokeratin 1 (K1) and loricrin (38). Epidermal development and stratification concludes on E19.5, just prior to birth.

In adult mice, the epidermis and its appendages experience continuous turnover to replenish damaged and dying cells, and to maintain the integrity of the tissue structures. Multiple stem cell compartments reside within the IFE and the various epidermal appendages, consisting of cells that can self renew and produce more differentiated progenitors (39-42). The IFE is continuously replenished by the proliferation of basal keratinocytes, which includes basal stem cells and transit amplifying cells (TACs) (36). These cells express K5 and K14 and lay atop the basement membrane. This structure contains a dense extracellular matrix (ECM) and secretes important growth factors that supports the IFE. Basal stem cells and TACs express multiple integrins, including α6β4 and α3β1, which bind to laminin-5 in the basement membrane and contribute to cell polarity (43). Adherens junctions and desmosomes also mediate cell polarity, through their abilities in establishing intercellular connections between the various epithelial cells within the epidermis (44).

Together, basal stem cells and TACs fuel the stratification of the epidermis. This process is regulated by two primary mechanisms: (1) asymmetric cell division, in which cells divide in a vertical plane, relative to the basement membrane (45), and

(2) delamination, which is the process by which basal keratinocytes detach from the basement membrane and migrate out towards the suprabasal layers (46). This process results in a proliferative basal cell and a suprabasal daughter cell that is committed to differentiation (45). As basal keratinocytes detach from the basement membrane, they exit the cell cycle, and migrate from the inner basal layer to the outer, apical layer of the epidermis. During this process, keratinocytes undergo differentiation, which includes a tightly regulated program of biochemical and morphological changes, including permanent cell cycle arrest, enucleation, and cornification (47). These changes result in several distinct layers of keratinocytes in various stages of differentiation. These layers are referred to as the basal layer, spinous layer, granular layer and the stratum corneum, which lines the apical surface (Figure 2). The outermost layer consists of dead, enucleated squamous cells (referred to as *squames*). These cells lack most of its organelles and consist primarily of insoluble bundles of keratin filaments. Adjacent squames are fused to one another via lipid bilayers that are secreted during terminal differentiation. This adhesion forms a tight barrier that prevents fluid loss and blocks microbes from entering the host. Squames are continuously sloughed off from the apical surface and are replenished by the underlying keratinocytes.

Most mammals, including mice and humans, develop and maintain a hair coat, which consists of HFs found throughout the organisms skin. Proper HF development and maintenance requires frequent regeneration of new hairs throughout the life of the animal (48). In contrast to the IFE, which undergoes continuous regeneration, hair follicles undergo cycles of regeneration interrupted by

periods of quiescence. This process is driven by signaling between stem cells located in a region known as the *bulge*, clusters of cells below the bulge known as the *hair germ*, and dermal fibroblasts (36). Hair cycles are driven by two populations of hair follicle stem cells (HFSCs): (1) a quiescent population found in the bulge (Bu-SCs) and (2) another proliferative population located within the hair germ below the bulge region (49). Together, these stem cells are responsible for follicular morphogenesis and homeostasis.

The hair cycle is characterized by distinct phases, including *anagen* (hair follicle growth), *catagen* (follicle regression), and *telogen* (quiescence). During anagen, the hair shaft grows from the root via proliferation and differentiation of hair matrix cells within the bulb. At the beginning of anagen, the cells within the hair germ begin to proliferate (49). These cells develop into a pool of transit amplifying matrix cells, which proliferate prior to terminally differentiating into the inner root sheath (IRS) and the hair shaft (HS). Bu-SCs primarily develop into the outer root sheath (ORS), which is a group of cells with features of stem cells that surround the differentiating core of each HF (50).

Following anagen, HFs begin to regress and enter catagen. During this phase, cell proliferation within the hair bulb stops, differentiation ceases, and cells undergo extensive apoptosis (48). Subsequently, during the catagen-to-telogen transition, apoptosis ceases, a HS club is anchored, and the HF enters the quiescent telogen phase. ORS cells give rise to a new hair germ and form a new bulge adjacent to the previous one (50). The cells in the new bulge contain HFSCs, which are required for the subsequent hair cycle. Interestingly, the HFSCs present in the

original bulge are a reserve of HFSCs, which can be recruited during epidermal wounding.

Throughout telogen, HFSCs in the bulge and hair germ communicate with a dermal structure known as the dermal papilla (DP). This process involves several inhibitory and growth promoting signaling pathways (49, 51). When the balance of signaling cues favors activation, HFSCs within the hair germ divide and initiate renewed hair morphogenesis (49).

The DP derives from mesenchymal precursors and they are essential for hair follicle induction (52). The adult DP comprises a niche for a stem cell population known as skin derived precursors (SKPs) (53, 54). These stem cells derive from dermal precursors that express SOX2 and exhibit features of embryonic neural crest stem cells (53). SKP cells are found in both the DP and the dermal sheath (DS). These cells are necessary for normal HF morphogenesis, tissue maintenance, and can reconstitute the dermis during wound healing.

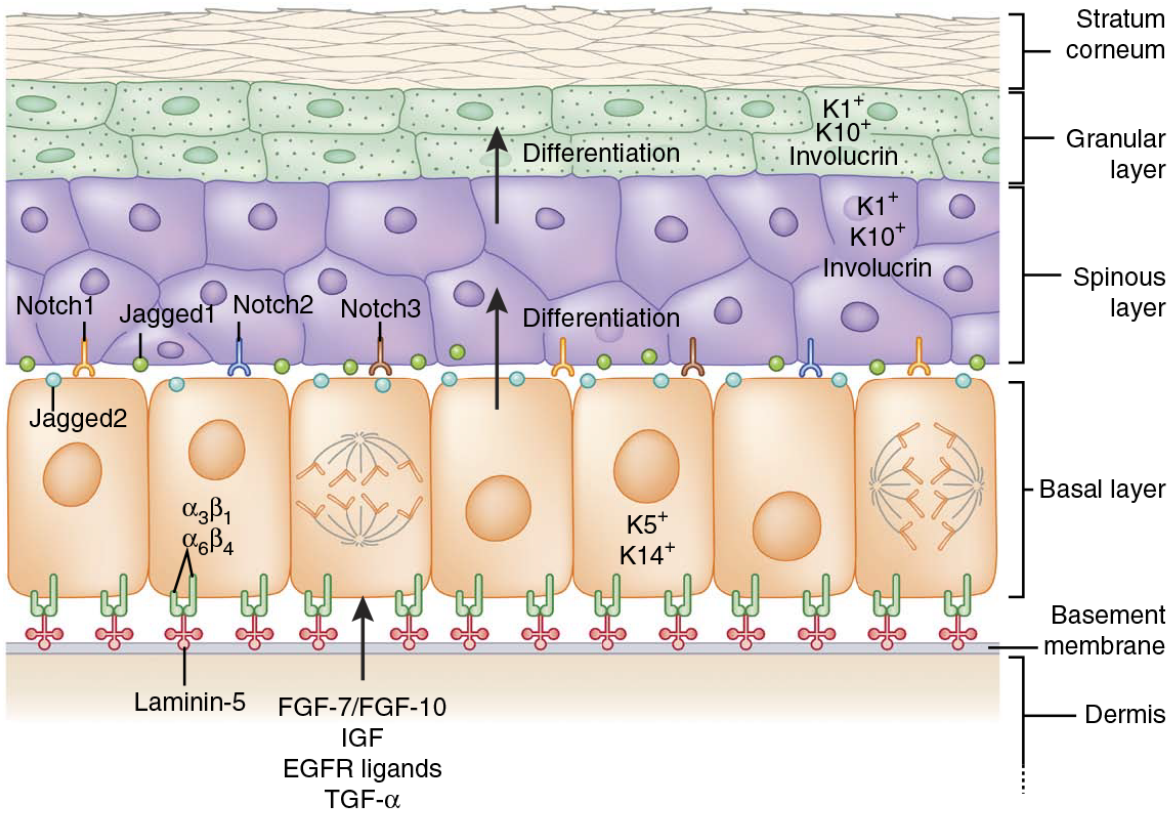

Figure 2: The stratified interfollicular epidermis: structure, cell types, and regulatory genes. Stratification of the epidermis is dependent on complex interactions between basal stem cells and transit amplifying cells (TACs) present in the basal layer. These cells adhere to the basement membrane via interactions between α6β4 and α3β1 integrins and laminin-5. Fibroblasts present in the dermis secrete growth factors that diffuse across the basement membrane and promote the proliferation and survival of basal keratinocytes. Basal stem cells and TACs divide and migrate apically, and begin the process of differentiation, resulting in the characteristic layers of the epidermis.

(This figure is reproduced from Hsu Y.C., Li L., Fuchs E. Emerging interactions between skin stem cells and their niches. Nature Medicine. 2014; 20(8):847-856 (36), with permission from Copyright Clearance Center).

1.2.2. p63 isoforms in epithelial development and homeostasis

Epidermal development and homeostasis are tightly regulated by the transcription factor p63, through its ability to coordinately regulate multiple transcriptional programs involved in keratinocyte survival, replication, and differentiation (15, 23, 55). The importance of p63 in this process is highlighted by the fact that p63-null (*Trp63*$^{-/-}$) mice fail to develop a stratified epithelium, and exhibit perinatal lethality due to desiccation and dehydration (

Appendix 1) (21, 23). *Trp63*$^{-/-}$ mice also exhibit incomplete limb development and craniofacial malformations due to the inability to form the embryonic apical ectodermal ridge. This structure relies on coordinated epithelial-mesenchymal interactions, and is essential for limb and facial development. Notably, a number of human ectodermal dysplastic syndromes are frequently caused by mutations in the human p63 gene (56).

p63 expression is first detected prior to epidermal stratification around E8.5. Isoform-specific RT-PCR analysis has demonstrated that the ΔNp63 isoforms are the most abundant isoform expressed in the epidermis during all stages of embryonic development (57). Conversely, TAp63 expression is first detected at E13, and accounts for approximately 1% of all p63 mRNA expressed in the epidermis (58, 59). ΔNp63α is the predominant isoform expressed in basal keratinocytes, however its expression is diminished in the differentiated suprabasal layers of the epidermis (Figure 2 and Figure 3) (60-63). The specific role of p63 in epidermal development and maintenance has been somewhat controversial, considering slight differences in

the epidermal phenotypes of the *Trp63*$^{-/-}$ mice developed in the Roop (*tm1Brd*) (23) and Mckeon (*tm1Fmc*) (21) laboratories (

Appendix 1). Specifically, the p63-knockout mouse developed in the Mckeon laboratory *Trp63*$^{-/-}$ (*tm1Fmc*) contains small regions in the skin that exhibit features of differentiation, including the expression of filaggrin, involucrin, and loricrin. This led to the hypothesis that p63 is not required for epidermal differentiation, but rather is necessary for the proliferation and survival of basal stem cells. Alternatively, the p63-knockout mouse developed in the Roop laboratory *Trp63*$^{-/-}$ (*tm1Brd*) showed a complete lack of epidermal differentiation markers, suggesting that p63 is absolutely essential for epidermal stratification and development. Despite these differences, it was clear that p63 plays an essential role in the proper development and function of the epidermis. Neither model however could could determine which of the particular p63 isoform(s) regulate these processes.

Using a transgenic strategy, the Melino laboratory demonstrated that ΔNp63 overexpression in the basal layer of *Trp63*$^{-/-}$ mice (*Trp63*$^{-/-}$*; ΔN*) almost completely rescued the epidermal phenotypes observed in p63-null mice, resulting in a significant basal layer showing evidence of stratification (64). Alternatively, TAp63 overexpression in the same compartment (*Trp63*$^{-/-}$*; TA*) showed no difference with *Trp63*$^{-/-}$ mice (64). Instead, overexpression of both ΔNp63 and TAp63 isoforms in the basal layer resulted in a near full epithelialization of the epidermis, compared to either isoform alone. These conclusions are supported by the fact that isoform-specific deletion of ΔNp63 in mice (ΔNp63$^{-/-}$) exhibit significant defects in epidermal stratification and differentiation (29, 65). These results suggest that ΔNp63 essential

for epithelial development and stratification, whereas the function of TAp63 may be limited to terminal differentiation.

These hypotheses are further supported by subsequent observations, which showed that ΔNp63 and TAp63 have non-overlapping transcriptional targets related to epidermal development and differentiation. Specifically, ΔNp63 promotes the expression of *KRT14* (64), and is required for maintaining the replicative potential of basal keratinocytes. ΔNp63 also binds to the promoters of $p21^{WAF1/Cip1}$ and 14-3-3 and inhibits their transcription. This activity may account for the significantly reduced proliferation observed in $Trp63^{-/-}$ keratinocytes (32). ΔNp63 has also been shown to exhibit an antagonistic relationship with Notch signaling in the basal epidermis. Specifically, ΔNp63 negatively regulates the expression of Hes-1 (66), an important downstream mediator of Notch1 (67). Conversely, Notch1 inhibits the expression of p63 through suppression of the interferon signaling pathway. The complex crosstalk between p63 and Notch signaling is essential for the stratification and proper functioning of the epidermis.

Alternatively, TAp63 induces the expression of Ets1, involucrin, K1, and K10, each of which are involved in terminal differentiation of epidermal keratinocytes (64). Taken together, these studies support the notion that ΔNp63 contributes to the proliferation and stratification of basal keratinocytes, whereas TAp63 plays a minor role in terminal differentiation.

While TAp63 is expressed at very low levels in the epidermis and has a limited role in terminal differentiation, studies from our laboratory have nevertheless implicated TAp63 as a critical factor in skin homeostasis and regeneration. These

observations were made using TAp63 knockout mice, which were generated in our laboratory (*TAp63*$^{-/-}$ (*tm1.1Elrf*)) (Appendix 2) (14). While *TAp63*$^{-/-}$ mice develop a normal epidermis, they exhibit skin blisters, premature aging, and reduced wound healing. In addition, *TAp63*$^{-/-}$ mice have reduced hair follicle morphogenesis. This led to the discovery that TAp63 plays a critical role in maintaining a hair follicle stem cell compartment known as skin-derived precursors (SKPs) (14, 53, 54). Notably, it was discovered that TAp63 is the predominant isoform expressed in SKP cells (Figure 3). TAp63 was found to transcriptionally regulate the cyclin-dependent kinase inhibitor $p57^{Kip2}$, which, in turn, maintains SKP cells in a state of quiescence and prevents their hyperproliferation and premature senescence. In the absence of TAp63, SKP cells are depleted in early adulthood, and this process accounts for the premature aging phenotypes and skin defects observed in TAp63$^{-/-}$ mice.

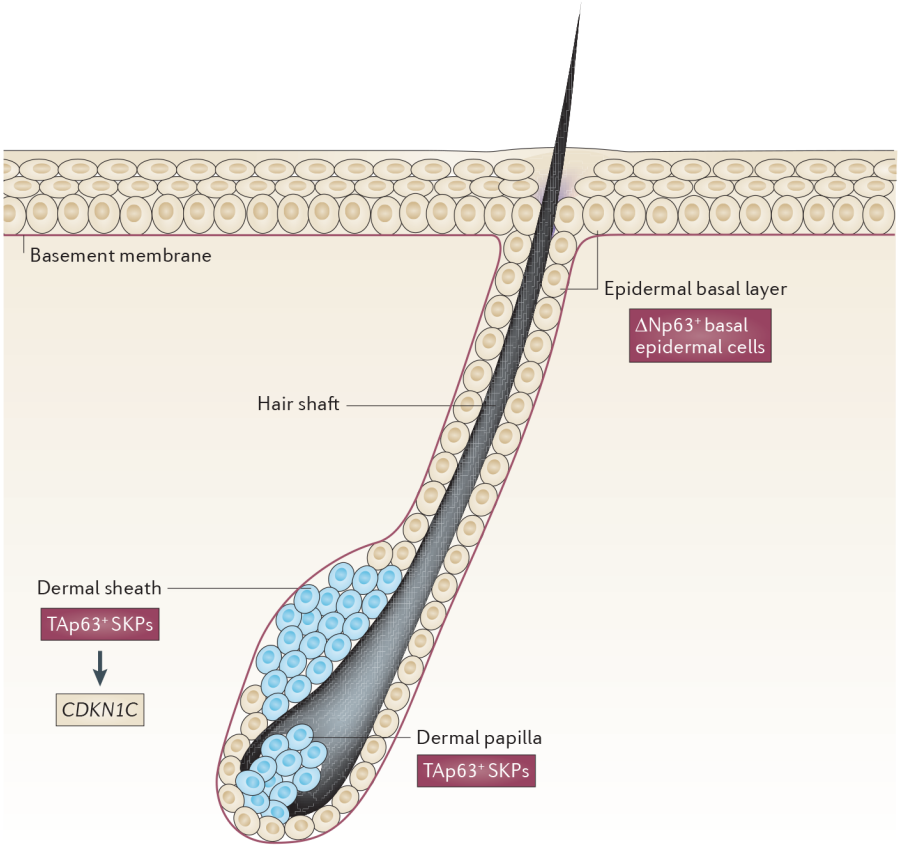

Figure 3: p63 isoforms are expressed in distinct stem cell compartments within the interfollicular epidermis and hair follicle. ΔNp63 expression is restricted to the basal epidermis, where it functions to maintain the proliferative capacity, self-renewal, and terminal differentiation of basal keratinocytes. Alternatively, TAp63 expression is detected exclusively in a dermal stem population present in the hair follicle, known as skin-derived precursors (SKPs). TAp63 maintains SKPs in quiescence, via transcriptional activation of CDKN1C (which encodes p57).

(This figure is reproduced from Su X, Chakravarti D, Flores ER. p63 steps into the limelight: crucial roles in the suppression of tumorigenesis and metastasis. Nat Rev Cancer. 2013; 13(2):136-43 (1) with permission from Copyright Clearance Center)

1.3 p63 isoforms in squamous cell carcinomas (SCC)

1.3.1 Classical features of SCC

Squamous cell carcinomas (SCCs) are a common malignancy that occurs throughout the human body in organs that are lined by a squamous epithelium. These tumors frequently arise within the epithelium of the lung (LUSC), skin (cuSCC), esophagus (ESCC), upper aerodigestive tract (HNSCC), and genitourinary tract (68-74). These tumors share common characteristics that resemble normal squamous epithelium, which has led to the hypothesis that all SCCs arise from normal squamous epithelial cells. These cells line many organ surfaces throughout the human body, and primarily serve as a barrier to the external environment. Due to their location, squamous epithelial cells are frequently exposed to physical and chemical insults. As a result, squamous-derived tumors are found to be primarily driven by exposure to carcinogens, such as UV radiation, tobacco, or alcohol. To protect the integrity of the tissue and the organism as a whole, squamous epithelium has evolved a sophisticated pattern of cell turnover. This process relies on the presence of long-lived stem cells and progenitors, which divide, differentiate, and migrate in an apical or outward direction. This process creates the tight, protective surfaces that define squamous epithelial tissues.

As squamous cells encounter genetic insults, they employ protective mechanisms to prevent the accumulation of precancerous lesions and to protect the integrity of the host tissue. These processes include, but are not limited to, cell cycle arrest, DNA repair, terminal differentiation, and programmed cell death. Multiple signaling pathways and transcriptional programs regulate each of these cellular

processes. Understanding how these processes become disrupted during tumor initiation and progression has led to breakthrough observations that may ultimately inform and improve therapeutic interventions for squamous cell carcinomas.

1.3.2. Histological and clinical features of cutaneous squamous cell carcinoma (cuSCC)

Non-melanoma skin cancer (NMSC), which primarily includes basal cell carcinoma (BCC) and cutaneous squamous cell carcinoma (cuSCC), is the most common malignancy diagnosed in the United States (75). Moreover, the global incidence of NMSC continues to rise, with an estimated 3.5 million new diagnoses of skin cancer each year (76). Fortunately, BCC rarely metastasizes and has a very high cure rate. While primary cuSCC also has a high cure rate of about 95%, a subset of lesions fail to respond to therapy, metastasize, and have a high rate of patient mortality (77). While cuSCC accounts for approximately 20% of all NMSC lesions, this tumor type accounts for the majority of NMSC-related metastatic death and disease (78). As a result, cuSCC is one of the most costly cancers to treat in the United States (79).

Exposure to ultraviolet radiation (UVR) has been implicated as the primary environmental risk factor for NMSC, including cuSCC (80). Elderly individuals with pale complexions and a history of moderate chronic UV exposure have the highest likelihood for developing cuSCC. On a molecular level, UVR induces specific photochemical reactions that alter the chemical bonds of DNA, resulting in characteristic DNA mutations. Such mutations are common in cuSCC and are frequently observed in tumor suppressors such as *NOTCH1* and *p53 (81, 82).*

Additionally, UVR exposure can induce immune suppression in the skin, by promoting the expression of immunosuppressive neuropeptides, cytokines, and melanocortins (83).

BCC accounts for approximately 75% of all diagnosed NMSCs in immunocompetent patients while cuSCC encompasses 20% of this tumor type. Interestingly, however, these percentages are inverted in immunocompromised patients (78). In fact, patients taking immunosuppressive drugs following organ transplantation surgery exhibit a nearly 250-fold increase in developing cuSCC (84). In addition to chronic immunosuppression, patients with a history radiation exposure, or who have suffered from chronic skin wounding or burns, are at an elevated risk of developing cuSCC (85).

Cutaneous SCC (cuSCC) encompasses a broad spectrum of histologically diverse lesions, which display highly varied clinical outcomes. The current paradigm for the development and progression of cuSCC includes a progression from normal skin, to actinic keratosis (AK), to SCC in situ (SCCS), and finally, invasive SCC (SCCI) (

Table 1). While AK and SCCS exhibit minimal invasiveness and favorable outcomes, a significant percentage of SCCI lesions fail to respond to therapy and metastasize (86, 87). As with many other malignancies, the early detection and treatment of high-risk tumors with an aggressive treatment regimen can result in improved patient outcomes. As a result, the ability to identify and distinguish between the stages of disease progression is critical in the clinical treatment of a given tumor.

Actinic keratosis (AK) is a premalignant lesion that is generally accepted to be the primary precursor to most cuSCC lesions (88). In line with the connection of cuSCC to UV-exposure, AKs frequently develop on sun-exposed skin surfaces, such as the head, neck, forearms, and back (89). Light-skinned individuals with a propensity for sunburn are at the highest risk of developing AKs. Clinical presentations of AK include scaly patches or papules, which are frequently red in color, and are typically found in areas of the skin that exemplify other indications of solar damage (90).

Histologically, AKs are restricted to epidermal foci that contain abnormal, pleomorphic keratinocytes (91). These cells frequently exhibit nuclear atypia, abnormal keratinization, and the loss of apical-basal polarity. Abnormal keratinocytes within the basal layer frequently extend into the upper layers of the epithelium, but by definition they do not span the full thickness of the epidermis.

The possible clinical outcomes for AKs include regression, persistence as an identifiable AK, or progression into SCCS (92). The majority of AKs never progress to bonafide cuSCC (93). However, the majority of cuSCC lesions are diagnosed in

close physical association with AKs, leading to the hypothesis that AK is a direct precursor to cuSCC (94).

SCCS (used interchangeably with ‘Bowen’s disease’) is typically diagnosed in elderly patients (95) and, as is the case with AK, is most often found on the skin of sun-exposed surfaces such as the face, neck, and hands (96). SCCS typically presents as a slow growing erythematous scaly lesion, with an irregular border. Such lesions may appear hyperkeratotic and ulcerated, and a small percentage will appear pigmented (97). Most clinical studies have reported that a given SCCS lesion has a risk of progression to SCCI of 3%–5% (98).

Histologically, the epidermis in SCCS will exhibit significant acanthosis with elongation, in addition to an increase in the size of epithelial extensions into the underlying dermis (i.e. rete ridges). SCCS lesions also frequently show features of hyperkeratosis and parakeratosis, which are found above abnormal keratinocytes. The majority of SCCS lesions will also frequently involve the interfollicular epithelium and neighboring hair follicle and adnexal structures (86).

The conventional term “cutaneous SCC” typically refers to invasive squamous cell carcinoma (SCCI). The observation that most SCCI lesions (>95%) are associated with the malignant progression of an AK, has led to the general consensus that AKs are the premalignant precursor for SCCI (99). SCCI shares many histological features of AK and SCCS, however SCCI can be identified by the presence of cells invading the basement membrane into the underlying dermis (90, 100). During the early stages of the disease, this invasion may be difficult to detect histologically. However, the presence of atypical structures and keratinocytes

through the full length of the epidermis may enable a diagnosis of SCCI (101). In late stage SCCI, large pockets of abnormal tumor cells may be present in the underlying dermis, in addition to infiltrating inflammatory cells.

SCCI can be subgrouped into three histologic grades depending on the associated degree of nuclear atypia and the extent of keratinocyte differentiation. The most common of the three subtypes is referred to as well differentiated SCCI, which is characterized histologically by large, hyperchromatic nuclei, along with extensive keratin production, which typically presents as atypical structures known as keratin pearls (91). These tumors however will maintain intercellular bridges and will have a very low probability of metastasis. On the other end of the spectrum are poorly differentiated SCCI, which is characterized by significantly enlarged, atypical nuclei and multiple mitotic figures. The most obvious distinguishing characteristic of poorly differentiated SCCI is reduced keratin production. While these tumors are far less common than the well-differentiated type, they harbor an enhanced risk for recurrence and metastasis, and are typically found on the ear and lip (77). The third and final subtype is moderately differentiated SCCI, which as its name suggests, is characterized by features of both well- and poorly-differentiated SCCI.

Retrospective studies have shown that a given cuSCC lesion has an estimated 4% risk of metastasis and an estimated death rate of about 2% (102). The majority of metastatic spread is identified in nearby lymph nodes, however cuSCC infrequently metastasize to more distant organs, including but not limited to the brain, liver, and lungs (103-105). One of the most important determinants for diagnosing and predicting the malignant potential for a given cuSCC lesion is its

individual histological features. Additionally, however, are other factors that demonstrate clinical utility when evaluating the risk for a given tumor. Several clinical studies have demonstrated that the following characteristics are highly informative when assessing risk of metastatic spread: differentiation status, anatomical location, tumor diameter, immunosuppression, and perineural/perivascular invasion (102, 106-108).

Tumors located on the lip or the ear tend to have a very poor prognosis, particularly SCCI with a poorly differentiated histology (77). Nevertheless, most metastatic tumors will be well differentiated SCCI. Therefore it is essential to examine other important clinical features as well (77). Another highly informative prognostic characteristic is the size of the tumor and how deeply it has invaded into the underlying dermis (77). In general, tumors with a diameter of more than 2 cm have a high likelihood for recurrence and metastasis, whereas those with smaller sizes have a significantly reduced risk of progression (109). The presence of perineural and perivascular spread is also indicative of high-risk cuSCC. Another clinical feature to be assessed is the presence of immunosuppression in the patient harboring the tumor, as this can significantly increase the likelihood of cuSCC development and progression (110, 111). Possible causes of immunosuppression include the use of immunosuppressive drugs following transplant surgery, the presence of a secondary cancer, and infection with HIV. Moreover, cuSCC lesions in the context of immunosuppression tend to exhibit an elevated capacity for metastasis (112), leading to significantly higher mortality rates in immunocompromised patients (85).

The primary treatment for most cuSCC lesions is surgical excision as it has been shown to have a cure rate of 95% (113). The primary benefit for excisional surgery is that it enables the histological examination of the tumor and the surrounding skin tissue. Depending on the stage of disease, a surrounding margin of normal skin will be removed (4-6 mm for low-risk and 6-10 mm for high-risk cuSCC) (114, 115). These tissue samples are subsequently examined by a dermatopathologist to determine if the entire tumor was successfully removed.

Mohs micrographic surgery (MMS) describes a commonly used surgical technique that allows a detailed microscopic examination of excised tumor tissue. As a result, MMS enables a more precise assessment of the tumor margins, thereby improving the likelihood of total tumor removal, which is essential for minimizing tumor recurrence. Due to the success of this technique, MMS has become the primary treatment option for high-risk cuSCC (116).

Radiation therapy has been the non-surgical treatment of choice in cases of cuSCC where patients are poor candidates for surgical treatments (e.g. tumors are inoperable based on anatomical location). While it is highly effective for cuSCC (particularly low-risk tumors), it entails a long treatment schedule and it does not allow for extensive histological examination of the treated lesion. In addition there are significant side effects of radiation therapy including but not limited to nausea, malaise, and treatment-induced malignancies (117). Given these drawbacks, radiation therapy alone is only used in cases where surgery is not feasible or when other therapeutic options have failed (118).

The current treatment recommendation for high-risk cuSCC consists of

adjuvant treatments including radiation therapy, due to the enhanced risk of tumor recurrence and metastasis (119). Several options for adjuvant therapies to surgery exist, however there is no consensus regarding the proper management of high-risk cuSCC (120). As a result, more clinical research is required to correctly identify the most efficacious therapy modalities.

Current efforts to improve the outcome of patients harboring high-risk cuSCC include development of targeted molecular therapies. This includes the epidermal growth factor receptor (EGFR), which is frequently overexpressed in many SCC subtypes and has been shown to be essential for driving tumor cell survival and proliferation (121, 122). Multiple therapeutic agents inhibiting EGFR or its downstream signaling pathways have been identified, including the small molecule tyrosine kinase inhibitors such as erlotinib and gefitinib and the monoclonal antibody cetuximab (123). EGFR targeting has shown some clinical benefit in recent clinical trials, however these observations are limited to a small and poorly defined subset of cuSCC patients (124, 125). Therefore, further characterization of the underlying molecular and genetic characteristics of high-risk cuSCC is necessary to identify other pathways to target therapeutically.

Field cancerization is a concept that refers to an area of tissue that is significantly altered and primed for malignancy due to exposure to carcinogenic insults (126). Field cancerization in the skin is typified by the presence of multiple AKs, SCCS, and SCCI, and is typically the result of UVR exposure (127). After these primary lesions are treated, clinical focus typically shifts towards treating the surrounding region of potentially damaged skin. One way of addressing field

cancerization in the context of actinically-damaged skin includes topical medications such as ingenol mebutate and fluorouracil, which function by clearing the skin of potentially premalignant epithelial cells (128). Another option shown to exhibit significant preventative benefits is photodynamic therapy, which includes the use of a photosensitizer such as methyl aminolevulinate (MAL), visible light exposure, and reactive oxygen species to similarly clear the tissue of cancerized cells (126, 129).

Table 1: Clinical and histological features of the cuSCC spectrum of disease.

Normal skin	Actinic Keratosis (AK)	SCC in situ (SCCS)	Invasive SCC (SCCI)
• Well-defined epidermal layers • Normal keratinocytes with low number of mitotic figures	• Scaly patches or papules • Abnormal, pleomorphic keratinocytes restricted to epidermal foci • Atypical keratinocytes do not span full length of epidermis • Minimal risk for malignant progression	• Scaly erythematous lesions, with irregular borders and possible ulceration • Significant acanthosis with possible hyperkeratosis • May involve adjacent follicular and adnexal structures • 3%–5% risk of progression to SCCI	• Atypical structures and keratinocytes through the full length of the epidermis • Invasion of tumor cells into the underlying dermis • Varying degrees of differentiation, with poorly differentiated lesions as having higher risk for recurrence and metastasis.

1.3.3. Genomic and molecular features of cutaneous squamous cell carcinoma

The advent of improved and cost effective high throughput genetic and molecular technologies has made it possible to comprehensively characterize thousands of human patient tumors. Large-scale research consortiums that leverage these technologies along with relevant clinical data have been established in order to identify the common genetic and epigenetic traits of human cancer. The Cancer Genome Atlas (TCGA) Research Network is one of the largest consortiums, consisting of 20 collaborating institutions in the United States and Canada. Since its inception in 2005, it has generated a comprehensive characterization of over 11,000 patient tumors, consisting of 33 different pathologically defined tumor types. This massive collection of data has become an invaluable resource for researchers and clinicians, and has led to several important observations with regards to the underlying biology of human tumors.

Interestingly, a recent cross-platform analysis of 12 different cancer types led to the observation that several common genetic and molecular features are shared, not only within the same tumor type, but also across divergent, pathologically distinct cancers as well (73). One of the most striking findings was the convergence, based on genetic and molecularly defined similarities of LUSC, HNSCC, and some bladder cancers (BLCA). Using an unbiased approach, Hoadley et al demonstrated that these tumors, which they termed *C2-Squamous like*, shared significant overlap with regards to specific gene mutations, copy number alterations (CNAs), and gene expression patterns (73). The specific alterations in C2-squamous like tumors included TP53 mutations, TP63 and SOX2 amplification, as well as hyperactivation

of cell proliferation and immune pathways (73). Interestingly, many of these same genetic aberrations are also seen in human SCCs arising in other tissues, including esophageal SCC (ESCC) (130), cuSCC (72, 131), and cervical squamous cell carcinoma (CESCC) (132). The convergence of SCCs in terms of their underlying genetics suggest that targeted therapies discovered to be effective in one SCC subtype may prove to be effective for the treatment of multiple SCC subtypes.

As of this publication, cuSCC has not been included in TCGA. However, similar efforts to provide a comprehensive molecular and genetic characterization of cuSCC have been made. In one such study, Pickering et al. investigated aggressive cuSCC using exome sequencing of DNA from frozen tumors and matched normal blood form 39 patients (131). Strikingly, they found a mutation rate of 61.2 mutations/Mb, which is one of the highest mutation rates amongst human cancers, including LUSC and HNSCC (133). Previous studies have found that inactivation of TP53, CDKN2A, NOTCH1 and NOTCH2 are common genetic alterations in cuSCC (134-140). Similarly, Pickering et al. found that nine of the most commonly mutated genes, including TP53 (94.9%), CDKN2A (43.6%), NOTCH1 (59.0%), HRAS (20.5%), CASP8 (23.1%), AJUBA (17.9%), RASA1 (12.8%), FAT1 (43.6%), and KMT2D (69.2%), are also commonly mutated in HPV-negative HNSCC and LUSC (131).

RNA sequencing (RNA-seq) of UV-driven mouse and human patient skin (NS), actinic keratosis/papillomas (AK/PAP), and cuSCC identified the dysregulation of multiple pathways, which may be relevant to disease progression (72). For example, it was found that β-catenin/Wnt signaling is activated throughout the

progression of cuSCC (72). In addition, the transcriptional targets of AP1 are downregulated across the progression of cuSCC, indicating that epidermal differentiation is disrupted in cuSCC (141). This conclusion is further supported by the preponderance of mutations in genes involved in NOTCH signaling in cuSCC tumors (72, 131, 137, 142, 143). In addition, transcriptional drivers of cuSCC, including NFY, E2F, and ELK1 were found to be activated early in tumor development (e.g. during the NS to AK/PAP transition), whereas MYC-dependent transcriptional programs are activated in the progression of AK/PAP to cuSCC. Pathway analysis of differentially expressed genes of both mouse and human cuSCC showed enrichment for pathways related to the DNA damage response, cell cycle progression, and mitotic roles of polo-like kinase (72).

These transcriptional changes were frequently associated with recurrent CNAs, which resemble those observed in both HNSCC and LUSC. These include chromosomal gains of 3q and 8q, and the loss of chromosomes 5q, 8p, and 18 (70, 71, 131). Gain of 3q is of particular interest due to the fact that this region harbors PI3KCA, SOX2, and TP63, each of which have been shown to exhibit oncogenic roles in cuSCC and other tumors (1, 144, 145). Targeted sequencing of 29 human cuSCC lesions found that ~24% of tumors showed specific amplification of TP63, however they did not find amplification of PIK3CA or SOX2 (143). This suggests that TP63 overexpression is the critical factor that favors the amplification of 3q in cuSCC. Importantly, ΔNp63 isoforms are typically overexpressed, whereas TAp63 isoforms are lost or underexpressed (31, 61). Studies in mice show that cuSCC tumors rely on the expression of p63, as the inhibition or deletion of p63 results in

apoptosis and cuSCC regression (31, 146). Conversely, decreased expression of TAp63 promotes the formation of metastatic sarcomas and carcinomas, including cuSCC (147). These observations support the notion that ΔNp63 isoforms function as oncogenes in cuSCC, whereas TAp63 isoforms function as tumor suppressors.

The disruption of normal miRNA expression has been causally linked to the pathogenesis of many tumor types (148, 149), including cuSCC (72, 150, 151). Using functional pair analysis, which relies on miRNA-mRNA targeting predictions, Chitsazzadeh et al. found that miRNAs 15a/b, 17, 20a, 21, 31, 200a and 340b were frequently overexpressed in cuSCC (72). Likewise, miR-21 and miR-31 have been previously shown to be causally linked to the development and progression of tumors, including cuSCC (152-154). Conversely, miRNAs 30a, 125b, and members of the let-7 family were found to be significantly downregulated in cuSCC tumors (72).

Taken together, these observations suggest that cuSCC exhibits distinctive molecular and genetic characteristics, many of which overlap with SCCs that arise in other tissues, most notably HNSCC and LUSC. These include mutations in TP53, CDKN2A, FAT1/2, CASP8, and NOTCH, chromosomal CNAs involving 3q, 5p, and 8p, and aberrant mRNA and miRNA expression of genes related to squamous differentiation, epithelial-to-mesenchymal transition, cell cycle progression, and DNA damage responses.

1.3.4. Regulation of miRNA expression and biogenesis

miRNAs are a class of evolutionally conserved non-coding RNAs that ~20-24 nt in length. They are found in most organisms, including plants, animals, and protists (155). The primary function of miRNAs is to repress mRNA stability and translation. This occurs through Argonaute-mediated binding to specific mRNAs by binding to partially complementary sequences in the 3' UTR, and, albeit less frequently, the coding sequence (CDS), or 5' UTR of target mRNAs (156). Depending on the degree of complementarity between the miRNA and mRNA, the miRNA-Argonaute complexes suppress translation or can induce mRNA decay.

miRNA genes are transcribed by RNA polymerase II into long precursor transcripts known as *pri-miRNAs* (Figure 4) (157). Following transcription, the majority of pri-miRNAs are spliced, capped, polyadenylated, and cleaved by a protein complex known as the Microprocessor (158-160). This complex includes DGCR8 and the RNAse III enzyme Drosha. The Microprocessor cleaves pri-miRNAs into shorter hairpin RNAs, which are referred to as *pre-miRNAs*. The pre-miRNA forms a complex with XPO5 and RAN-GTP, which facilitates the nuclear export of the pre-miRNA into the cytoplasm (161, 162). This process requires the hydrolysis of GTP, which also results in the disassembly of the complex and the release of the pre-miRNA.

In the cytoplasm, pre-miRNAs are cleaved by another RNAse III-type endonuclease known as Dicer (Figure 4) (163-165). Dicer cleaves the pre-miRNA near the terminal loop, resulting in a short RNA duplex. This duplex then binds argonaute (AGO) proteins and TRBP to form a functional RNA:protein complex

known as the RNA-induced silencing complex (RISC) (166, 167). After loading, the RNA duplex unwinds and one of the strands (referred to as the *passenger strand,* or *miRNA**) is ejected from the RISC complex. Typically, the miRNA strand with the less stable 5' terminus is preferentially selected to function as the guide strand in the mature RISC complex (168, 169). Once released from RISC, the passenger strand is degraded. Importantly, strand selection may vary in different cellular contexts. Occasionally the passenger strand can be favored, and exert its inhibitory functions on target genes that are typically mutually exclusive of the targets of the corresponding guide strand (153, 170).

1.3.5. Regulation of miRNAs by the p53 family in epithelial development and cuSCC

The p53 family of transcription factors has been shown to play an essential regulatory role in miRNA expression and processing (Figure 4) (29, 147, 171, 172). Conversely, p53, p63, and p73 are themselves targets of specific miRNAs, indicating a complex interaction between p53, p63, p73 and miRNA expression. Recent studies have implicated this network in normal epithelial development and tumorigenesis.

miRNAs play an important role in normal skin development and homeostasis. Multiple studies have implicated miRNA expression in keratinocyte differentiation and epidermal development. This is exemplified by the fact that the disruption of miRNA expression and processing results in severe defects in epidermal stratification. Notably, miR-203 has been shown to be a critical regulator of ΔNp63,

specifically by restricting its expression to the basal layer of the epidermis (18, 173). Transgenic expression of miR-203 in the basal layer of the epidermis results in perinatal lethality due to incomplete epidermal development and significantly reduced expression of ΔNp63. These phenotypes mimic the phenotypes observed in ΔNp63$^{-/-}$ mice (29), demonstrating the strong inhibitory effect of miR-203 on ΔNp63 expression in the epidermis. It was found that miR-203 expression induces cell cycle arrest and significantly reduces the self-renewal capabilities of basal keratinocytes. These effects were dependent on the suppression of ΔNp63, as well as the inhibition of Skp2 and Msi2 (18). Through this regulation, miR-203 was found to be a critical regulator of epidermal stratification.

Conversely, ΔNp63 itself is a regulator of miRNA expression through its ability to transactivate DGCR8, which is an important component of the Microprocessor complex (Figure 4). This regulation mediates the downstream biogenesis of select miRNAs, which have been found to be important in regulating epithelial homeostasis stemness (29). Importantly, disruption of this regulatory axis has been linked to the pathogenesis and progression of cuSCC (33). In fact, our laboratory has found that targeting ΔNp63 and DGCR8-dependent miRNAs, including miR-128 and let-7d, can be an effective therapeutic strategy in treating cuSCC.

While ΔNp63 functions through DGCR8, our laboratory has shown that TAp63 is a potent transactivator of Dicer transcription, and therefore a global regulator of miRNA biogenesis and expression (Figure 4) (147). These observations are noteworthy, as TAp63 isoforms have also been implicated in skin homeostasis and regeneration, albeit in a different stem cell compartment. The *TAp63$^{-/-}$* (*tm1.1Elrf)*

mice generated in the Flores lab exhibit premature aging phenotypes that were most pronounced in the skin of adult mice (14) (Appendix 2). It was discovered that the loss of TAp63 results in the hyperproliferation and subsequent premature senescence of hair follicle stem cells, known as SKP cells. Interestingly, genome-wide miRNA profiling of senescent and proliferative human keratinocytes found that miRNA expression is significantly dysregulated in senescent keratinocytes (174, 175). Whether or not TAp63-mediated mIRNA expression plays a role in the senescence of keratinocytes or SKP cells remains to be explored.

Interestingly, recent studies have found that *TAp63*$^{-/-}$ (*tm1.1Elrf)* mice develop a number of metastatic carcinomas and sarcomas, including cuSCC (Appendix 2) (147). Of particular significance, it was found that decreased expression of miRNAs was responsible, in part, for TAp63-mediated tumor suppression. This coincides with the observation that miRNA expression is frequently reduced in human cancers, suggesting that most miRNAs exert tumor suppressive functions (176, 177). In addition, components of the miRNA biogenesis pathway, including Dicer, are also frequently mutated or expressed at low levels (178-180). Taken together, these studies show that TAp63 exerts tumor suppression in part through the regulation of miRNAs. The specific miRNAs involved in these processes, however, remain to be identified and characterized.

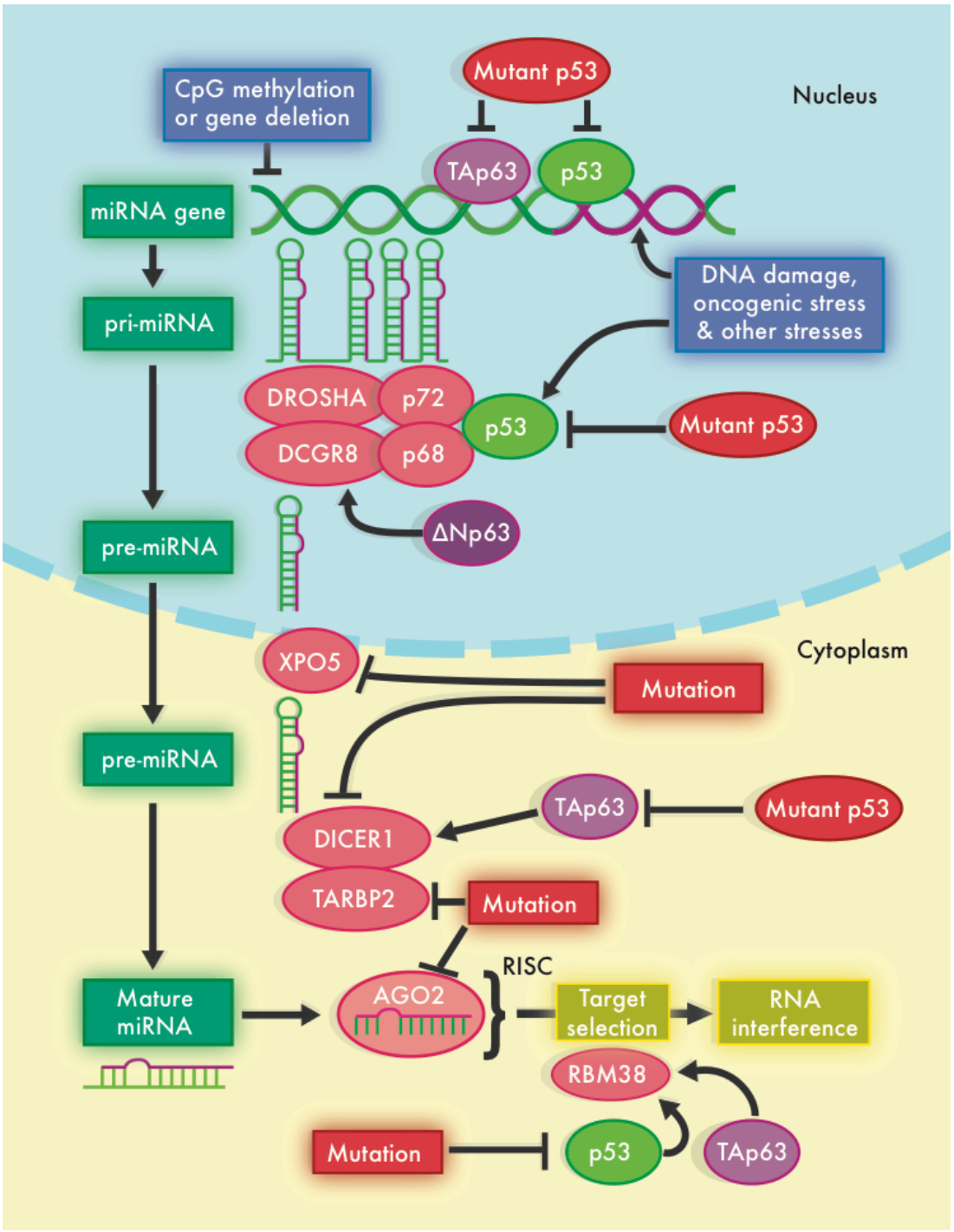

Figure 4: Regulation of miRNA biogenesis by p53 family members. Dysregulation of miRNA expression has been implicated in the pathogenesis of human cancer. In general, expression of miRNAs and members of the miRNA biogenesis pathway is reduced in human patient tumors. Notably, these

observations coincide with mutations or downregulation of p53 family members. Indeed, functional experiments have implicated p53, TAp63, and ΔNp63 in the expression of miRNAs and miRNA biogenesis. Both p53 and TAp63 have been shown to directly promote transcription of miRNA genes. Further, TAp63 regulates the transcription of Dicer, and this regulation has been shown to be important for tumor suppression. Mutant p53 has been shown to inhibit TAp63-mediated transcriptional activation of Dicer, which enhances the invasive capacity of tumor cells. Interestingly, ΔNp63 has been found to promote miRNA biogenesis through the transcriptional activation of DGCR8.

1.4. p73 and tumorigenesis

1.4.1 Tumor suppressive functions of TAp73

The p53 family member p73 was discovered in the late nineties along with p63 (181). Similar to p63, p73 is expressed as multiple isoforms, due to the occurrence of alternative splicing, and the presence of two alternative promoters (Figure 1). There are at least 6 isoforms that are expressed in humans, and they are generally grouped into 2 primary classes of p73 isoforms, depending on the presence or absence of the N-terminal acidic transactivation domain (TA). Isoforms expressed from the upstream 5' promoter are typically referred to as TAp73, whereas the isoforms expressed from the downstream 3' promoter are known as ΔNp73. TAp73 isoforms structurally resemble p53 and TAp63, and therefore mimic many of their transcriptional functions (24). ΔNp73 isoforms, which lack the TA domain, have been shown to inhibit the transcriptional activity of p53 and TAp73 (182). As a result, the general paradigm is that TAp73 exerts tumor suppressive functions, similar to TAp63 and p53, whereas ΔNp73 isoforms exhibit oncogenic potential.

To ascertain the physiological functions of p73, the Mckeon laboratory generated the fist p73 knockout mouse (*Trp73*$^{-/-}$) (

Appendix 1) (183). In contrast to *Trp53*$^{-/-}$ or *Trp63*$^{-/-}$ mice, *Trp73*$^{-/-}$ mice show reduced body size, and exhibit neurological defects, highlighting a critical function for p73 in neurogenesis. In addition, the majority of the *Trp73*$^{-/-}$ mice die from chronic infections, including rhinitis, otitis, perioorbital oedema, and conjunctivitis, around 4-5 weeks of age (183, 184). This observation suggested that p73 isoforms play a role regulating proper immune development. Subsequent studies found that p73-deficient

mice are also tumor prone, supporting the notion that p73 functions as a tumor suppressor (

Appendix 1) (184). In fact, 60% of *Trp73*$^{-/-}$ mice that survive into late adulthood develop LUAC. Interestingly, *Trp73*$^{+/-}$ mice are also tumor prone, developing both LUAC (10%), as well as thymic lymphomas (12.5%) and hemangiosarcomas (12.5%) (

Appendix 1). These observations suggest that p73 is a haploinsufficient tumor suppressor. Taken together, these early studies indicated that p73 isoforms played critical roles in the development of the immune system and the central nervous system, as well as in tumorigenesis. Unfortunately, however, these early studies using total p73-knockout mice precluded the possibility of attributing any of these functions to a specific isoform.

Early studies into the specific functions of each p73 isoform suggested that TAp73 and ΔNp73, in general, have opposing functions (24, 182). Specifically, it was found that TAp73 is capable of inducing cell cycle arrest and apoptosis, mimicking many of the canonical tumor suppressive functions of p53 and TAp63 (24). The tumor suppressive functions of TAp73 were confirmed in vivo, as TAp73 knockout mice (*TAp73*$^{-/-}$ (*tm1Mak)*) were found to be tumor prone (Appendix 2) (185, 186). Specifically, *TAp73*$^{-/-}$ mice develop lymphoma, LUAC, and colon carcinoma. These mice also exhibit hippocampal dysgenesis, suggesting that TAp73 may be at least partially responsible for the neurological defects observed in *Trp73*$^{-/-}$ mice (183). Moreover, *TAp73*$^{-/-}$ mice show evidence of premature aging, and shorter lifespans. These phenotypes may be caused by genomic instability, which has been observed

in multiple cell types of *TAp73*$^{-/-}$ mice. Likewise, it has been hypothesized that the increased genomic instability may also contribute to the increased tumor phenotype of *TAp73*$^{-/-}$ mice. Indeed, subsequent studies have shown that DNA damage stabilizes the TAp73 protein, through direct interaction with the DNA mismatch repair protein PMS2 (187). In turn, it was found that TAp73 transcriptionally activates DNA repair genes, including MUYTH, SMUG1 (188), Mre11, RAD51, and BRCA2 (4). Studies have also shown that TAp73 can facilitate cell cycle arrest in both G1 and G2/M through the transcriptional activation of p21 or GADD45 (189, 190). TAp73 is also capable of inducing mitochondria-dependent apoptosis via transcriptional activation of BAD, BAX, BIK, NOXA, and PUMA (191, 192). Taken together these studies led many to conclude that TAp73 functions as a tumor suppressor, with specific functions that overlap with p53 and TAp63, as well as unique and tissue specific functions.

1.4.2. Genomic and molecular features of lung adenocarcinoma

Lung cancer is the number one cause of cancer-related deaths worldwide (193, 194). Non-small cell lung cancer (NSCLC), which includes lung squamous cell carcinoma (LUSC) and lung adenocarcinoma (LUAC), accounts for approximately 85% of all lung cancer cases. LUAC is the most common subtype of NSCLC and is responsible for nearly one million deaths per year, making it the deadliest cancer worldwide (195). In recent years, molecularly targeted therapies have improved survival for patients whose tumors express mutated oncogenes, including EGFR and ALK (196, 197). Unfortunately, the majority of LUAC tumors lack an identifiable

driver mutation that can be treated with molecularly targeted therapy. Instead, LUAC tumors frequently exhibit activating KRAS mutations and/or mutations in tumor suppressor genes, such as TP53, KEAP1, STK11, RB1, and CDKN2A (198). Attempts to target KRAS or reactivate mutant tumor suppressors as therapeutic strategies have largely failed. As a result, the majority of LUAC patients are treated with conventional chemotherapy, albeit with limited success.

The therapeutic application of antibodies that target the programmed death-1 (PD-1)-programmed death-ligand (PD-L1) immune checkpoint pathways has resulted in significant improvements cancer treatment outcomes (199), including for patients with NSCLC (200). This is due to the intrinsic capacity of endogenous cytotoxic $CD8^+$ T cells to eliminate cancer cells (201, 202), which can lead to tumor regression and improved survival (203, 204). Clinical studies have shown however, that the effectiveness of checkpoint blockade immunotherapy is limited to a subset of patients. Therefore, a major goal of recent clinical research has been focused on understanding the mechanisms that dictate the effectiveness of immune checkpoint inhibitors. This research has shown that the presence of tumor-infiltrating T cells is a predictor for responsiveness to these therapies (205). Understanding the mechanisms that regulate T cell infiltration and activity may lead to new therapeutic strategies that may increase the number of patients who benefit from checkpoint blockade immunotherapies.

1.4.3. Modeling lung adenocarcinoma in the mouse

Genetically engineered mouse models (GEMM) are particularly useful as they allow

cancer researchers to study different aspects of tumorigenesis in a genetically distinct system, in the natural microenvironment of a given tumor type. This allows cancer researchers to more accurately investigate the potential contribution of a given genetic mutation to the development and/or progression of a particular cancer. In addition, autochthonous tumor models allow researchers to investigate non-cell autonomous mechanisms that act on tumor development, including the effect of the tumor microenvironment and the immune system.

To better understand the fundamental biology and genetics of LUAC, multiple groups set out to develop preclinical animal models that faithfully recapitulate the features of the human disease. The most commonly used mouse models of LUAC contain conditional alleles for oncogenic Kras (206, 207) and/or conditional deletion of p53 (208), which are the two most frequently mutated genes in human LUAC (198). The oncogenic *Kras*$^{LSL\text{-}G12D/+}$ mouse developed in the laboratory of Tyler Jacks is frequently used in such studies (206-211). The intratracheal delivery of replication-deficient viral vectors expressing Cre recombinase induces recombination in the lung cells of the trachea, bronchioles and distal lung. The conditional expression of the oncogenic KrasG12D mutant protein is sufficient to induce lung adenomas in mice in as little as 2 weeks (206). The combination of *Kras*$^{LSL\text{-}G12D/+}$ with other conditional alleles (such as mutant p53) (208, 211) has been shown to significantly accelerate tumor development and progression, resulting in tumors that are highly invasive and metastatic.

To monitor tumor development and progression in a systematic and quantifiable way, the laboratory of Tyler Jacks developed a 4-stage system of

grading tumors that develop in these models (208, 209). The earliest lesions, which encompass atypical adenomatous hyperplasias (AAH) and small adenomas, feature uniform (e.g. normal) nuclei, and are thus designated at Grade 1 lesions. Grade 2 adenomas are larger in size, and contain nuclei that are enlarged and exhibit prominent nucleoli. Bona fide adenocarcinomas resembling human lesions are designated as Grade 3 lesions. These tumors exhibit a higher degree of pleomorphic nuclei, conspicuous nucleoli, and nuclear molding. Grade 4 adenocarcinomas exhibit similar cellular characteristics as Grade 3 lesions, along with a higher mitotic index, tumor giant cells, an invasive stromal reaction, and invasive edges along blood vessels and/or the pleura.

Together these model systems are incredibly useful for preclinical studies of the underlying mechanisms that drive the development and progression of LUAC. Ultimately, the conclusions drawn from such studies have a high probability of informing the development of newer, more effective therapies for LUAC.

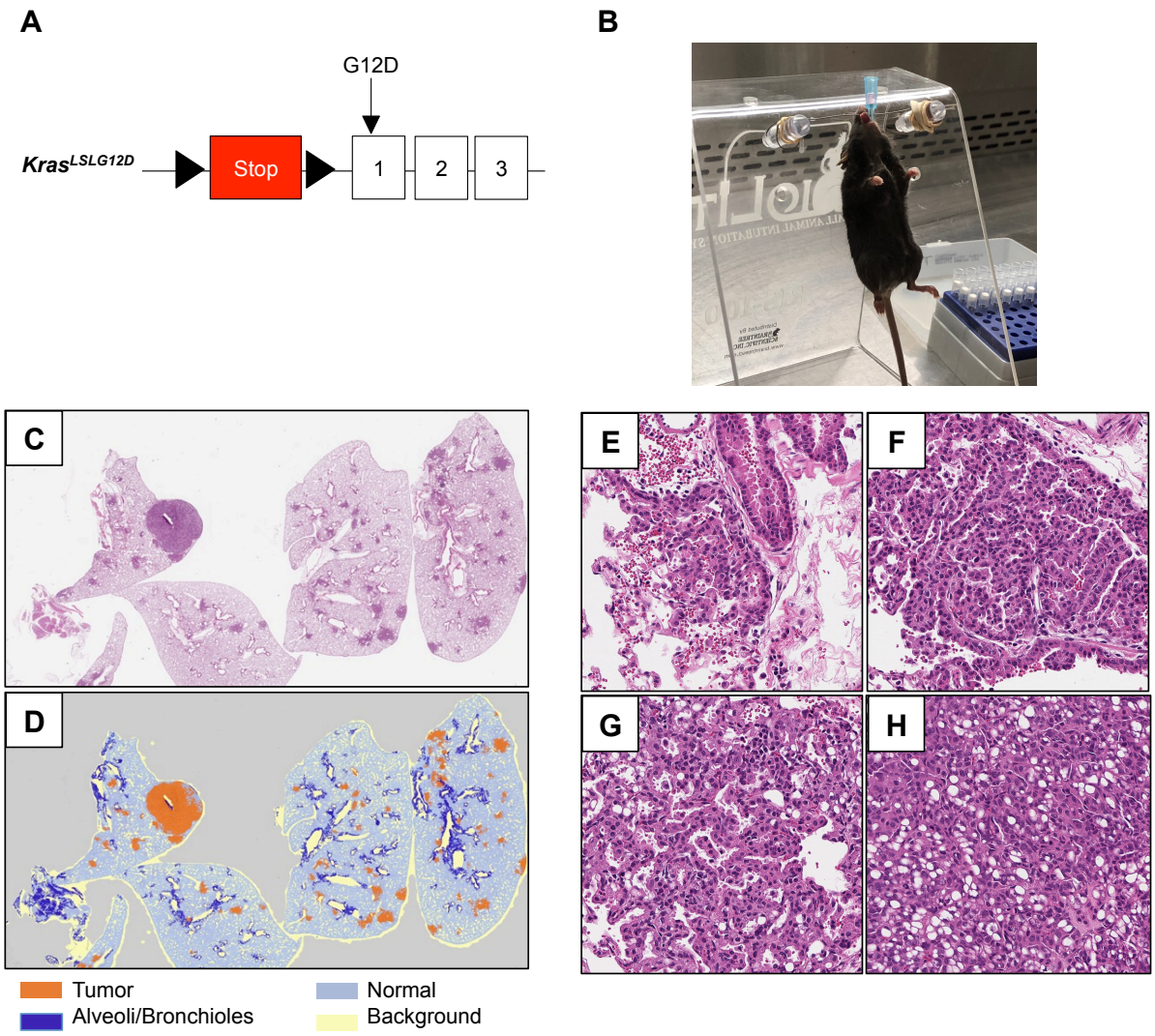

Figure 5: Modeling lung adenocarcinoma in the mouse. (A) The oncogenic *Kras*^{LSLG12D} mouse allele generated in the Jacks lab. (B) Anesthetized mice are aligned onto a platform with their teeth across a thin metal bar, such that the head, neck, and chest are positioned perpendicular to the base of the platform, allowing effective insertion of a catheter into the trachea. Adenovirus suspended in media is administered into the catheter and is inhaled by the mouse (C and E) Representative H&E stainings (C) and tissue segmentation (E) of lung sections from *TAp73*$^{fltd/fltd}$; *Kras*$^{LSLG12D/+}$ mice 30 weeks after intratracheal adenovirus infection. (E-H)

Representative images of oncogenic $Kras^{G12D}$-driven lung tumors, including grade 1 (E), grade 2 (F), grade 3 (G), and grade 4 (H) tumors.

CHAPTER 2: MATERIALS AND METHODS

Chapter 2: Materials and Methods

Content of this chapter is partly based on the following article:

Martin-Lopez M, Maeso-Alonso L, Fuertes-Alvarez S, Balboa D, Rodríguez-Cortez V, Weltner J, Diez-Prieto I, **Davis A**, Wu Y, Otonkoski T, Flores ER, Menéndez P, Marques M, and Marin MC. p73 is required for appropriate BMP-induced mesenchymal-to-epithelial transition during somatic cell reprogramming. Cell Death and Disease (2017) 8(9), e3034.

2.1 Animal studies

Mouse studies were approved by the IACUC at the University of Texas MD Anderson Cancer Center or the IACUC at Moffitt Cancer Center. *TAp63*$^{fl/fl}$ and *TAp63*$^{-/-}$ mice were generated previously (14). *TAp63*$^{-/-}$ mice (14) were backcrossed over 10 generations to generate *TAp63*$^{-/-}$ and *WT* mice on a pure C57BL/6 background. Athymic nu/nu mice were purchased from Envigo. *SOX2-CreER* (212), *Rosa*$^{mT/mG}$ (213) were purchased from JAX labs. The *Kras*^{LSLG12D} (214) mouse was a gift from Jonathan M. Kurie. Age- and sex-matched mice were used for all experiments, unless noted otherwise.

2.2 Generating the *TAp73*$^{fltd/fltd}$ and *TAp73*$^{\Delta td/\Delta td}$ mice

The cre-loxP strategy was used to generate the TAp73 conditional knockout reporter allele (*TAp73*^{fltd}). Genomic DNA encompassing the *Trp73* locus from intron 1 to intron 3 was amplified from mouse genomic DNA (C57BL/6). A neomycin resistance gene (neo) flanked by frt sites was inserted in intron 3. LoxP sites were cloned into

the endogenous locus upstream (5') to exon 2 and downstream (3') of the frt-flanked neo cassette. tdTomato was cloned upstream of the 5' loxP site in an antisense orientation, while the synthetic CAG promoter was cloned, in an antisense orientation, downstream of the 3' loxP site. The modified p73 locus was cloned into the pL253 plasmid vector (215). Mouse embryonic stem cells (G4) electroporated with the targeting vector were analysed by Southern blot analysis for proper targeting of the *TAp73*^{fltd} allele. Resulting chimaeras were mated with C57BL/6 albino females and genotyped as described below. Mice with germline transmission of the targeted allele (*TAp73*^{fltd}) were intercrossed to generate homozygous mice (*TAp73*$^{fltd/fltd}$). Total knockout mice (*TAp73*$^{\Delta td/\Delta td}$) were generated by crossing *TAp73*$^{fltd/fltd}$ mice with transgenic mice expressing an oocyte-specific cre recombinase (*Zp3-Cre*) (216). *TAp73*$^{fltd/+}$*; Zp3-Cre* mice were intercrossed to generate *TAp73*$^{fltd/\Delta td}$*; Zp3-Cre* mice, which were subsequently intercrossed to generate *TAp73*$^{\Delta td/\Delta td}$ mice.

2.3 4-hydroxytamoxifen (4OHT) treatment of mice

To induce recombination in the SOX2^{+} skin-derived precursor (SKP) cell compartment, 3 week old *SOX2*$^{CreER/+}$; *Rosa*$^{mT/mG}$; *TAp63*$^{+/+}$ and *SOX2*$^{CreER/+}$; *Rosa*$^{mT/mG}$*; TAp63*$^{fl/fl}$ mice were shaved on their dorsal side, and treated with 3 consecutive days of 1mg 4OHT (Sigma; H6278) diluted in ethanol at 5mg/ml via topical administration to the back skin.

2.4 UVR treatments

To model UVR-driven cuSCC, 4-week-old mice were shaved on the entire dorsum prior to irradiation, and as needed throughout the experiment. Mice were exposed to low-dose UVR (2.5kJ m^{-2}, 3x a week) using a bank of 4 FS40 T12 fluorescent sunlamps (Westinghouse, NJ). Control mice were regularly shaved but not exposed to UVB. Mice were irradiated for up to 60 weeks or until tumors exceeding 2mm in diameter developed, at which point the mice were euthanized and the tissues were collected for RNA extraction and/or histological processing.

2.5 Tumor xenograft studies

To model human cuSCC, we modified the use of a previously described xenograft model of cuSCC (217). COLO16 cells stably expressing RFP and luciferase were reverse transfected with miRNA mimics or scrambled mimic control. Six hours later, the transfected cells were harvested and diluted in a 1:1 mixture of PBS and matrigel (Corning). 2 x 10^5 COLO16 cells transfected with either miRNA mimic were subcutaneously injected into one side of 6-week-old female athymic nu/nu mice. The side of injection was randomized such that the each mouse received an injection of cells transfected with miRNA mimic on one side, while the other flank was injected with cells transfected with the scrambled control mimic. Tumor growth was measured with calipers and tumor volume was calculated using the following formula: tumor volume (mm^3) = (D x d^2) / 2, where D and d are the longest and the shortest diameters of the tumor, respectively. In parallel, tumor growth was

monitored using bioluminescence imaging of luciferase activity using a Bruker In Vivo Xtreme Imaging system. 3 mg of D-luciferin (GoldBio) was administered to each mouse via intraperitoneal injection, 6 minutes prior to bioluminescence imaging. Radiance (photons/sec/cm^2/steridian) was determined within a consistent region that encompassed each flank of all imaged mice using the Molecular Imaging Software "MI" version 7.2.0 (Bruker). Mice were euthanized when the biggest tumors of the respective controls were 1,000mm^3, or if the mice exhibited symptoms of distress.

2.6 Intratracheal adenoviral infections

Intratracheal administration of viral particles was carried out as described previously (209, 214). Briefly, 8-to-10 week old mice were anesthetized using xylazine/ketamine and were intratracheally infected with 2.5 x10^7 or 7.5 x10^7 Pfu of adenovirus expressing Cre (Ad5-CMV-Cre) or empty vector (Ad5-CMV-empty) co-precipitated with $CaCl_2$ suspended in 50 microliters (μl) of minimum essential media (MEM). Infected mice were kept on a heating pad and monitored until consciousness was fully regained.

2.7 Histology

Mouse tissues were harvested and fixed in 10% neutral-buffered formalin, and embedded in paraffin. Assistance in processing murine tissue samples was provided by the MD Anderson Research Histopathology Facility or the Moffitt Cancer Center Tissue Core Histology Core. Five-micron (μm) sections were cut from formalin-fixed,

paraffin-embedded (FFPE) skin and tumors and de-waxed in xylene and re-hydrated using decreasing concentrations of ethanol. FFPE samples were stained with hematoxylin and eosin, using standard protocols, or were used for immunostaining purposes.

2.8 Immunohistochemistry of murine skin and cuSCC

Five-micron (μm) sections were cut from formalin-fixed, paraffin-embedded (FFPE) skin and tumors and de-waxed in xylene, followed by re-hydration in decreasing concentrations of ethanol. Antigens were unmasked using citrate buffer unmasking solution (Vector Laboratories) and samples were subsequently incubated in blocking solution for one hour at room temperature. Primary antibody incubation was performed overnight at 4°C with the following primary antibodies: cytokeratin 5 (1:1000) (Abcam ab53121). Visualization was performed using ImmPRESS secondary antibodies (Vector Laboratories) and the ImmPact DAB peroxidase substrate kit (SK4100, Vector Laboratories). Immunostained slides were then counterstained with hematoxylin, dehydrated, and mounted following standard protocols. Images were acquired using an Olympus IX83 microscope or Zeiss Imager 2, and analyzed using the CellSens Dimensions software or Zeiss Zen software. Alternatively, bright field images were acquired using an Aperio™ Scanscope AT2 digital whole slide scanner (Leica). Tumor pathology was characterized with the assistance of Kenneth Y. Tsai, M.D.

2.9 Immunohistochemistry for lung tissues

Five-micron (μm) sections were cut from formalin-fixed, paraffin-embedded (FFPE) tissues and were stained using the Ventana Discovery XT automated system and associated proprietary reagents (Ventana Medical Systems) as per the manufacturer's protocol. Slides were deparaffinized using the EZ Prep solution (Ventana Medical Systems) and the heat-induced antigen retrieval method was used in Cell Conditioning 1 Mild (Ventana Medical Systems). The following antibodies were used: rabbit anti-CD31, (1:200; #ab28364, Abcam), rabbit anti-CD3 (1:100; M307, Spring Biosciences), and rabbit anti-CD11b, (1:700; #LS-C141892, Lifespan Bioscience). All primary antibodies were diluted in Dako antibody diluent and incubated for 32 minutes. The Ventana ChromoMap kit was used for detection. Immunostained slides were then counterstained with hematoxylin, dehydrated, and mounted following standard protocols.

2.10 Double-staining immunohistochemistry for CD4/CD8 on lung tissues

Five-micron (μm) sections were cut from formalin-fixed, paraffin-embedded (FFPE) tissues and were stained using the Ventana Discovery XT automated system and associated proprietary reagents (Ventana Medical Systems, Tucson, AZ) as per the manufacturer's protocol using. Slides were deparaffinized using the EZ Prep solution (Ventana) and heat-induced antigen retrieval method was used in Cell Conditioning 1 (Ventana). Primary rabbit anti-CD8 (#98941, Cell Signaling, Danvers, MA) was incubated for 60 min. Slides were incubated with the Ventana OmniMap anti-rabbit

secondary Antibody for 16 min and detected with the Ventana ChromoMap DAB kit. Subsequently, the slides were incubated for 32 minutes with rabbit anti-CD4 (#50134-R001, Sino Biological, Wayne, PA). Slides were incubated with the Ventana UltraMap Anti-rabbit secondary antibody for 16 minutes with ChromoMap Red detection. Immunostained slides were then counterstained with hematoxylin, dehydrated, and mounted following standard protocols.

2.11 Immunofluorescence

Paraffin embedded tissue sections were prepared as described previously (184). Sections were incubated with rabbit anti-SOX2 (EPR3131, Abcam, 1:100), chicken anti-GFP (ab13970, Abcam, 1:200), guinea pig anti-Cytokeratin 14 (LS-C22637, LifeSpan Biosciences, 1:500). For secondary antibodies, AlexaFluor 568 goat anti-rabbit (703-545-155, Life Technologies, 1:500), Alexa Fluor 633 goat anti-guinea pig (A-21105, Life Technologies) or Alexa Fluor 488 goat anti-chicken (A-11039, Life Technologies) antibodies were used. Slides were mounted with coverslips and Vectashield® Hardset™ Mounting media with DAPI (H-1500).

2.12 Imaging and lung tumor segmentation

H&E stainings of FFPE tissue sections were scanned using the Aperio™ ScanScope AT2 (Leica Biosystems, Vista, CA) with a 200x/0.8NA objective lens. These images and their meta-data were then imported into the Definiens Tissue Studio v4.2 suite or Visiopharm v 7.2 for segmentation analysis. A machine-learning algorithm was used to segment each tissue section image into "tumor", "alveoli", "normal", and

"background". Segmentation was further refined using size, shape, and proximity classifiers. This refinement step was necessary to correct regions that were misclassified during the initial learning iterations. Data features to determine the number of tumors and percent tumor area were extracted from the final segmentation. In addition to the tumor level segmentation each cell (nucleus and cytoplasm) within each tumor was segmented and identified for future analysis considerations.

2.13 Generating mouse embryonic fibroblasts (MEFs)

WT and *TAp73*$^{\Delta td/\Delta td}$ mouse embryonic fibroblasts (MEFs) were generated as described previously (24).

2.14 Cell culture

Human cutaneous squamous cell carcinoma (cuSCC) cell lines (COLO16 and SRB12) were kindly provided by Dr. K.Y. Tsai. Normal human epidermal keratinocytes (NHEKs) were purchased from Lonza. All cuSCC cell lines were maintained in culture conditions as previously reported (218, 219). NHEKs were cultured in KGM-Gold^{TM} Keratinocyte Growth media (Lonza).

2.15 Lenti-virus infection

COLO16 and SRB12 cells were seeded at a density of 5 x 10^6 cells in 10-cm dishes prior to infection. Approximately 16 hours later, cells were infected with lenti-rLV-

EF1a-mCherry-Nuc-IRES-Puro-WPRE (Vectalys™) or lenti-FLuc-T2A-RFP (BioSETTIA), at a multiplicity of infection of 5 particles per cell, and supplemented with polybrene (2μg/ml) for 24 hours. After infection, cells were subjected to 48 hours of puromycin (2μg/ml) selection, at which point transduction efficiency was quantified by assessing mCherry or RFP-positive cells.

2.16 Reverse transfections

Cells were transfected with 55.5 nM hsa-miR-30c-2-3p (*miR*Vana™ miRNA mimic, ambion®, MC12646), hsa-miR-497 (*miR*Vana™ miRNA mimic, ambion®, MC10490), Negative Control (*miR*Vana™ miRNA mimic, ambion®, 4464061), siAURKA (MISSION® siRNA, Sigma, SASI_Hs01_00079240), siCDK6 (MISSION® siRNA, Sigma, SASI_Hs01_0004879), siFAT2 (MISSION® siRNA, Sigma, SASI_Hs01_0033187), siORC1 (MISSION® siRNA, Sigma, SASI_Hs01_00038886), siKIF18B (MISSION® siRNA, Sigma, SASI_Hs02_00314896), siPKMYT1 (MISSION® siRNA, Sigma, SASI_Hs01_00199784), siORC1 (MISSION® siRNA, Sigma, SASI_Hs01_00038886), siControl (MISSION® siRNA, Sigma, SIC001), or siControl-Cy5 (MISSION® siRNA, Sigma, SIC005) using Lipofectamine® RNAiMAX (Invitrogen™). The mixture of oligos and Lipofectamine were added to tissue culture-treated plates and incubated for 20 minutes, after which trypsinized cells were plated on top. The effects on target gene levels were tested 48 hrs post transfection.

2.17 RNA isolation

Tissue specimens were flash frozen in liquid nitrogen and homogenized with a mortar and pestle and subsequently lysed in Qiazol reagent from the miRNeasy RNA isolation kit (Qiagen). Total RNA was extracted according to the manufacturer's instructions. RNA concentration was determined by measuring the total absorbance at 260nm using a Nanodrop™ 2000 spectrophotometer.

2.18 RNA sequencing and analysis

RNA sequencing (Illumina Hi-Seq) yielded 30–40 million read pairs for each sample. The mRNA-Seq mouse sample reads were aligned onto the mouse genome build UCSC mm10 (NCBI 38). The HTSeq software platform was used to quantify overlaps between aligned sequence reads and annotated genomic features, including genes and exons. The scaling factor method was used to normalize the resulting counts.

2.19 Small RNA-seq analysis

Illumina small RNA adapter sequences were removed from sequence reads. Reads shorter than 10 nt or ending in homopolymers greater than or equal to 9 nt were discarded. From this, the total number of usable reads for each sample was calculated. Sequence reads were then mapped to the miRBase (220) reference (http://www.mirbase.org/) using BLAST. The relative abundance of each individual miRNA sequenced in the experiment was counted as a fraction of the total usable

reads (parts per million). The ComBat normalization algorithm (221) (http://www.bu.edu/jlab/wp-assets/ComBat/ Abstract.html) was used to minimize potential batch effects. Differentially expressed miRNA were identified following a cut-off of absolute fold-change greater than 1.5, and a p value less 0.05 (*t*-test) using the R statistics software. Principal Component Analysis (PCA) was used to examine sample clustering.

2.20 miRNA-mRNA Functional Pair Analysis

We evaluated the enrichment of miRNA–mRNA pairs using the SigTerms methodology (222). Briefly, a one-sided Fisher exact test was applied along with microRNA target predictions using TargetScan (223) to determine the miRNAs for which its predicted gene targets are significantly enriched (false discovery rate-adjusted q less than 0.25; fold-change greater than 1.25) in a given gene signature. Finally, we determined the conserved miRNAs enriched the mouse *TAp63*$^{-/-}$ cuSCC signature, as well as the human cuSCC signature. Enriched microRNA–mRNA pairs were visualized using the Cytoscape software (http://www.cytoscape.org/).

2.21 RT-qPCR

Total RNA from cells and tumors was used to synthesize complementry DNA using the qScript™ XLT cDNA Synthesis Kit (QuantaBio) followed by qRT-PCR using the PerfeCTa SYBR® Green SuperMix reagent (QuantaBio) according to the manufacturer's protocols. The following primers were used, as described previously: *histone H3* (224), *TAp63* (225), and *Dicer* (226). Alternatively, gene expression was

assessed using the qScript™ XLT One-Step RT-qPCR ToughMix, Low ROX kit (QuantaBio) and TaqMan® assays (Applied Biosystems™). For human samples, the following TaqMan® assays were used: *POL2RA* (Hs00172187_m1), *GAPDH* (Hs03929097_g1), *AURKA* (Hs01582072_m1), *CDK6* (Hs01026371_m1), *FAT2* (Hs01087234_m1), *ITGA6* (Hs01041011_m1), *KIF18B* (Hs00977735_m1), *ORC1* (Hs01069758_m1), *PKMYT1* (Hs00993620_m1), *pri-miR-30c-2* (Hs03302833_pri), and *pri-miR-497* (Hs03303903_pri). For mouse samples, the following assays were used: *TAp73* (Mm00660223_m1), and *Gapdh* (Mm99999915_g1). qRT-PCR was performed using an Applied Biosystems™ QuantStudio™ 6 Flex Real-Time PCR System. Reactions were performed in triplicate and ΔΔCt values were calculated using *H3* (SYBR® Green), *POL2RA* (Taqman), or *GAPDH* (Taqman) as an internal control.

2.22 miRNA Taqman Real Time qPCR assays

Expression of mature miRNAs was assessed using TaqMan® miRNA assays (Applied Biosystems™). Total RNA (10ng per reaction) was used to synthesize complementary DNA using the TaqMan® MicroRNA Reverse Transcription Kit (Applied Biosystems™) and TaqMan® primers for the specific miRNAs being assayed. The following assays from were used: hsa-miR-30c-2* (002110), hsa-miR-497 (001043), mmu-miR-17* (002543), *snoRNA234* (001234), and *RNU6B* (001093) (Applied Biosystems™). qRT-PCR was performed using the TaqMan Universal Master Mix II (no UNG) with TaqMan primers for the specific miRNAs and run on a QuantStudio™ 6 Flex Real-Time PCR System (Applied Biosystems™). Reactions

were performed in triplicate and ΔΔCt values were calculated using *RNU6B* (human samples) *or snoRNA234* (murine samples) as an internal control.

2.23 Western blot analysis

Fifty microgram (µg) of protein lysates were electrophoresed on a 6%, 8%, 10% or 12.5% SDS PAGE gel and transferred to nitrocellulose membranes as described previously (147). High molecular weight proteins (e.g. FAT2) were transferred (without ethanol) in a 70C water bath for 40min at 40V as described previously (227). Blots were probed with anti-AURKA (1:1000) (ab13824, Abcam), anti-CDK6 (1:1000) (3136S, Cell Signaling), anti-FAT2 (1:100) (sc59985, Santa Cruz), anti-ITGA6 (1:500) (ab97760, Abcam), anti-ORC1 (1:100) (sc23887, Santa Cruz), anti-PKMYT1 (1:1000) (ab134108, Abcam), or anti-TAp73 (A300-126A, Bethyl laboratories) at 4 °C for appx. 18 hr, followed by incubation for 1 hr at room temperature with the appropriate secondary antibodies conjugated to horseradish peroxidase (1:5,000) (Jackson Lab), IRDye® 800CW (1:10,000) (LI-COR®), or IRDye® 680LT (1:10,000) (LI-COR®). HSP90 (1:10,000) (ab13495, Abcam), mouse β-Actin (1:5,000) (Sigma), and rabbit β-Actin (1:5,000) (Sigma) were used as loading controls. ECL™ Prime reagent was used for chemiluminescent detection when HRP-conjugated secondary antibodies were utilized. All Westerns were imaged using the Odyssey® Fc imaging system (LiCOR®) and analyzed using the Image Studio™ software (LiCOR®).

2.24 Real time cell growth and apoptosis analysis

All proliferation and apoptosis imaging experiments were performed with the IncuCyte ZOOM imaging platform (Essen Bioscience). Cells were plated at a density of 5 x 10^3 cells per well. Experiments were conducted for 72-96 hours, with data collection every 6 hours. Four planes of view were imaged per well of a 96-well plate using a 10X objective. Images were collected in phase contrast, green fluorescence (Ex: 440/80 nm; Em: 504/44 nm), and red fluorescence (Ex: 565/05 nm; Em: 625/05 nm) for all experiments. Spectral unmixing was set at 5% of red fluorescence removed from the green channel. Processing definitions were developed for each particular experiment, however the same processing definition was utilized for each replicate experiment. For transfection experiments, cells were reverse transfected using Lipofectamine® RNAiMax (Invitrogen) in suspension and plated at a density of 5 x 10^3 cells per well in 6 replicate wells of a 96-well plate. For drug treatment experiments, cells were plated at 5 x 10^3 cell per well, and treated with the indicated drugs 24 hours after plating, at which point the cells were imaged every 6 hours. Cells were plated in media containing IncuCyte® Annexin V-AlexaFluor 488 Reagent (Essen Bioscience). Total cells were calculated based on the number of nucRed-mCherry$^+$-positive nuclei detected in each well. The percentage of apoptotic cells was calculated for each time point by counting the number of overlapping green (Annexin V$^+$) and red (nucRed-mCherry$^+$) cells and dividing it by the total number of nuclei in each well. Cells were scanned 6 hours after transfection, and every 6 hours thereafter.

2.25 Edu incorporation assays

Cells were plated at a density of 5 x 10^4 cells in 6 replicates in a 96-well dish. Three independent replicate experiments were performed for each assay. To evaluate cell proliferation, the cells were pulse labeled for 3 hours with 10 mM EdU (5'-ethynyl-2'-Apoptosis was monitored by incubating the cells with Annexin V-Alexa Fluor 488 (Essen BioScience) according to the manufacturer's instructions. Total nuclei were labeled using NucRed™ Dead 647 Readyprobes reagent. Images were captured and percentage of edu-positive cells was quantified using the IncuCyte high-throughput plate reader and accompanying software (Essen Bioscience).

2.26 Cell migration and invasion assays

Cells were incubated for 2 hours with 4ug/ml of mitomycin C to arrest the cells. Cells were trypsinized in resuspended in RPMI media without serum, and subsequently plated in 6 replicate wells at 1 x 10^3 cells per well in an IncuCyte ClearView 96 well cell migration plate (Essen BioScience), whose wells were either left uncoated (for migration assays) or coated with 20 µL of 200 µg/mL growth factor reduced matrigel (Corning®) (for invasion assays). RPMI media containing 10% horse serum was added to the bottom chambers of each well to serve as a chemo-attractant. Images of the top and bottom of each well were captured using the IncuCyte high-throughput plate reader and accompanying software (Essen Bioscience). Cell migration and invasion were quantified as the percentage of cell confluence on the bottom of each well and was normalized to the initial confluence of cells on the top of each well

2.27 Cell viability assays:

Cell viability was assessed in 96-well format using the CelltiterGlo® (Promega) luminescence measured on a GloMax® Discover System plate reader (Promega) according to the manufacturer's instructions. Cell viability of drug treated cells was calculated as a percentage of luminescence relative to the vehicle-treated cells. Dose response parameters, including the half maximal inhibitory concentration (IC50) were calculated using nonlinear regression using GraphPad Prism 7 software, based on the results from at least 3 independent experiments.

2.28 Cell cycle profiling using flow cytometry

Cells to be collected for cell cycle profiling were grown in 6cm TC-treated dishes. Trypsinized cells were fixed in 1% formaldehyde (1X PBS) on ice for 15 minutes, and subsequently post-fixed with ice-cold 80% ethanol for a minimum of 4 hours. Fixed cells were pelleted and resuspended in 1mL of 0.25% Triton X-100 and incubated on ice for 5 minutes. Cells were resuspended in 5mL of 1X PBS and pelleted. Cell pellets were resuspended in 100uL of PBS containing 1% BSA and 0.5ug of rat anti-phospho-histone H3 (S28) (BD BioSciences; HTA28) or normal IgG, and then incubated for 30 minutes at room temperature, in the dark, with gentle agitation. Cell suspensions were then rinsed with an additional 5mL of 1X PBS plus 1% BSA and then pelleted. Cell pellets were then resuspended in 100ul of 1X PBS containing 0.1% Triton X-100 and 1µg/ml DAPI and incubated in the dark for 20 minutes with gentle agitation. Cell cycle profiles were analyzed by flow cytometry using a BS LSR II cell analyzer (BD Biosciences). The flow cytometer was set for UV

excitation (340-380nm wavelengths) and detection of DAPI emission at blue wavelengths (450-495nm). DNA content was analyzed using the ModFit LT V3.3.11 software, whereas phospho-H3 staining was analyzed using FCS express 6 plus (DeNovo Software). Different cell populations were quantified based on DNA content to discern cells with 2N (G1), 2-4N (S), and 4N (G2/M). The percentage of cells in G2 was determined by subtracting the percentage of mitotic cells (e.g. the phospho-H3-positive population) from the G2/M population as determined by DNA content measurements.

2.29 Sample Preparation for Proteomics

Cells were lysed in denaturing lysis buffer containing 8M urea, 20 mM HEPES (pH 8), 1 mM sodium orthovanadate, 2.5 mM sodium pyrophosphate and 1 mM β-glycerophosphate. A Bradford assay was carried out to determine the protein concentration. Equal amount of heavy and light proteins were mixed together. The mixed proteins were reduced with 4.5 mM DTT and alkylated with 10 mM iodoacetamide. Trypsin digestion was carried out at room temperature overnight. Tryptic peptides were acidified with 1% trifluoroacetic acid (TFA) and desalted with C18 Sep-Pak cartridges according to the manufacturer's protocol.

2.30 TMT Labeling

100 microgram of peptide from each sample was labeled with TMT reagent. LC-MS/MS and spectral counting was used to analyze the incorporation of the TMT

label. 98% or greater label incorporation was achieved for each channel. The 6 samples were then pooled and lyophilized.

2.31 High pH Reversed Phase Peptide Separation

After lyophilization, the peptides were re-dissolved in 400 micro liter of 20 mM Ammonium Formate, (pH 10.0). The high pH reversed phase separation was performed on a Xbridge 4.6 mm x 100 mm column packed with BEH C18 resin, 3.5 µm, 130Å. (Waters) The peptides were eluted as follows: 5% B (5 mM Ammonium Formate, 90% acetonitrile, pH 10.0) for 10 minutes, 5% - 15% B in 5 minutes, 15-40% B in 47 minutes, 40-100% B in 5 minutes and 100% B held for 10 minutes, followed by re-equilibration at 1% B. The flow rate was 0.6 ml/min, and 24 concatenated fractions were collected. Speedvac centrifuge was used to dry the peptides.

2.32 Liquid chromatography-tandem mass spectrometry

A nanoflow ultra high performance liquid chromatograph (RSLC, Dionex) coupled to an electrospray bench top orbitrap mass spectrometer (Q-Exactive plus, Thermo) was used for tandem mass spectrometry peptide sequencing experiments. Samples were first loaded onto a pre-column (2 cm x 100 µm ID packed with C18 reversed-phase resin, 5µm, 100Å) and washed for 8 minutes with aqueous 2% acetonitrile and 0.04% trifluoroacetic acid. Trapped peptides were eluted onto an analytical column, (C18, 75 µm ID x 25 cm, 2 µm, 100Å, Dionex). A 90-minute gradient was programmed as follows: 95% solvent A (2% acetonitrile + 0.1% formic acid) for 8

minutes, solvent B (90% acetonitrile + 0.1% formic acid) from 5% to 38.5% in 60 minutes, then solvent B from 50% to 90% B in 7 minutes and held at 90% for 5 minutes, followed by solvent B from 90% to 5% in 1 minute and re-equilibrated for 10 minutes. The flow rate on the analytical column was 300 nl/min. Sixteen tandem mass spectra were collected in a data-dependent manner following each survey scan. Both MS and MS/MS scans were performed in Orbitrap to obtain accurate mass measurement using a 15 second exclusion for previously sampled peptide peaks.

2.33 Data Analysis

MaxQuant (version 1.5.2.8) (228) was used to quantify the TMT reporter ion intensities.

2.34 Human cytokine antibody array

Relative cytokine levels in conditioned media (CM) were determined using the Human Cytokine Antibody Array C5 (RayBiotech®) according to the manufacturer's instructions. Chemiluminescent detection was performed using the Odyssey® Fc imaging system and was quantified using the associated ImageStudio software (Li-COR®). Following background subtraction, the relative levels of individual cytokines present in CM were normalized based on the relative intensities of the positive control spots.

CHAPTER 3: UNDERSTANDING THE REGULATION OF MIRNAS BY TAP63 IN CUTANEOUS SQUAMOUS CELL CARCINOMA

Chapter 3: Understanding the regulation of miRNAs by TAp63 in cutaneous squamous cell carcinoma

3.1. Introduction and rationale

Cutaneous squamous cell carcinoma (cuSCC) is the second most common cancer type diagnosed in the United States, with an estimated incidence of 700,000 new cases each year (76). Cumulative exposure to ultraviolet radiation (UVR) is the most common environmental risk factor for the development of cuSCC, in part through its ability to induce mutagenesis in the skin epithelium. The most effective course of treatment for cuSCC is surgical excision, which is occasionally accompanied with adjuvant radiotherapy (113, 119). While the management of cuSCC generally has a favorable outcome, there is a small but significant percentage of patients, whose lesions fail to respond to therapy, resulting in severe morbidity and reduced survival. Efforts to develop more effective targeted therapies for treatment-resistant cuSCC have largely been unsuccessful. A better understanding of the underlying genetic and molecular determinants of cuSCC will likely facilitate the development of more effective treatments.

miRNAs are a class of small, highly conserved non-coding RNAs that have been shown to have significant roles in many different biological processes and cellular contexts. Interestingly, studies have shown that they are frequently disrupted in disease states, including cancer (229). The primary function of miRNAs is to inhibit the translation of mRNAs, via direct interaction between miRNAs and specific mRNAs via Watson-Crick base pairing between nucleotides 2-7 of the miRNA and complementary sequences in targeted mRNAs (156). Consequentially,

understanding the functions of a given miRNA depends upon identifying the mRNAs that it targets, which may be numerous, and may also be cell- and context-specific (230).

Large percentages of cuSCC (72, 131), as well as squamous cell cancers of the lung (LUSC), head and neck (HNSCC), esophagus (ESCC), and bladder (BSCC) share mutations in *TP53*, along with overexpression of *TP63* and de-regulated miRNA expression (70, 71, 73, 231). Our lab and others have shown that *TP63* encodes a diverse group of p63 isoforms, including TAp63 and ΔNp63, which exhibit non-overlapping and even antagonistic functions (1). ΔNp63 isoforms have been shown to promote tumor cell survival (31), whereas the downregulation of TAp63 isoforms is sufficient to initiate tumor development and promote metastasis (147). Notably, both *TAp63*$^{-/-}$ and *TAp63*$^{+/-}$ mice are highly susceptible to spontaneous sarcoma and carcinoma development, including cuSCC (147). Mechanistic studies found that TAp63 directly transactivates the expression of primary miRNA transcripts encoding miR-130b and miR-34a, as well as Dicer, an endoribonuclease that cleaves pre-miRNAs into short double-stranded RNA fragments called miRNAs. In addition, we found that ΔNp63 isoforms can affect miRNA expression through transactivation of DGCR8, another critical component of the miRNA biogenesis pathway (29). DGCR8 binds to Drosha in the nucleus to form the Microprocessor complex, which cleaves primary miRNA transcripts (pri-miR) into precursor miRNA (pre-miR) molecules (158, 159), which are transported out of the nucleus into the cytoplasm, where Dicer subsequently processes it into functional mature miRNAs. Interestingly, ΔNp63-mediated regulation of DGCR8 and downstream miRNAs,

including let-7d and miR-128, are necessary for the viability and proliferative potential of cuSCC (33). Together, these studies describe critical functions for both ΔNp63 and TAp63 in the regulation of miRNA expression in tumorigenesis.

Given these observations we set out to investigate the mechanisms through which TAp63 regulates miRNA expression in UVR-induced skin carcinogenesis. Our results show that *TAp63*-deficient mice develop UVR-driven cuSCC at a significantly higher rate compared to wild-type (WT) mice. Through the use of next generation sequencing, we identified several miRNAs whose expression are deregulated in *TAp63*$^{-/-}$ tissues, most notably miR-30c-2* and miR-497. We also found that several predicted and verified mRNA targets of these miRNAs are conversely overexpressed in human cuSCC. Reintroduction of miR-30c-2* and miR-497, or inhibition of their validated targets was sufficient to halt tumor cell proliferation and survival. Among these targets, we found that the miR-497 target AURKA was frequently overexpressed in cuSCC, and was associated with poor survival in patients with HNSCC. Moreover, inhibition of AURKA was effective at suppressing cuSCC proliferation and inducing cell death. Thus, we propose that dysregulation of these miRNAs and their downstream targets promote tumor development and progression.

3.2 Results

3.2.1. Loss of TAp63 promotes UVR-induced tumorigenesis

To investigate the role of TAp63 in skin tumorigenesis, we first compared UVR-induced tumor formation among mice with normal TAp63 (*WT*) and homozygous

deletion of TAp63 (*TAp63*$^{-/-}$) (14) (Figure 6A). As anticipated, this treatment induced cutaneous tumors in both cohorts, including pre-malignant papillomas and fully malignant cuSCC (Figure 6B and Figure 6E). While the number of papillomas did not differ between the two genotypes, we observed a higher frequency of cuSCC in the *TAp63*$^{-/-}$ cohort (Figure 6C-D). These results suggest that the loss of TAp63 promotes malignant progression.

An important prognostic feature of cuSCC is differentiation status. Tumors with a poorly differentiated histology harbor an enhanced risk for recurrence and metastasis (77). Close histopathological examination found that all of the identified tumors, regardless of genotype, were well-differentiated cuSCC, indicating that the loss of TAp63 does not impact primary tumor differentiation (Figure 6E). Since we have previously shown that TAp63-deficient mice are prone to metastatic tumorigenesis (147), we examined the organs of irradiated mice for evidence of metastasis. While no metastases were found in WT mice, multiple lung micrometastases, which stained positive for the squamous cell marker keratin 5, were found in one of the TAp63$^{-/-}$ mice bearing cuSCC lesions (data not shown). Taken together, these results indicate that TAp63 may be an essential tumor-suppressor in UVR-induced cuSCC.

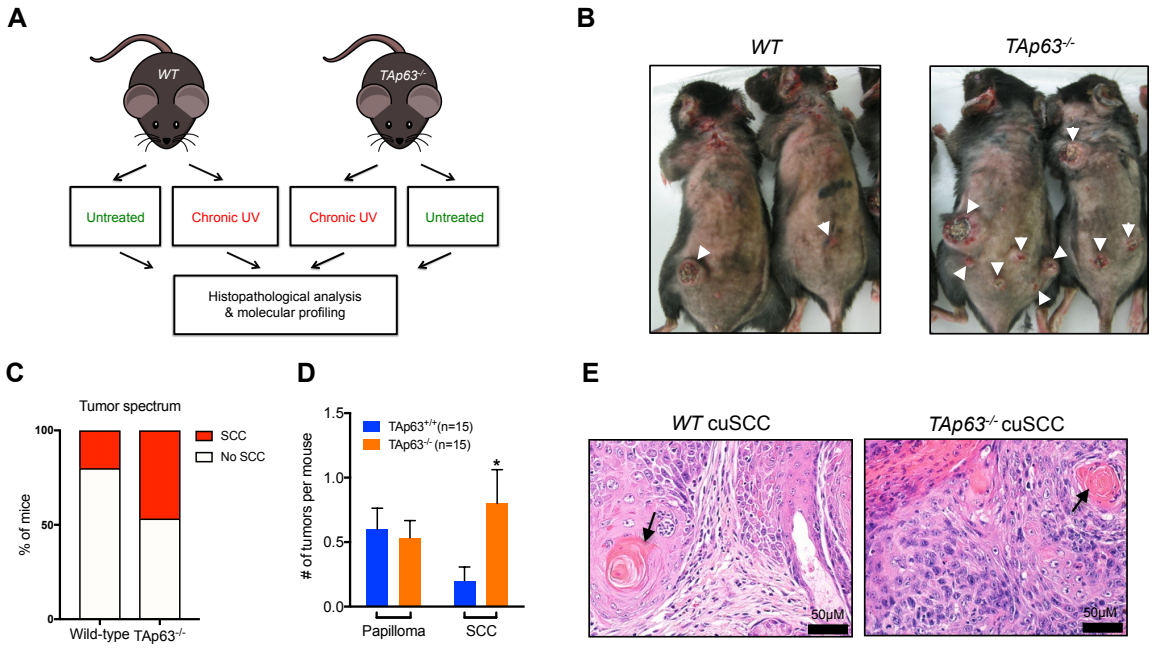

Figure 6: Loss of TAp63 promotes UVR-induced tumorigenesis. (A) *WT* and *TAp63*$^{-/-}$ mice were aged with or without chronic UVR (5kJ/m^2, 3x a week, for up to 60 weeks) and subsequently analyzed for tumor development. (B) Gross pathology images of chronically irradiated mice. White arrowheads indicate the presence of cuSCC tumors. (C) Quantification of the percentage of mice harboring histopathologically-verified cuSCC lesions for both genotypes. (D) The average number of pre-malignant papillomas and cuSCCs per mouse were quantified for each genotype. * $p<0.05$, two-tailed t test. (E) Representative H&E stainings of well-differentiated cuSCC tumors from the indicated genotypes. Keratin pearls (black arrow) indicate squamous differentiation.

3.2.2. Lineage tracing SOX2-positive stem cells during cuSCC development

Our laboratory previously demonstrated an essential role for TAp63 in preventing the hyperproliferation of a SOX2-positive stem cell population referred to as skin-derived precursors (SKPs) (14). In addition, recent studies in mice have shown that SOX2 plays a critical role in tumor initiation and tumor maintenance, and may function as a master regulator of cancer stemness (232, 233). Given the enhanced UVR-induced cuSCC phenotype of *TAp63*$^{-/-}$ mice, we asked whether SKPs may be a cell of origin for cutaneous SCC. To address this question we first immunostained *WT* and *TAp63*$^{-/-}$ skin and cuSCC for the expression of SOX2. As expected, SOX expression was limited to the dermal papilla (DP) and dermal sheath (DS) of anagen hair follicles (data not shown) (14). Consistent with previous reports however, we found that SOX2 was expressed in a small but significant fraction of both *WT* and *TAp63*$^{-/-}$ cuSCC tumors (Figure 7A). Notably, this expression was most frequently observed along the tumor-stroma interface, which has been shown to be highly enriched for cells with high tumor-initiating potential (234, 235). We did not however see a significant difference in the percentage of SOX2-positive cells across the two genotypes. These results suggest that our UVR-induced cuSCC model produces tumors that express SOX2, similar to what has been observed previously in chemically-induced mouse models of cuSCC (232, 233).

While previous studies have shown that SOX2-expressing cells have significantly increased tumor initiating potential, it remains to be determined if cuSCC tumors develop from a SOX2-expessing cell in the skin. Alternatively, it remains possible that cuSCC originates in a SOX2-negative cell (e.g. basal

keratinocytes) and acquires the capacity for de novo SOX2 expression during tumor progression. To definitively evaluate the capacity SOX2-positive skin cells to serve as cancer initiating cells, I have designed and initiated a lineage tracing experiment combined with our UVR-induced cuSCC model (Figure 7B). Mice bearing a tamoxifen-inducible CreER knocked into the SOX2 locus (*Sox2*$^{CreER/+}$) (212) were intercrossed with mice expressing a conditional fluorescent reporter (*Rosa*$^{mT/mG}$) (213). These mice were then intercrossed with mice harboring the TAp63 conditional knockout allele (14). This genetic strategy enables SOX2-specific recombination of the fluorescent reporter, thus permanently labeling cells originating from SOX2-specific cells in the skin (e.g. SKP cells). The presence or absence of the TAp63 conditional knockout allele also allows us to address whether or not the loss of TAp63, specifically in the SOX2-positive SKP cell compartment, accounts for the increased susceptibility of cuSCC development in *TAp63*$^{-/-}$ mice.

To verify specific recombination of the reporter allele in SOX2-positive SKP cells, mice bearing the above genotypes were treated at post-natal day 21 with topical 4-hydroxytamoxifen (4OHT) or ethanol for 3 consecutive days. As expected, nuclear SOX2 expression was detected in the nuclei of DP cells in anagen hair follicles (Figure 7D). Importantly, GFP expression was restricted to DP cells of *Sox2*$^{CreER/+}$*; TAp63*$^{fl/fl}$*; Rosa*$^{mT/mG}$ and *Sox2*$^{CreER/+}$*; TAp63*$^{+/+}$*; Rosa*$^{mT/mG}$ mice treated with 4OHT. Conversely, mice treated with ethanol, or *Sox2*$^{+/+}$*; Rosa*$^{mT/mG}$*; TAp63*$^{fl/fl}$ mice did not show GFP expression.

After verifying the efficiency and accuracy of the reporter strategy, we generated mice bearing the following genotypes: 1) *Sox2*$^{+/+}$*; Rosa*$^{mT/mG}$*; TAp63*$^{fl/fl}$ 2)

Sox2$^{CreER/+}$*; Rosa*$^{mT/mG}$*; TAp63*$^{+/+}$ and 3) *Sox2*$^{CreER/+}$*; Rosa*$^{mT/mG}$*; TAp63*$^{fl/fl}$ (Figure 7C). These mice were then treated at post-natal day 21 with topical 4-hydroxytamoxifen (4OHT) or ethanol for 3 consecutive days. On p24 or p25, the treated mice were subjected to chronic solar-simulated UVR-treatment (5kJ/m^2, 3x a week). As of the date of this publication, we have analyzed a subset of the irradiated cohort. Interestingly, we have detected multiple GFP-positive hair follicles in a *Sox2*$^{CreER/+}$*; Rosa*$^{mT/mG}$*; TAp63*$^{fl/fl}$ mouse after 43 weeks of irradiation (Figure 7E). We also identified a cuSCC tumor from this mouse that contained a significant population of SOX2-positive cells (Figure 7F and Figure 7G). This tumor was GFP-negative however, suggesting that it did not arise from a GFP-positive SKP cell. We are currently in the process of finishing these irradiations at which point we will fully analyze each tumor for SOX2 and GFP expression.

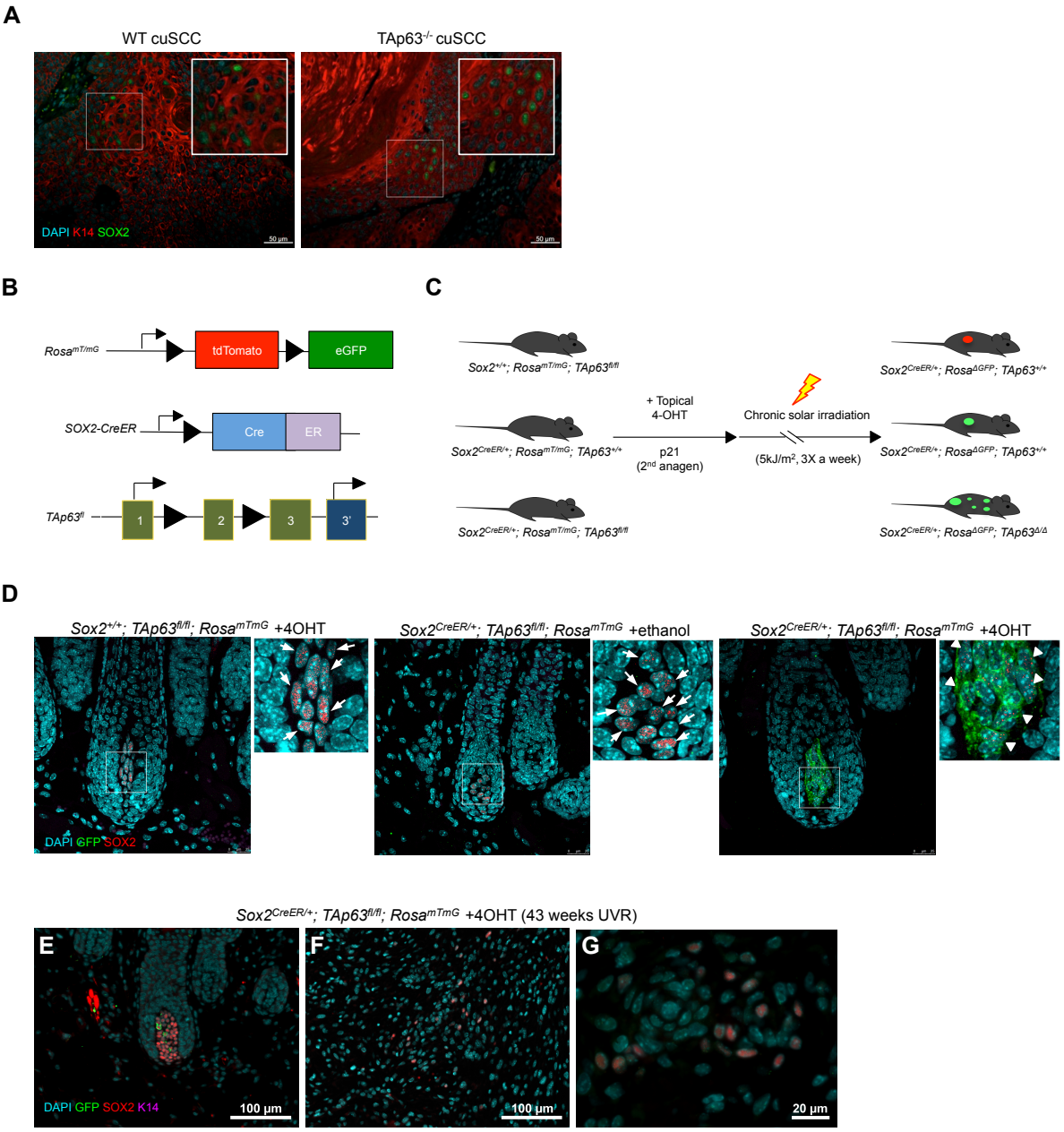

Figure 7: Lineage tracing SOX2-positive stem cells during cuSCC development. (A) Representative merged immunofluorescence images of *WT* and *TAp63*$^{-/-}$ murine cuSCC sections immunostained for K14 (red) and SOX2 (green), and counterstained with DAPI (cyan). (B) Alleles included in the lineage tracing experiment. The *Rosa*^{mTmG} allele harbors an inducible fluorescent reporter knocked into the Rosa26 locus. Unrecombined cells constitutively express tdTomato,

however following cre-mediated recombination, tdTomato and a stop codono are excised enabling expression of the GFP allele. The *SOX2-CreER* allele harbors cre recombinase conjugated to an estrogen-receptor domain (CreER), which requires the binding of tamoxifen to translocate into the nucleus, thus enabling recombination. Mice will also have WT TAp63, or the floxed TAp63 (TAp63fl) allele as shown. Cre-mediated recombination of this allele deletes exon 2, and therefore the expression of TAp63 isoforms. (C) Experimental design for the lineage tracing experiment. Mice bearing the indicated genotypes, were treated with 1mg 4OHT for 3 consecutive days. On the fourth day, these mice were subjected to chronic UVR treatment, 3x per week, and analyzed for intratumoral expression of GFP or tdTomato. (D-F) Representative confocal microscopy images of longitudinal sections of mouse hair follicles from P24 mice with the indicated genotypes following 3 consecutive days of 200ul with vehicle (ethanol) or 5mg/ml 4-hydroxytamoxifen (4OHT). SOX2 expression is restricted to the cells in the dermal papilla (DP) (red). GFP expression (green) is restricted to SOX2-expressing cells in $SOX2^{CreER/+}$; $TAp63^{fl/fl}$; $Rosa^{mT/mG}$ mice treated with 4OHT. Right panels show SOX2-positive (red, arrows) and EGFP-positive (green, arrowheads) DP cells at higher magnification. (E-G) Representative merged immunofluorescence images of skin (E) and tumor sections (F and G) from $Sox2^{CreER/+}$; $TAp63^{fl/fl}$; $Rosa^{mTmG}$ mice treated with 4OHT, followed by 43 weeks of UVR exposure. Sections were immunostained for K14 (magenta), GFP (green), and SOX2 (red), and counterstained with DAPI (cyan).

3.2.3. TAp63-deficient tumors exhibit deregulated mRNA and miRNA expression

Since TAp63 has been implicated in miRNA biogenesis (147), we asked whether the increase in cuSCC development was due to the dysregulation of miRNA expression in the skin. To answer this question, we performed RNA-seq and small RNA-seq on skin and histologically verifiable cuSCC lesions from both *WT* and *TAp63*$^{-/-}$ irradiated mice. In total, 3 *WT* normal skin, 3 *TAp63*$^{-/-}$ normal skin, 2 *WT* cuSCC tumors, and 3 *TAp63*$^{-/-}$ cuSCC tumor samples were sequenced and analyzed. Principal component analysis (PCA) of samples based on the differentially expressed mRNAs (Figure 8A) showed that the global expression pattern distinguished skin from cuSCC samples. Moreover, we found that the samples within each tissue type grouped according to genotype, indicating that the loss of TAp63 may have global effects on the transcriptional landscape of normal skin and cuSCC. Unsupervised hierarchical clustering of mRNAs (Figure 9A) and miRNAs (Figure 9B) also showed clustering of normal skin and cuSCC samples, however the samples did not perfectly segregate according to genotype within each tissue type. Taken together these results suggest that the loss of TAp63 affects a significant proportion of the cuSCC transcriptome.

To identify TAp63-regulated mRNAs and miRNA networks, we generated *a TAp63*$^{-/-}$ cuSCC signature from the mRNA (Figure 8B) and miRNA (Figure 8C) expression datasets (fold change > 1.5, p-value <0.05). To identify those targets that are dependent on TAp63, we focused on genes and miRNAs that were differentially expressed in the *TAp63*$^{-/-}$ cuSCC signatures but were not similarly affected in *WT*

cuSCC (Figure 8D, blue). From this comparison we identified 1993 mRNA and 90 miRNAs that were differentially expressed in the *TAp63*$^{-/-}$ cuSCC signature.

In order to examine the possibility that TAp63-regulated miRNAs are functional in the pathogenesis of cuSCC, we performed miRNA-mRNA pair analysis by identifying differentially expressed miRNAs that complement miRNA response elements (MREs) within the 3' UTR of significantly anti-correlated mRNAs via Watson-Crick base pairing (222, 236). Functional pairs were identified within the *TAp63*$^{-/-}$ SCC signature and integrated network maps were generated to identify key miRNA-mRNA pairs that were associated with loss of TAp63 in cuSCC (Figure 10 and Figure 11). Altogether, the *TAp63*$^{-/-}$ cuSCC signature contained 28 underexpressed miRNAs with 311 overexpressed mRNAs (Figure 10), and 25 overexpressed miRNAs with 333 underexpressed mRNAs (Figure 11).

To determine if any of the TAp63-associated miRNAs and mRNAs are conserved in human cuSCC, we compared the *TAp63*$^{-/-}$ cuSCC signature to previously published human cuSCC mRNA and miRNA signatures generated from 9 cuSCC and 7 normal skin samples obtained from human patients (72) (Figure 8D). This comparison identified 263 mRNAs (93 upregulated, 170 downregulated) and 13 miRNAs (8 upregulated, 5 downregulated) (Appendix 3) that were differentially expressed in both mouse *TAp63*$^{-/-}$ cuSCC and human cuSCC. Gene set enrichment analysis (GSEA) revealed significant deregulation of genes in pathways related to the regulation of cell proliferation and cell death (Figure 8E). Both of these processes are identified as hallmarks of human cancer (237, 238). Moreover, previous studies have demonstrated that TAp63 is a transcriptional regulator of

protein coding genes involved in these two processes (2, 14, 24), and that this regulation is a major component of the tumor suppressive functions of TAp63. Prior to this study, however the role of TAp63-regulated miRNAs in these two processes remained unexplored. Interestingly, several of the miRNAs that were found to be overexpressed in this analysis have been previously implicated in the pathogenesis of cuSCC, including miRs-15b, 17, and 27b (72, 150, 152, 239). Conversely, several miRNAs that were underexpressed, including miRs-30c-2* and 497, were found to be frequently reduced in cuSCC and found to exhibit tumor suppressive functions (72, 150). Despite the implication of these miRNAs in cuSCC, the specific identities of the most significant mRNA targets and their functions remain to be characterized.

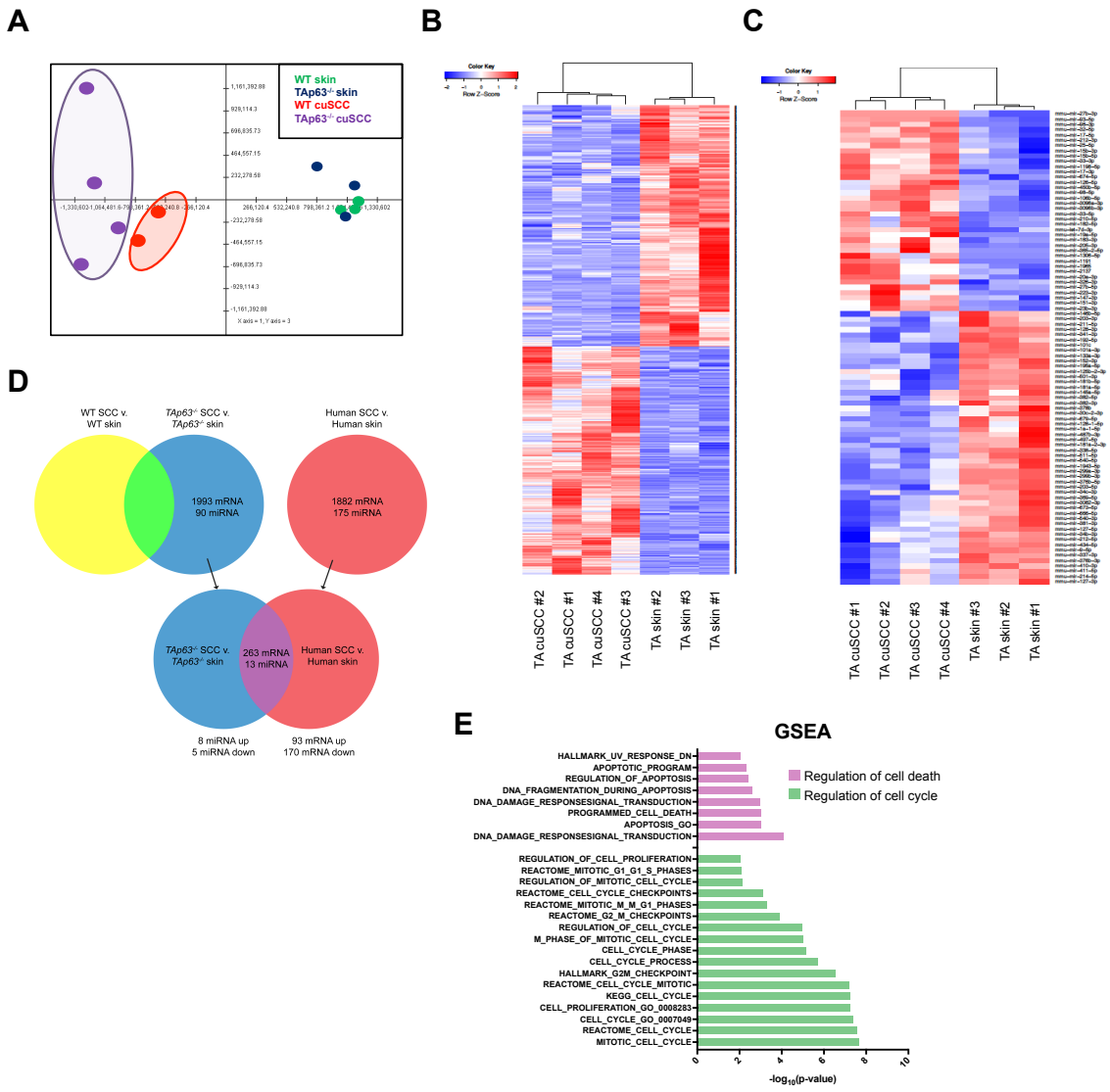

Figure 8: TAp63-deficient tumors exhibit deregulated mRNA and miRNA expression. (A) Principal component analysis (PCA) plot of global mRNA expression in murine WT and TAp63$^{-/-}$ skin and cuSCC (3 WT normal skin, 3 TAp63$^{-/-}$ normal skin, 2 WT cuSCC tumors, and 3 TAp63$^{-/-}$ cuSCC tumors). (B and C) Hierarchical clustering analysis based on differentially expressed mRNAs (B) and miRNAs (C) in TAp63$^{-/-}$ cuSCC tumors vs. TAp63$^{-/-}$ normal skin samples. Each row represents a single mRNA or miRNA, while each column represents a sample. The

Pearson correlation matrix is shown on top. The color scale shown in the map illustrates the relative expression levels of mRNAs and miRNAs across each sample. Blue shades correspond to reduced expression and red shades represent increased expression levels. (D) Comparison of the TAp63$^{-/-}$ cuSCC signature and human cuSCC identified similar differential expression of the indicated number of miRNAs and mRNAs. (E) GSEA Analysis of the overlapping targets (purple) identified in (D).

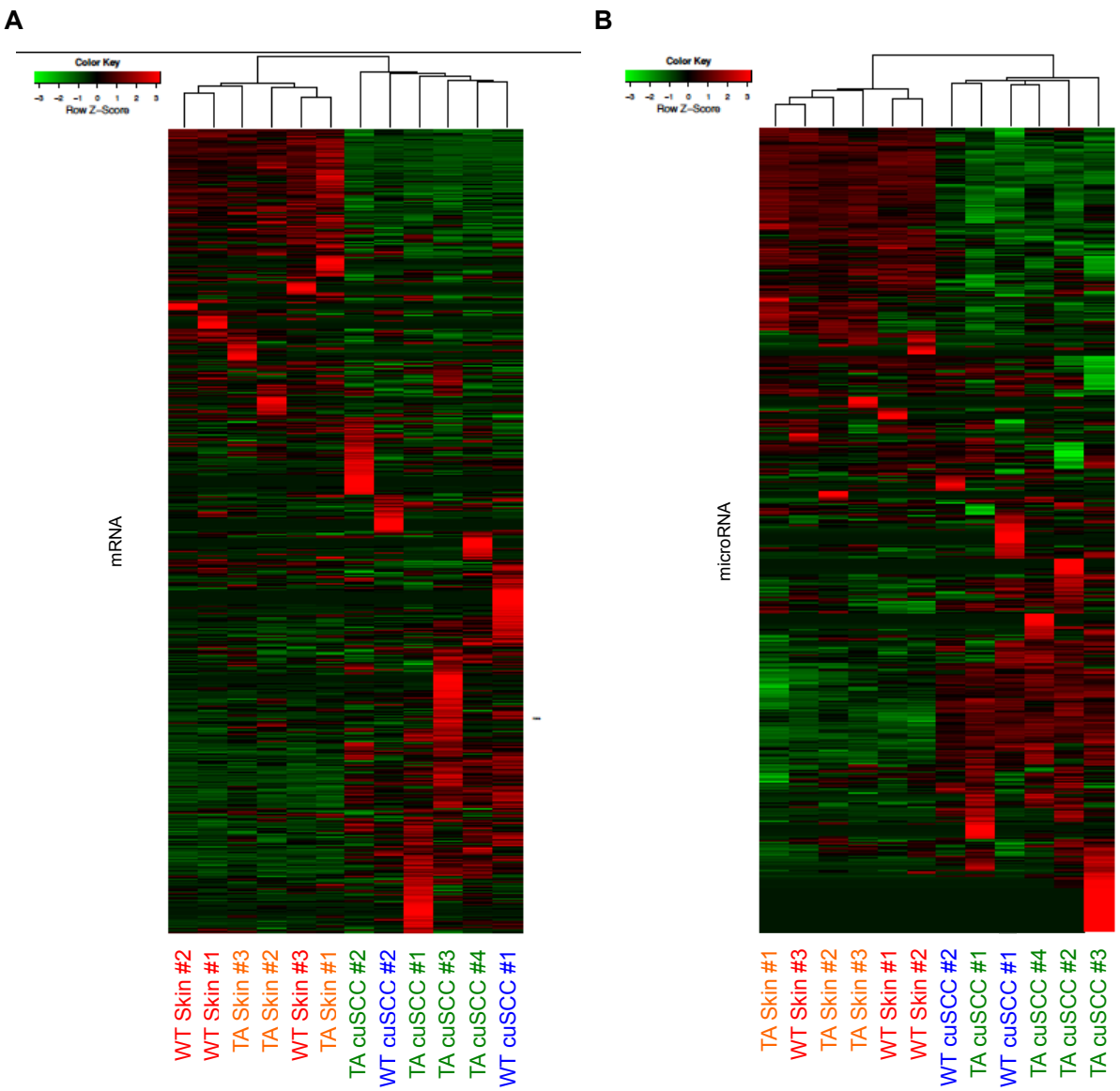

Figure 9: mRNA and miRNA profiling of WT and TAp63$^{-/-}$ skin and cuSCC. Unsupervised hierarchical clustering analysis based on differentially expressed mRNAs (A) and miRNAs (B) in WT and TAp63$^{-/-}$ skin and cuSCC. Each row represents a single mRNA or miRNA, while each column represents a sample. The Pearson correlation matrix is shown on top. The color scale shown in the map illustrates the relative expression levels of mRNAs and miRNAs across each

sample. Green shades correspond to reduced expression and red shades represent increased expression levels.

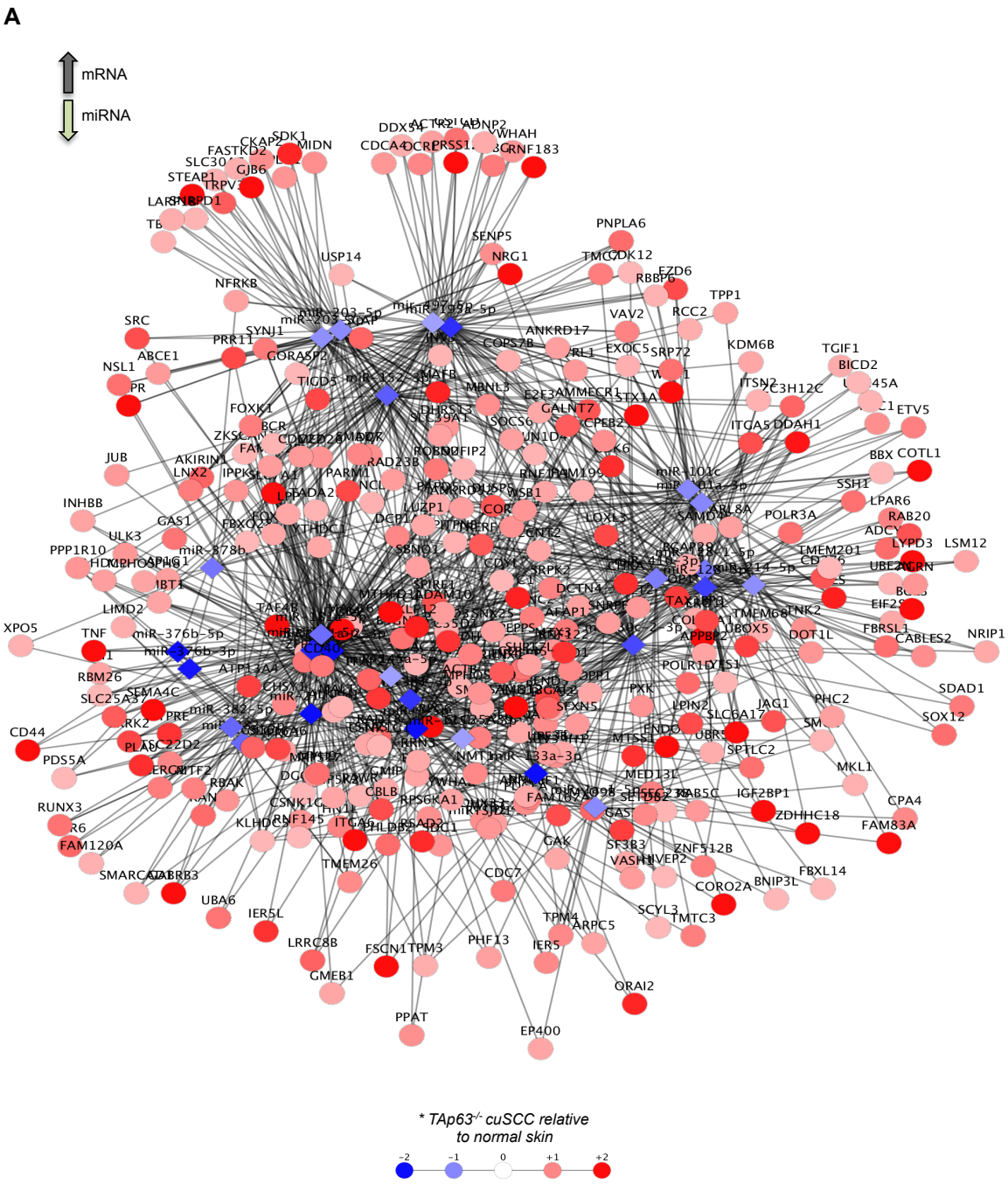

Figure 10: Functional pair analysis identifies TAp63-associated miRNA-mRNA regulatory networks in cuSCC. (A) Underexpressed miRNAs with predicted mRNAs that are overexpressed in the TAp63$^{-/-}$ cuSCC signature.

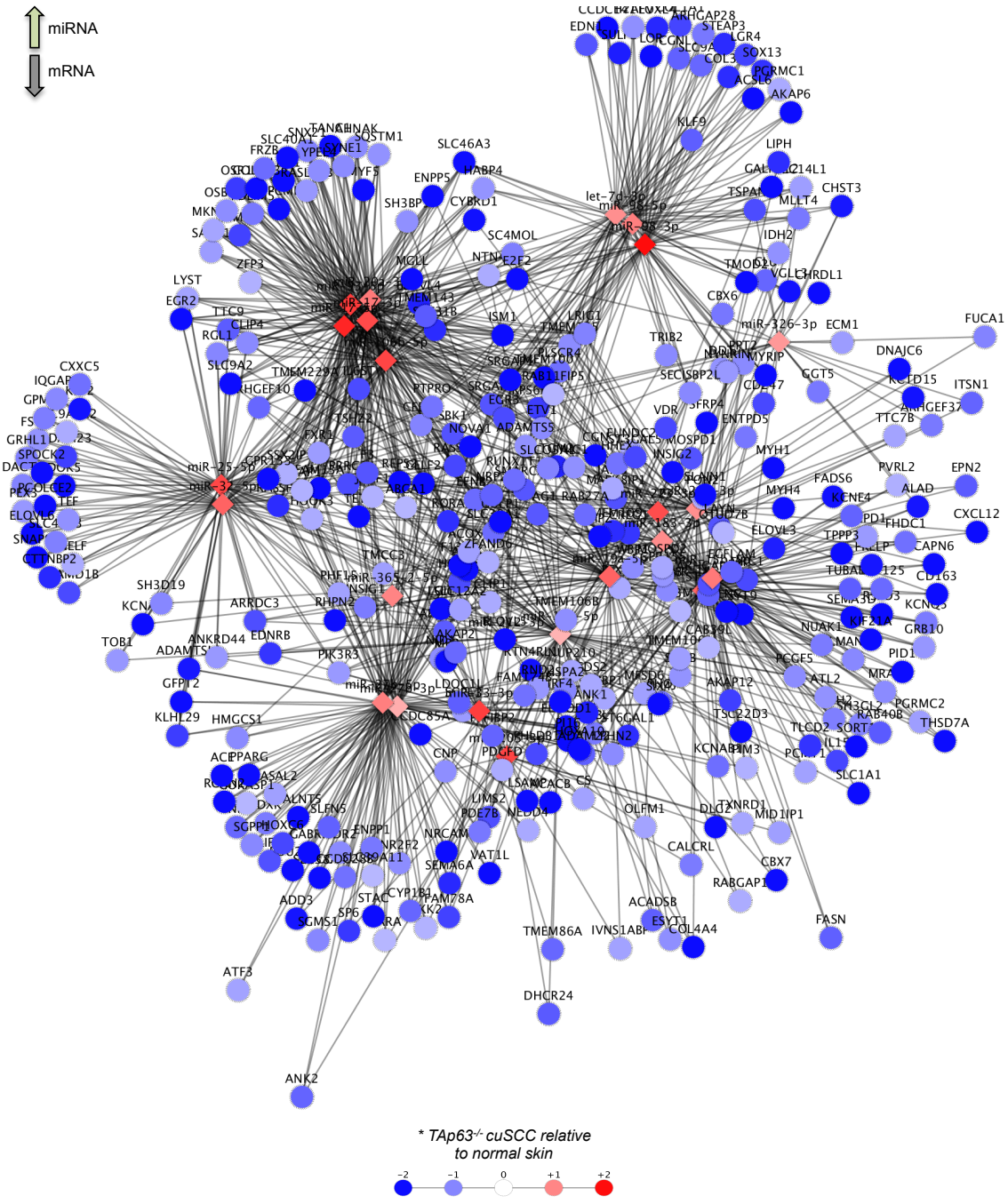

Figure 11: Functional pair analysis identifies TAp63-associated miRNA-mRNA regulatory networks in cuSCC. Overexpressed miRNAs with predicted mRNAs that are underexpressed in the TAp63$^{-/-}$ cuSCC signature.

3.2.4. TAp63-regulated miR-30c-2* and miR-497 suppresses cuSCC through induction of cell death and cell cycle arrest

We utilized Taqman qRT-PCR to validate the differential expression of the TAp63-associated miRNAs in *TAp63*$^{-/-}$ cuSCC compared to normal skin. Using these assays, we were able to validate the significantly increased expression of miR-17* and reduced expression of miR-30c-2* and miR-497 in murine *TAp63*$^{-/-}$ cuSCC (Figure 12A-C). We then profiled the expression of these miRNAs in 2 human cuSCC cell lines (COLO16 and SRB12) and compared it to their expression in normal human epidermal keratinocytes (NHEKs), which are believed to be the cell of origin for cuSCC (Figure 12D). As expected, we found that miR-30c-2* was underexpressed in both cell lines, while miR-497 was significantly reduced in COLO16 cells. In parallel, we also examined the expression of TAp63 and Dicer in these cell lines and found that they are both significantly underexpressed when compared to NHEKs (Figure 12E). Taken together, these results suggest that the reduced expression of TAp63 and Dicer is associated with reduced expression of miR-30c-2* and miR-497.

To further probe the interaction between TAp63, miR-30c-2* and miR-497 in cuSCC, we used short interfering RNA (siRNA) to knockdown TAp63 in NHEKs (Figure 12F). Knockdown of TAp63 resulted in diminished expression of miR-30c-2* (Figure 12H) and miR-497 (Figure 12I), supporting a model in which TAp63 positively regulates the expression of these miRNAs. To determine the mechanism through which TAp63 may regulate these miRNAs, we examined the expression of the primary transcripts that encode the mature forms of miR-30c-2* and miR-497.

While pri-miR-30c-2 was significantly reduced (Figure 12J), pri-miR-497 expression was increased upon knockdown of TAp63 (Figure 12K). These results suggest that TAp63 may promote miR-30c-2* expression through direct transcriptional activation of its precursor transcript. Indeed the promoter of the host gene encoding miR-30c-2* contains 2 predicted p63 binding sites (data not shown). Chromatin immunoprecipitation quantitative PCR (ChIP-qPCR) however failed to show p63 binding to either region (data not shown). These results suggest that TAp63 may regulate miR-30c-2* and miR-497 through an indirect mechanism. In line with previous observations, downregulation of TAp63 resulted in a significant reduction in *Dicer* mRNA expression (Figure 12G). To determine if this loss of *Dicer* expression is responsible for the diminished miR-30c-2* and miR-497 expression following the downregulation of TAp63, we transfected NHEKs with siRNAs targeting *Dicer* (Figure 12L). Downregulation of *Dicer* resulted in significant reductions of miR-30c-2* (Figure 12M) and miR-497 (Figure 12N) expression, similar to what is observed upon TAp63 knockdown. These observations suggest that TAp63 may regulate both miR-30c-2* and miR-497 through positive regulation of Dicer-mediated miRNA biogenesis.

To test the putative anti-tumor effects of miR-30c-2* and miR-497 we transfected chemically modified miRNA mimics into the human cuSCC cell lines COLO16 and SRB12 and analyzed cell growth. We found that both miR-30c-2* and miR-497 significantly inhibited proliferation of COLO16 (Figure 13A) and SRB12 (Figure 13B) cells when compared to a scrambled control mimic. To further dissect the anti-proliferative effects of these miRNAs, we assayed transfected cuSCC cells

for DNA synthesis, apoptosis, and cell cycle profiling. We found that miR-30c-2* led to a significant reduction in Edu incorporation, indicating decreased DNA synthesis (Figure 13D and Figure 13F). We also saw an even more striking induction of apoptosis in miR-30c-2*-transfected cells, as evidenced by increased annexin V staining (Figure 13C Figure 13E). Likewise, miR-497-transfected cells showed an even more significant reduction in DNA synthesis, as evidenced by a nearly 5-fold reduction in Edu incorporation (Figure 13D and Figure 13F). miR-497-transfected cell did not however show increased apoptosis (Figure 13C Figure 13E), as had been previously reported in breast cancer cells (240). Instead, cell cycle profiling demonstrated that miR-497-transfected cells exhibited a striking increase in the percentage of cells in G1, which is indicative of G1/S arrest (Figure 13G and Figure 13AH), and is in accordance with previous studies of miR-497 function in other cancer cell types (240-242). Alternatively, miR-30c-2*-transfected cells were found to have a slight, non-significant increase in the percentage of cells in G2 (Figure 13G and Figure 13H). Taken together these results suggest that miR-30c-2* and miR-497 suppress cuSCC cell growth through the induction of cell death and cell cycle arrest, respectively.

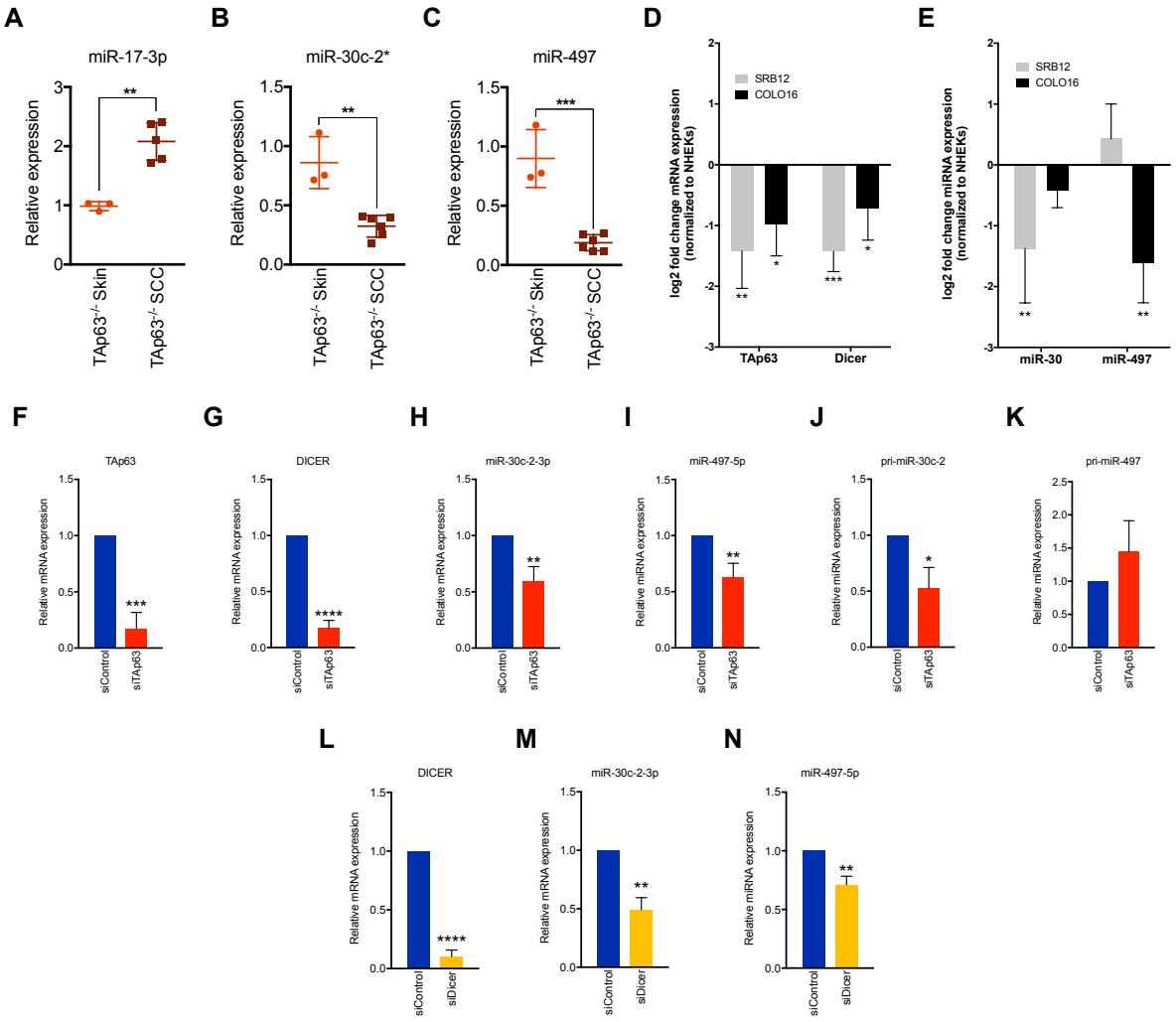

Figure 12: TAp63 promotes miR-30c-2* and miR-497 expression through Dicer. (A-C) Taqman qRTPCR of miR-17* (A), miR-30c-2* (B) and miR-497 (C) in TAp63$^{-/-}$ skin and cuSCC samples. (D) SYBR green qRT-PCR of TAp63 and DICER in human cuSCC cell lines SRB12 and COLO16. (E) Taqman qRTPCR of miR-30c-2* and miR-497 in human cuSCC cell lines SRB12 and COLO16. (F-G) SYBR green qRTPCR of TAp63 (F) and Dicer (G) in NHEKs following transfection with the indicated siRNAs. (H-K) Taqman qRTPCR of miR-30c-2* (H), miR-497-5p (I), pri-miR-30c-2 (J), and pri-miR-497 (K) in NHEKs following transfection with the indicated siRNAs. (L) SYBR green qRTPCR of Dicer in NHEKs following transfection

with the indicated siRNAs. (M and N) Taqman qRTPCR of miR-30c-2-3p (M) and miR-497-5p (N) in NHEKs following transfection with the indicated siRNAs. Data shown are mean ± SD, n=3. * $p<0.05$, ** $p<0.01$, *** $p<0.001$, **** $p<0.0001$ two-tailed t test.

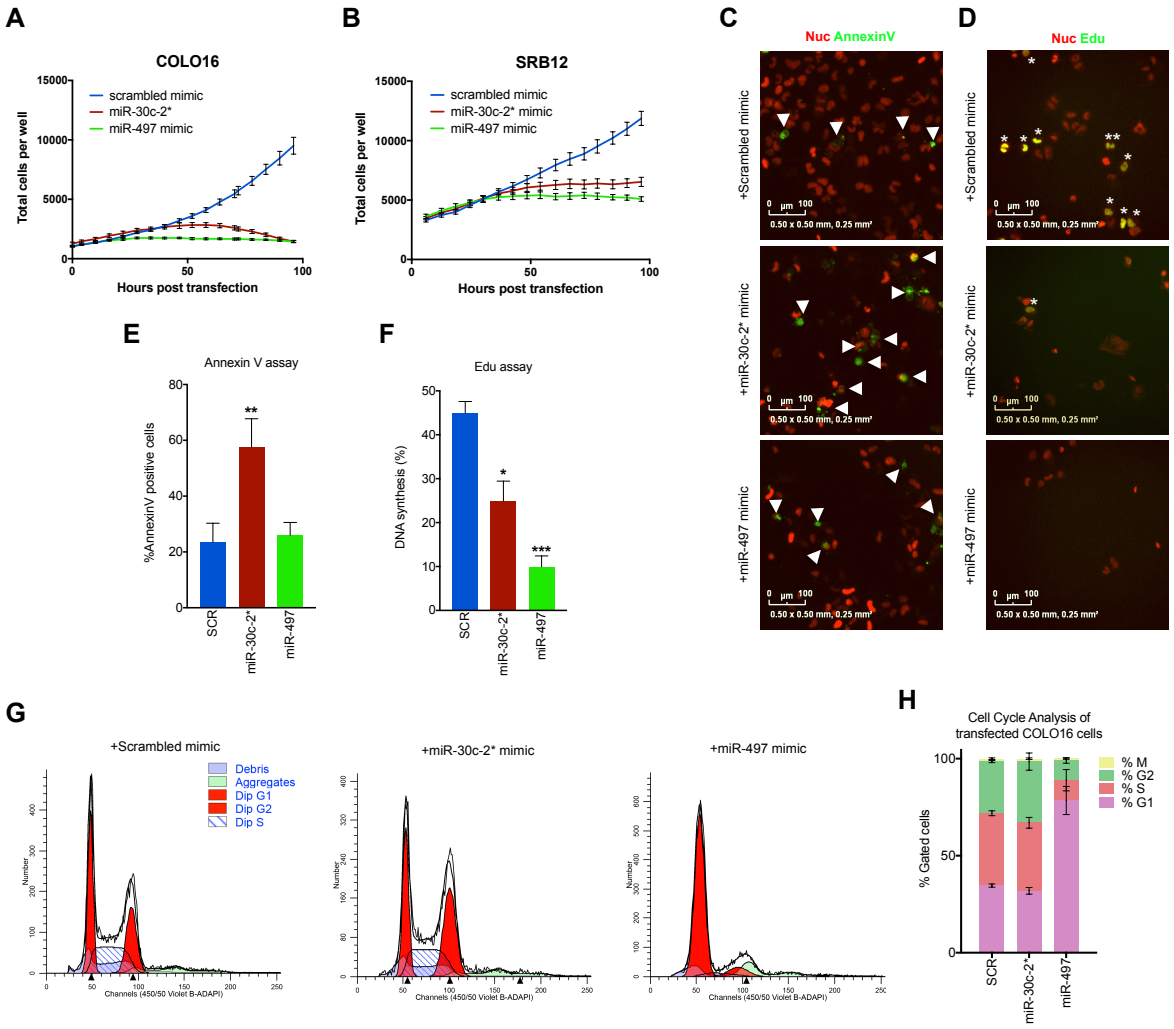

Figure 13: TAp63-regulated miR-30c-2* and miR-497-5p suppresses cuSCC through induction of cell death and cell cycle arrest. (A and B) Representative growth curve of nucRed-mCherry-labeled COLO16 (A) and SRB12 (B) cells transfected with the indicated miRNA mimics. (C and E) Immunofluorescence (C) and quantification (E) for Annexin V-488 (green)-positive COLO16 cells transfected with the indicated miRNA mimics. (D and F) Immunofluorescence (D) images and quantification (F) for Edu (green) incorporation in COLO16 cells transfected with the indicated miRNA mimics following a 3 hour Edu pulse. NucRed® dead 647 (red) was

used as a counterstain (G and H) Cell cycle profiles (G) and quantification (H) of COLO16 cells 48 hours after transfection with the indicated miRNA mimic as measured by FACS analysis. M phase was measured as the percentage of cells staining positive for Histone H3-pS28-AF647. Data shown are mean ± SD, n=3, unless noted otherwise. * $p<0.05$, ** $p<0.01$, ***$p<0.001$, two-tailed t test.

3.2.5. miR-30c-2* and miR-497 suppress cuSCC growth in vivo

To extend these observations to an in vivo setting, we generated COLO16 cells that stably express an RFP-luciferase reporter. These cells were then transfected with mimics of miR-30c-2*, miR-497, or negative control, and subsequently xenografted into athymic nu/nu mice (Figure 14A). In accordance with our in vitro observations, transfection of miR-30c-2* or miR-497 almost completely abolished the tumor growth of COLO16 cells compared to controls (Figure 14B-E). Collectively, these observations suggest that miR-30c-2* and miR-497 suppress cuSCC tumor growth in vivo.

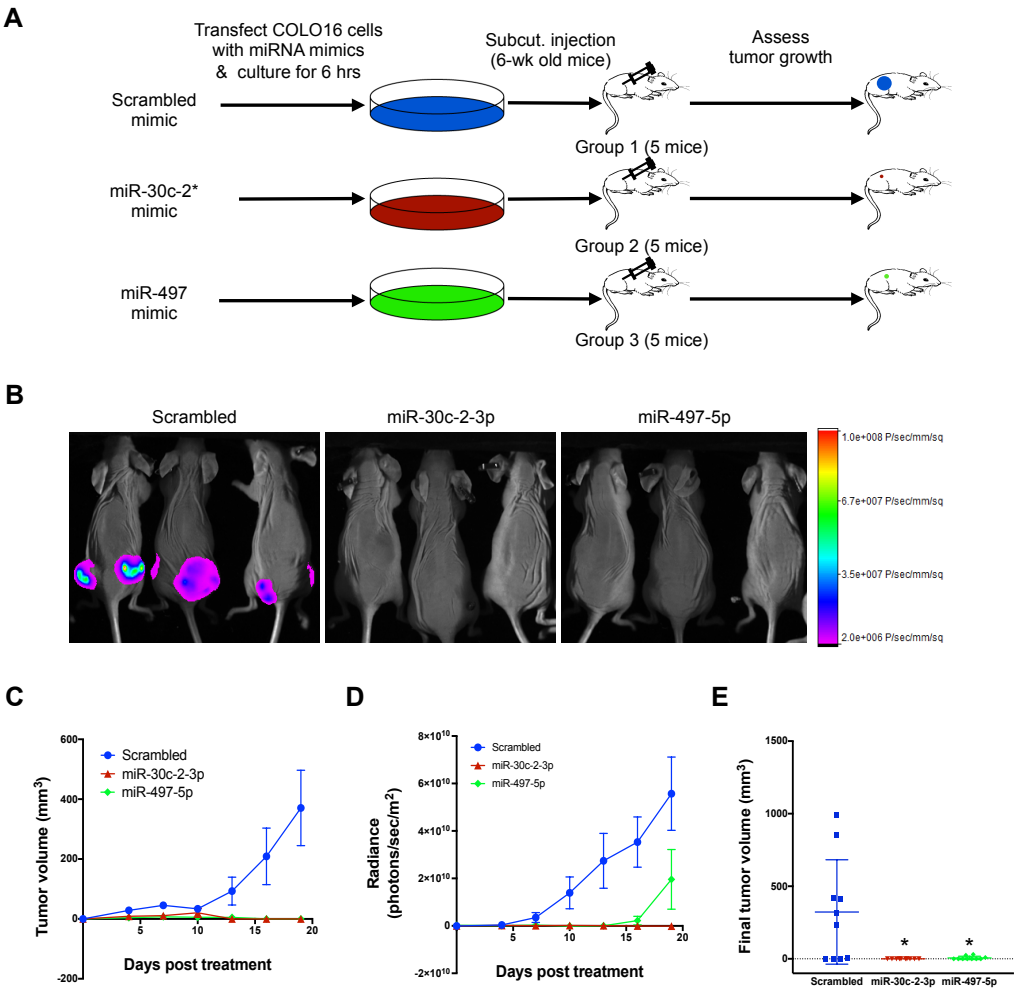

Figure 14: miR-30c-2* and miR-497 suppress cuSCC growth in vivo. (A) COLO16 cells stably expressing RFP and luciferase were transfected with the indicated miRNA mimics and subcutaneously injected into both flanks of athymic nu/nu mice. (B) Representative images of mice injected with COLO16 cells transfected with scrambled, miR-30c-2-3p, and miR-497-5p miRNA mimics on Day 19 prior to tumor harvest. (C-D) Tumor volume was assessed was assessed using caliper measurements (C) and luminescence imaging (D). (E) Quantification of extracted tumor volumes. Data shown are mean ± SEM, n=10.

3.2.6. Intravenous injection of miRNA mimics fails to inhibit growth of cuSCC xenografts.

Next, we assessed whether intravenous delivery of miR-30c-2* and miR-497 miRNA mimics showed anti-tumor effects in the COLO16 cuSCC xenograft model. Tumor-bearing athymic nu/nu mice were treated with intravenous injections of either miR-30c-2*, miR-497, or scrambled mimics complexed with *in vivo*-jetPEI® reagent, 3 times per week. Compared to the scrambled control, neither miR-30c-2*, nor miR-497 had a significant effect on tumor growth (Figure 15A). To determine if this lack of a tumor response was due to inadequate intratumoral delivery of the miRNA mimics, I performed Taqman qRT-PCR to assay the expression of either miRNA in the corresponding tumors and organs of the mimic-injected mice. Surprisingly, there was only a modest increase in the amount of miR-30c-2* present in the tumors of the miR-30c-2* mice relative to scrambled mimic injected mice (Figure 15B). In contrast, miR-497 injected mice showed no significant increase in miR-497 compared to control (Figure 15C). Notably, the amount of miR-30c-2* and miR-497 were increased dramatically in the livers of miR-30c-2* and miR-497-injected mice, respectively (Figure 15B and Figure 15C). Attempts to increase the dosage of miRNA mimic resulted in significant toxicity and caused lethality in mice, presumably due to the preferential accumulation in the liver versus tumor (data not shown). Taken together, these results indicate that the *in vivo*-jetPEI® reagent failed to adequately deliver the miRNA mimics to the xenograft tumors, and precluded the possibility to investigate their therapeutic potential.

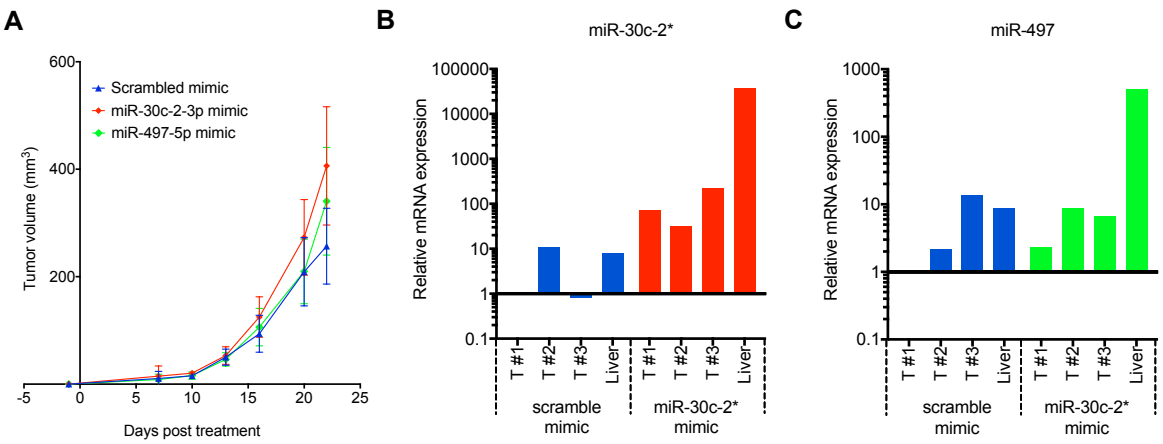

Figure 15: Intravenous injection of miRNA mimics fails to inhibit growth of cuSCC xenografts. (A) COLO16 cells stably expressing RFP were subcutaneously injected into both flanks of athymic nu/nu mice. Mice with palpable tumors were treated three times per week with intravenous injections of 2.5mg/kg of the indicated miRNA mimic in complex with the *in vivo*-jetPEI® reagent. Tumor volume was assessed was assessed using caliper measurements. Data shown are mean ± SEM, n=12. (B) Taqman qRT-PCR for miR-30c-2* (B) and miR-497 (C) in tumors and liver tissues isolated from mice injected with the indicated miRNA mimics. Data shown are normalized expression in individual tumors and liver tissues (normalized to scambled mimic tumor #1).

3.2.7. Cross-platform analysis identifies multiple direct mRNA targets for miR-30c-2* and miR-497

The ultimate consequence of miRNA function is the translational inhibition of the mRNAs that it targets. Therefore, to study the regulatory functions of miR-30c-2* and miR-497, we employed a quantitative mass spectrometry-based approach to measure global protein expression following overexpression of either miRNA (Figure 17A). COLO16 cells were transfected with miR-30c-2*, miR-497 or scrambled control mimics and collected 48 hours later. Cell lysates were alkylated and subjected to tryptic digestion, followed by Tandem mass tag (TMT) labeling. Peptides were then identified via LC-MS/MS and proteins that were quantified by at least 2 unique peptides were selected for further analysis. Differential protein expression was determined as the relative protein ratio of the differentially labeled peptide fractions in each mimic transfected sample compared to the scrambled mimic control.

A total of 1751 proteins were differentially expressed based on an absolute fold change greater than 1.5 in the miR-30c-2*-transfected sample relative to the scrambled mimic-transfected sample (Figure 17B). Among these proteins, 361 were underexpressed, while 1390 proteins were increased relative to control-transfected cells. Alternatively, 587 proteins were differentially expressed in the miR-497-transfected sample relative to control with 275 proteins being underexpressed, and 312 proteins were overexpressed (Figure 17C). Notably, we did not see reduced expression for any of the previously published targets of miR-30c-2* as being significantly reduced in the miR-30c-2* transfected cells. Likewise, we only found

two previously published targets of miR-497 (ANLN and CDK6) as being significantly underexpressed in the miR-497 comparison (243, 244). The discordance between our proteomics data and the previously identifed targets of miR-30c-2* and miR-497 suggest that the targets of a given miRNA may differ, according to the specific cellular and physiological context. As a result, the data generated in this study may reveal previously unidentified targets of miR-30c-2* and miR-497 that are functionally relevant to the pathogenesis of cuSCC.

Ingenuity pathway analysis (IPA) was performed to identify the significantly enriched canonical pathways among the underexpressed proteins in both comparisons. Interestingly, the proteins that were underexpressed in the miR-30c-2*-transfected cells were significantly enriched for pathways related to ErbB signaling, including Agrin Interactions at Neuromuscular Junction, Neuregulin Signaling, and ErbB2-ErbB3 Signaling (Figure 16A). Alternatively, the top pathway enriched in the underexpressed proteins in the miR-497 comparison was Mitotic Roles of Polo-like kinase (Figure 16B). Each of these pathways exhibited a negative z-score, indicating that the activity of the pathways are predicted to be reduced in the miRNA mimic transfected cells, which is corroborated by our phenotypic assays. Taken together these results indicate that the global proteomics changes identified by this method accurately reflect the phenotypic changes observed following the overexpression of the corresponding miRNA.

Given that miRNAs function to inhibit protein translation, it was surprising to see such a large percentage of proteins exhibiting an increase in expression following miR-30c-2* overexpression. This, however may be due to the increased

fraction of miR-30c-2* transfected cells in the G2 phase of the cell cycle, which is typically characterized by increased protein synthesis which prepares the cell for mitosis and cell division (Figure 13H). To test this hypothesis, we performed Ingenuity Pathway Analysis on the overexpressed proteins in the miR-30c-2* vs. scrambled control comparison (fold change > 1.5) (Figure 16C). This analysis showed enrichment for pathways related to protein synthesis, including EIF2 signaling, as well as enrichment for pathways related to cell growth and division, including Actin Cytoskeleton, Integrin Signaling, and RhoA signaling. These results suggest that miR-30c-2* expression induces a G2/M arrest.

To determine if the measured protein expression changes reflect direct regulatory effects of miR-30c-2* and miR-497, we profiled the corresponding mRNA for each of the differentially expressed proteins in each comparison for the presence of miRNA response elements (MREs) for the respective miRNA utilizing the miRwalk 2.0 software (245). This software allowed us to leverage 4 different miRNA target prediction algorithms, including miRwalk, miRanda (125), Targetscan (246), and RNA22 (247). From this analysis, we found that 243 of the 361 (67.3%) underexpressed proteins harbored a predicted MRE for miR-30c-2*. Unexpectedly, we found that 875 of the 1390 (62.9%) overexpressed proteins harbored a predicted MRE for miR-30c-2*, indicating that there was not a significant enrichment for the presence of predicted MREs in the underexpressed fraction, as was expected. Likewise, among the differentially expressed proteins following miR-497 overexpression, we found 160 of the 275 underexpressed proteins (58.18%) and 171 of the 312 overexpressed proteins (54.81%) to have predicted MREs for miR-

497. Interestingly, these analyses failed to show a significant enrichment for predicted MREs among the underexpressed proteins.

To prioritize targets for further validation, we compared the list of underexpressed proteins (fold change < 0.67) in the miR-30c-2* (Figure 17D) and miR-497 (Figure 17E) proteomics signatures against the mRNAs that were conversely overexpressed (fold change > 1.5, $p < 0.05$) in both the mouse TAp63$^{-/-}$ cuSCC and human cuSCC RNA-seq signatures. We then examined both lists of mRNAs for the presence of at least one MRE to focus our studies on likely targets of either miRNA. From this analysis we found 5 putative targets of miR-30c-2* (FAT2, ITGA6, KIF18B, ORC1, and PKMYT1) and 4 predicted targets of miR-497 (AURKA, CDK6, KIF18B, and PKMYT1) that are frequently overexpressed in both mouse TAp63$^{-/-}$ and human cuSCC. Interestingly, both miRNAs are predicted to target KIF18B and PKMYT1. We validated the LC-MS/MS observations for all 7 of the putative targets by Western blotting (Figure 17F-H). Interestingly, only AURKA and CDK6 appeared to be significantly reduced at the RNA level following overexpression of miR-497, whereas none of the miR-30c-2* targets were affected (Figure 17I and Figure 17J). These results confirm that all 7 targets are significantly downregulated following overexpression of the corresponding miR and suggest that they may be directly inhibited via miRNA-mRNA mediated targeting.

To determine if the putative targets of either miRNA are repressed via RISC-mediated miRNA-mRNA interaction we transfected COLO16 cells with miRNA mimics biotinylated at the 3'-end of the mature strand (bi-miR-30c-2*, bi-miR-497, or bi-scrambled). We then performed streptavidin pull-downs and performed qRT-PCR

for each of the putative targets of miR-30c-2* and miR-497, as well as GAPDH for normalization purposes (248). Relative mRNA abundance in the streptavidin pull-downs and inputs in the bi-miR-30c-2*- and bi-miR497-transfected cells were separately normalized to their levels in cells transfected with a biotinylated scrambled mimic (bi-scrambled). The putative miR-30c-2* targets FAT2, ORC1, KIF18B, and PKMYT1 were significantly enriched in the bi-miR-30c-2* pull-down (Figure 17K). While not significant, enrichment for ITGA6 trended towards significance. Similarly, all 4 putative targets of miR-497 (AURKA, CDK6, KIF18B, and PKMYT1) were enriched in the bi-miR-497 pull-down (Figure 17L). Taken together, these results suggest that FAT2, ITGA6, ORC1, KIF18B and PKMYT1 appear to be novel direct targets of miR-30c-2*, while AURKA, CDK6, KIF18B, and PKMYT1 seem to be bona fide targets of miR-497.

A

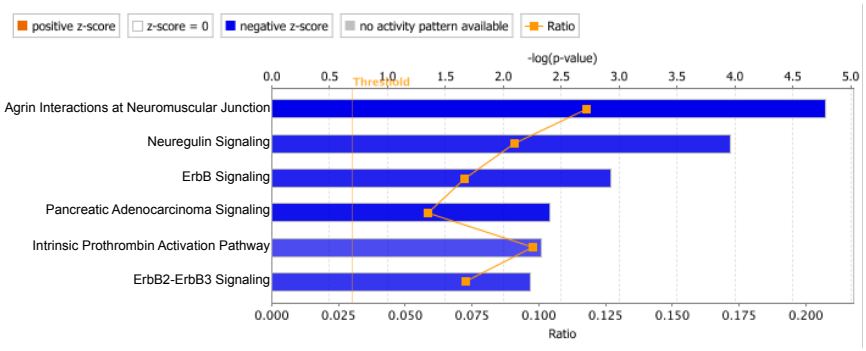

B

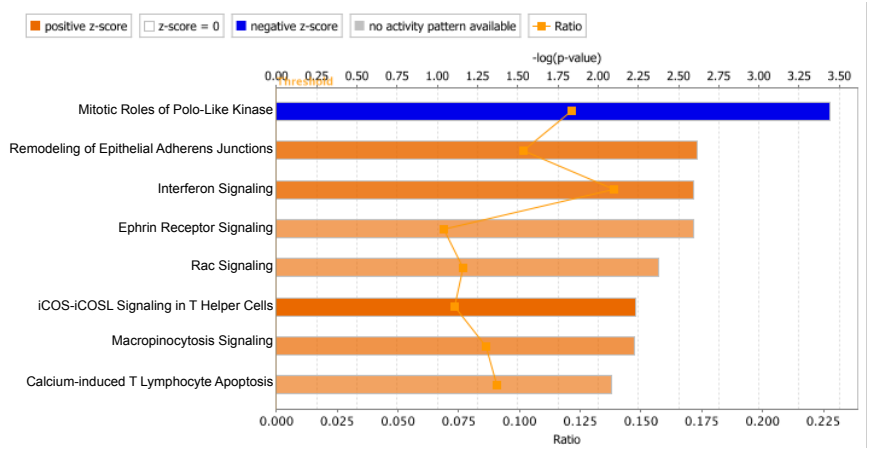

C

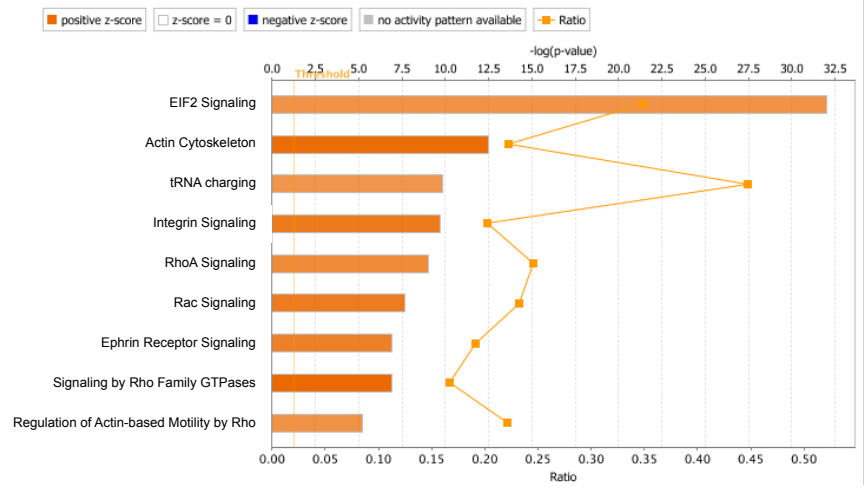

Figure 16: Identification of miRNA targets through the use of TMT-LC-MS/MS. (A and B) Ingenuity Pathway Analysis (IPA) of underexpressed proteins (fold change < 0.67) in cells transfected with miR-30c-2-3p (A) and miR-497-5p (B) compared to

scrambled control. The canonical pathways shown exhibited a -log(p-value) > 2, and an absolute z-score > 1.5. A positive (orange bars) or negative (blue bars) z-score indicates that a given pathway is predicted to be increased or reduced following overexpression of the corresponding miRNA mimic. (C) Ingenuity Pathway Analysis of the overexpressed proteins (fold change > 1.5) in cells transfected with miR-30c-2-3p compared to scrambled control. The canonical pathways shown exhibited a -log(p-value) > 5, and an absolute z-score > 4.

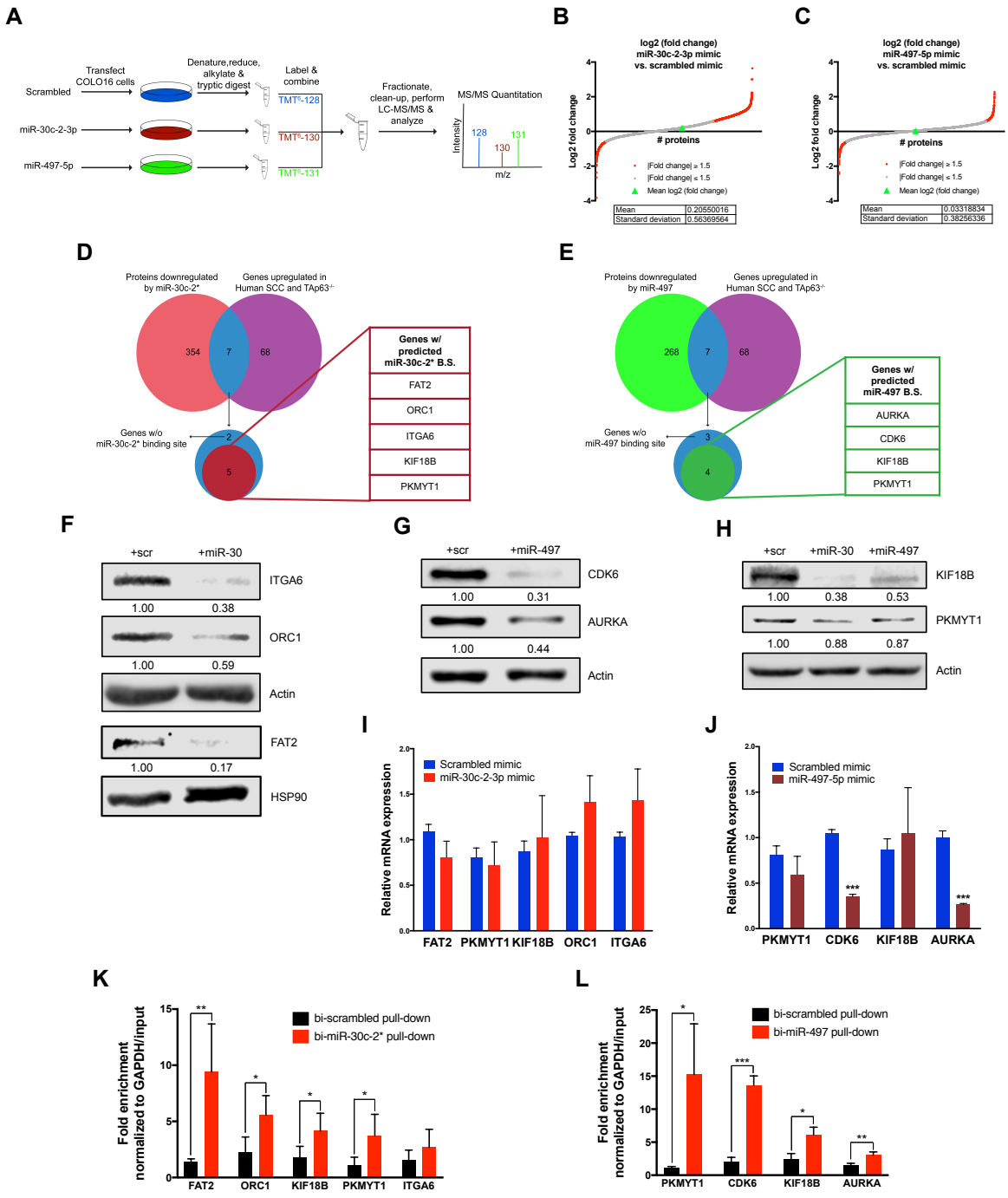

Figure 17: Cross-platform analysis identifies direct mRNA targets for miR-30c-2* and miR-497. (A) Schematic representation of experimental design. COLO16 cells transfected with the indicated miRNA mimic were collected, denatured, and subjected to tryptic digest prior to labeling of each sample with the indicated tandem

mass tag (TMT). Labeled peptides were then combined, fractionated and subjected to LC-MS/MS analysis to identify differentially expressed proteins. (B and C) Differential protein expression changes in cells transfected with miR-30c-2-3p (B) or miR-497-5p (C) mimics compared to scrambled control. (D and E) Comparison of significantly underexpressed proteins following transfection with miR-30c-2* (D) and miR-497 (E) with the overexpressed mRNAs in murine TAp63$^{-/-}$ cuSCC and human cuSCC by RNAseq. Overlapping targets were examined for the presence of MREs for miR-30c-2* and miR-497. Note that KIF18B and PKMYT1 were found to be predicted targets of both miR-30c-2* and miR-497-5p and were underexpressed in both proteomics experiments. (F-H) Western blot analysis for the indicated proteins following transfection with mimics of miR-30c-2* (F), miR-497 (I), and both miRs (J). (I and J) Taqman qRTPCR of the putative targets of miR-30c-2* (I) and miR-497-5p (J). COLO16 cells following transfection with the indicated mimics. (K and L) COLO16 cells were transfected with the indicated biotinylated miRNA mimics (bi-miR) and collected 24 hrs after transfection. Fold enrichment for the indicated targets in the streptavidin pull-down of bi-miR-30c-2-3p (n=5) (K) and bi-miR-497-5p (n=3) (L) was calculated using qRT-PCR. Data shown represent the mean ± SD of at least 3 independent experiments, unless noted otherwise. * $p<0.05$, ** $p<0.01$, *** $p<0.001$, two-tailed Student's t test.

3.2.8. miR-30c-2* and miR-497 targets promote tumor cell proliferation and survival

To determine if the verified targets of miR-30c-2* and miR-497 are relevant to human tumors, we profiled their expression by Western blot in 5 human cuSCC cell lines (COLO16, SRB12, SRB1, IC1, and RDEB2) and compared it to their expression in NHEKs (Figure 18A). From these experiments, we found that each of these targets are overexpressed in the majority of the cuSCC cell lines profiled, with the exception of FAT2 and PKMYT1, which showed variable expression across the different cuSCC cell lines.

Given that overexpression of miR-30c-2* and miR-497 can impair cell proliferation and induce cell death, we asked whether depletion of these putative targets could produce the same biological effects. To do so, we utilized siRNA-mediated gene silencing to knock down each individual target in COLO16 and SRB12 cells (Figure 18B). Knockdown of all 7 targets in SRB12 cells caused decreased growth of SRB12 cells (Figure 19A). Interestingly, knockdown of FAT2 and CDK6 caused an increase in cell proliferation in COLO16 cells, whereas knockdown of KIF18B, PKMYT1, ORC1, and AURKA resulted in significant reductions in COLO16 growth (Figure 18C). These results suggest that KIF18B, ORC1, PKMYT1, and AURKA may be oncogenic drivers of cuSCC.

To determine if inhibition of these targets may induce apoptosis, we performed Annexin V assays in COLO16 and SRB12 cells transfected with siRNAs targeting each of the 6 targets. Knockdown of FAT2, ORC1, KIF18B, PKMYT1, and AURKA led to significant increases in cell death in COLO16 cells, (Figure 18D and

Figure 18E). In SRB12 cells, however, only knockdown of FAT2 and AURKA caused significant increases in apoptosis (Figure 19B and Figure 19C).

We next asked whether inhibition of these targets can phenocopy the effects miR-30c-2* or miR-497 overexpression had on the cell cycle of COLO16 cells. Cell cycle profiling showed that ORC1 knockdown resulted in an apparent G2/M arrest, resembling the effects miR-30c-2* overexpression (Figure 18F). Knockdown of the miR-497 targets did not lead to a G1/S arrest, however, suggesting that miR-497 mediates this effect through the inhibition another target(s), or a combination thereof. Interestingly, AURKA inhibition resulted in significant reductions in the percentage of cells in G1 and S phase, and increases in the percentage of cells in G2 and M phase. Interestingly, the percentage of cells that stained positive for histone H3 S28 phosphorylation was significantly elevated in AURKA knockdown cells, indicating increased mitosis. This phenotype, along with increased apoptosis, is suggestive of mitotic cell death, a process in which aberrant mitotic activity results in cell death or irreversible cellular senescence (249). These results suggest that these targets may be viable therapeutic targets for the treatment of cuSCC.

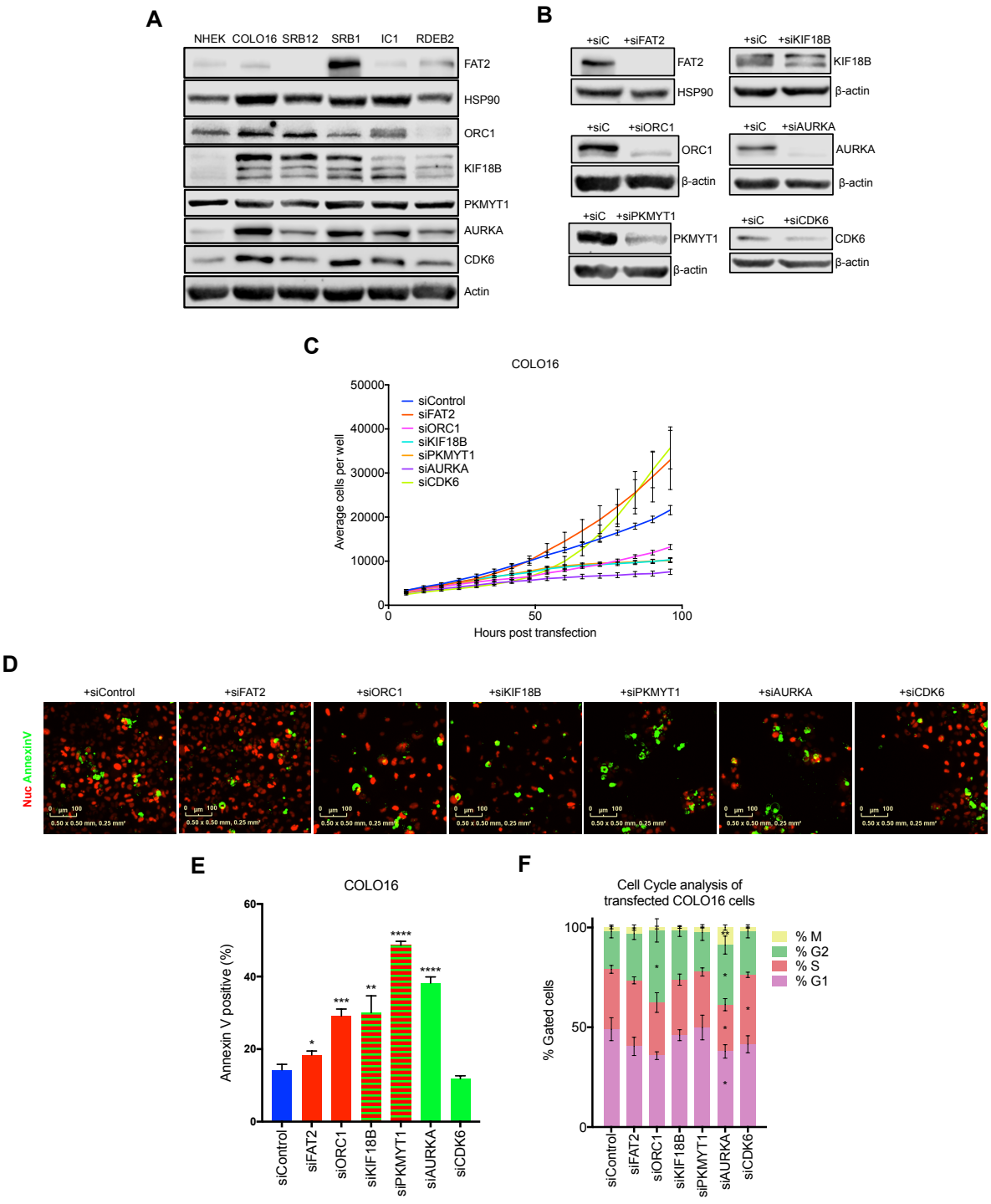

Figure 18: Inhibition of mIR-30c-2* and miR-497-5p targets affects cuSCC cell proliferation and survival. (A) Representative results of Western blotting of the validated miR-30c-2* and miR-497 targets in NHEKs and the cuSCC cell lines

COLO16, SRB12, SRB1, IC1, and RDEB2. (B) Representative Western blotting of the indicated targets following siRNA-mediated knockdown. (C-E) COLO16 cells stably expressing nuclear mCherry transfected with the indicated siRNAs, incubated with Annexin V-488, and scanned every 4 hours using the Incucyte® high-content live-cell imaging platform. (C) Growth curve of COLO16 cells transfected with the indicated siRNAs. (D and E) Immunofluorescence (D) and quantification (E) for annexin V-488 (green)-positive cells transfected with the indicated siRNAs. (F) Cell cycle profiles of COLO16 cells were assessed by FACS 48 hours after siRNA transfection. Data shown are mean ± SD, of at least 3 independent experiments. * $p<0.05$, ** $p<0.01$, ***$p<0.001$, two-tailed Student's t test.

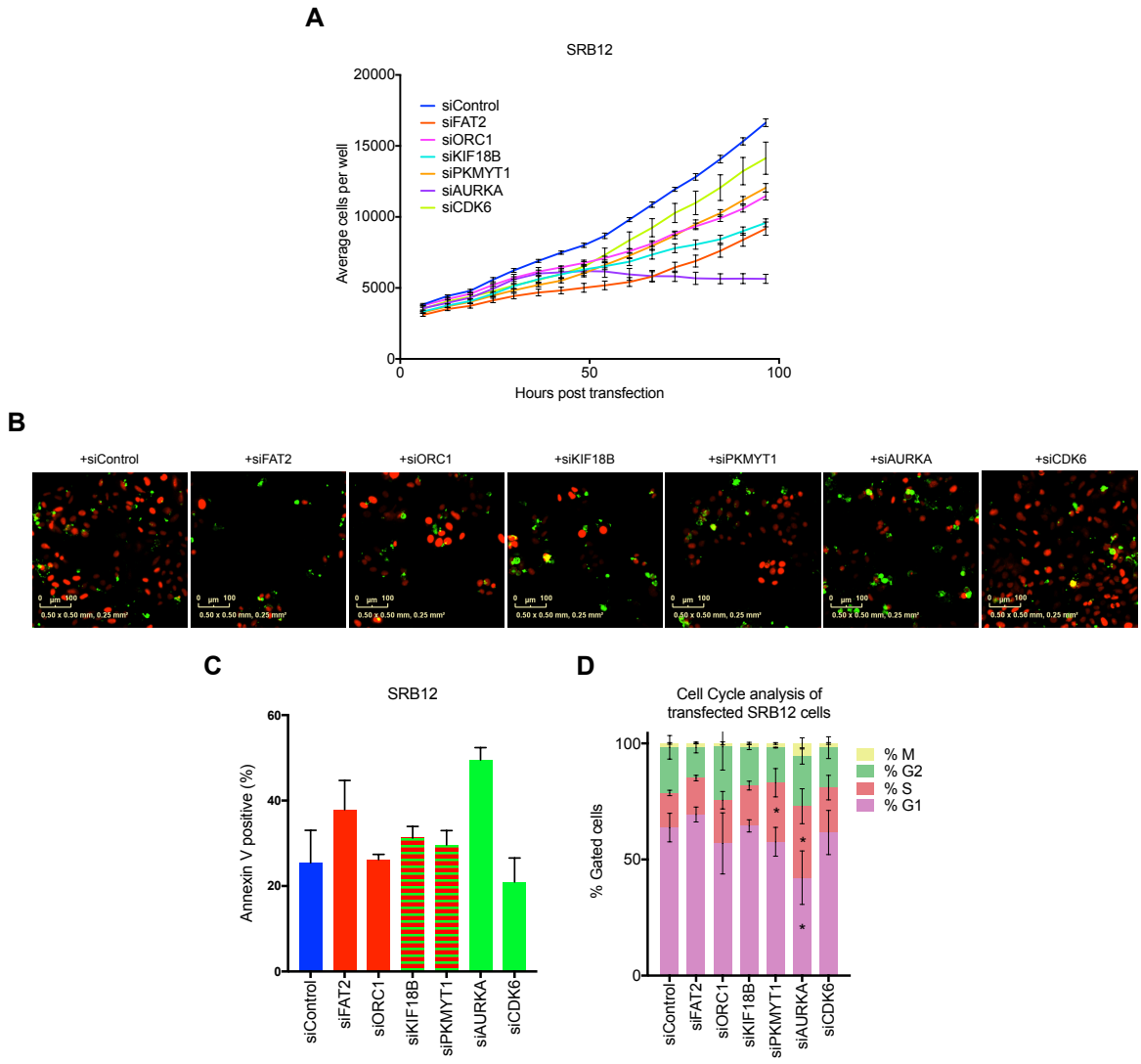

Figure 19: Inhibition of miR-30c-2-3p and miR-497-5p targets affects SRB12 cell proliferation and survival. (A-C) SRB12 cells stably expressing nuclear mCherry were transfected with the indicated siRNAs, incubated with Annexin V-488, and scanned every 4 hours using the Incucyte® high-content live-cell imaging platform. (A) Growth curve of SRB12 cells transfected with the indicated siRNAs. Immunofluorescence (C) and quantification (B) for annexin V-488 (green)-positive cells transfected with the indicated siRNAs. Data shown are mean ± SD, of at least 3

independent experiments. * $p<0.05$, ** $p<0.01$, ***$p<0.001$, two-tailed Student's t test.

3.2.9. AURKA is a viable therapeutic target in cuSCC

To investigate if TAp63 and these miRNAs interact in human patient cuSCC, we performed correlation analyses of miR-30c-2* and miR-497 with the mRNA expression of the 7 validated targets described above. While miR-30c-2* did not show significant correlation with any the targets identified in this study (data not shown), we found significant negative correlation between miR-497 and AURKA (Figure 20C) (r = -0.79, p-value=2.44 10^4) and PKMYT1 (Figure 20B) (r = -0.58, p-value-0.019) mRNA expression. The expression of miR-497 and KIF18B was negatively correlated, however this trend was not statistically significant (r = -0.46, p-value=0.07) (Figure 20A). These results suggest that miR-497 may regulate the expression of AURKA and PKMYT1 in human cuSCC.

We next asked whether the expression levels of miR-30c-2*, miR-497, or the targets validated in this study could predict patient survival. To do so, we leveraged the publically available data from the Cancer Genome Atlas (TCGA). We decided to focus our analyses on HNSCC, which has been shown to be the tumor type that is most closely related to cuSCC (72). From this analysis, we found that high expression of miR-497 correlated with improved survival outcomes in patients with HNSCC (Figure 20D). Conversely, HNSCC patients with high expression of AURKA showed significantly reduced survival (Figure 20E). Taken together these observations suggest that miR-497-mediated regulation of AURKA is functionally and clinically important in cuSCC and HNSCC.

To pursue the potential therapeutic significance of these findings, we treated COLO16 cells with the AURKA-selective kinase inhibitor alisertib. Using the

CellTiter-Glo® assay to quantify cell viability, we found that alisertib was particularly potent in its ability to reduce the viability of COLO16 cells (IC_{50} = 0.01225μM) (Figure 20F). We then asked whether alisertib could reduce cell proliferation and induce cell death in COLO16 cells to the same extent as siRNA-mediated knockdown of AURKA. High content live cell imaging demonstrated that cell proliferation was almost completely inhibited by alisertib treatment (0.01225μM) (Figure 20H). Additionally, alisertib treatment (0.01225μM, 72 hours) resulted in significant apoptosis to the same extent as siRNA-mediated knockdown of AURKA (Figure 20H and Figure 20I). Overall, these results highlight the therapeutic potential of alisertib in the treatment of cuSCC.

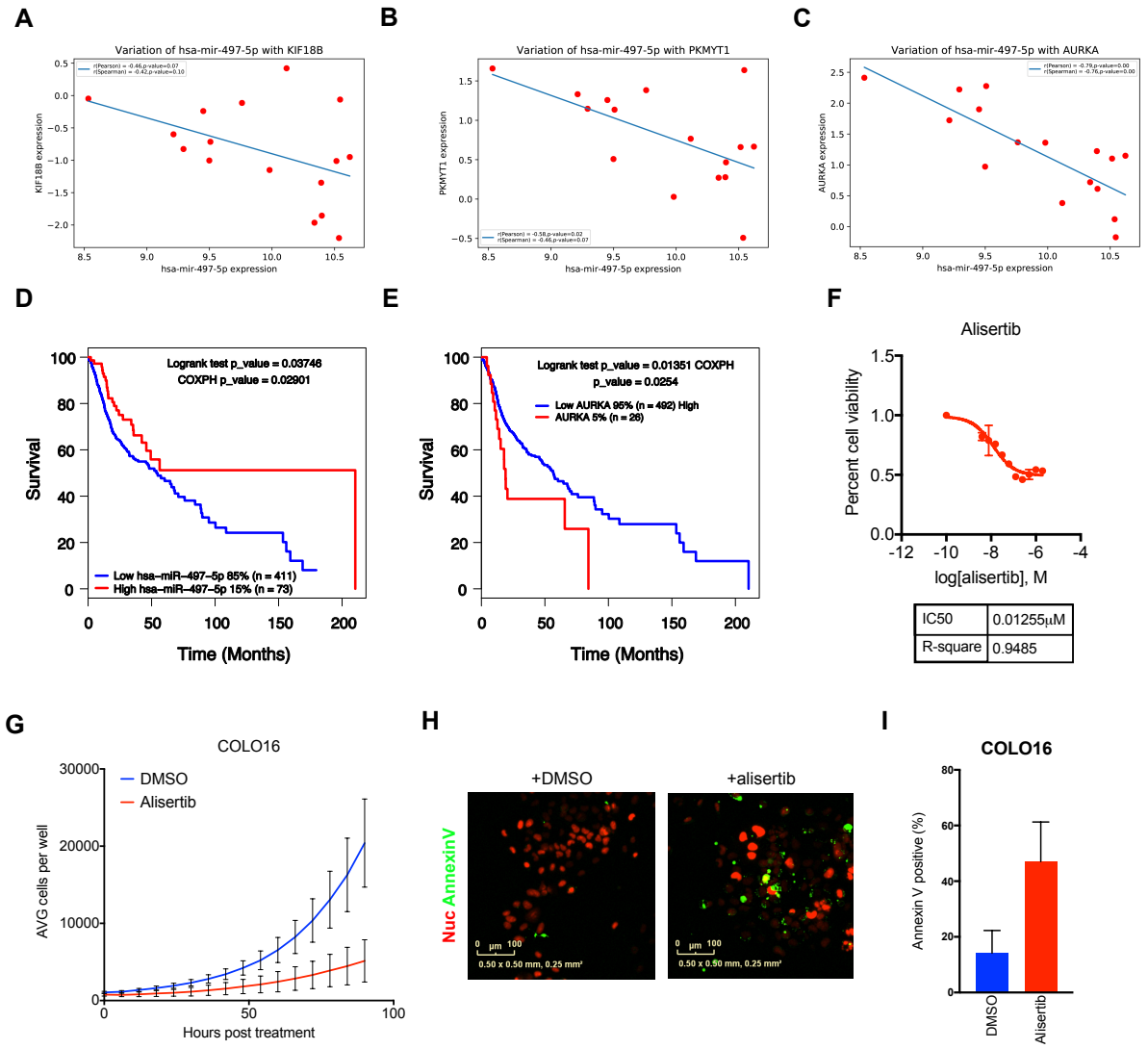

Figure 20: AURKA is a viable therapeutic target in cuSCC. (A-C) Correlation analysis of miR-497 and KIF18B (A), PKMYT1 (B), and AURKA (C) in human cuSCC tumors. Pearson's correlation coefficient (r) values and p values are listed. (D and E) Kaplan-Meier survival curves from HNSCC patients with high vs. low expression of miR-497 (D) and AURKA (E). (F) Effect of alisertib treatment on COLO16 cells. (G-I) COLO16 cells stably expressing nuclear mCherry treated with DMSO vs. alisertib (0.01225uM), incubated with Annexin V-488, and scanned every 6 hours using the Incucyte® high-content live-cell imaging platform. (G) Growth

curve of COLO16 cells treated with alisertib vs. DMSO. (H and I) Immunofluorescence (H) and quantification (I) for annexin V-488 (green)-positive cells following treatment with alisertib or DMSO.

3.2.10. Discussion

Recent genomic and molecular pan-cancer profiling studies of human patient tumors indicate that *TP63* gene plays a central role in the pathogenesis of almost every type of SCC, including the skin, head and neck, lung, esophagus, bladder, and cervix (68, 70-74, 250). In fact, amplification of chromosome 3q, which harbors the *TP63* gene, is the most common copy number alteration across all human SCC (68). Importantly, however, *TP63* is expressed as two different groups of isoforms due to the presence of two alternative promoter regions. TAp63 isoforms contain an N-terminal acidic transactivating domain (TA), which is highly homologous to the TA domain present in the p53 gene. ΔNp63 isoforms on the other hand lack this domain and frequently exert inhibitory function on TAp63 and p53 (21, 24). The use of isoform-specific reagents and next generation sequencing led to the discovery that ΔNp63 isoforms are frequently overexpressed in human tumors, including SCC, whereas TAp63 isoforms are typically not expressed or are expressed at very low levels (63). The differential expression of the N-terminal isoforms may be due to the differential methylation status of the alternative transcriptional start sites for TA and ΔN isoforms (68, 251). Together, these studies support a paradigm where TAp63 functions as a tumor suppressor, while ΔNp63 predominantly functions as an oncogene.

In this study, I found that TAp63 functions as a tumor suppressor in UVR-induced cuSCC. Using a commonly employed mouse model for this disease I found that mice lacking TAp63 are more susceptible to UVR-induced cuSCC. We previously demonstrated that TAp63 promotes miRNA expression through transcriptional regulation of *Dicer*. Therefore, we asked whether or not TAp63-

mediated miRNA expression might account for the increased tumor susceptibility of *TAp63*$^{-/-}$ mice. To answer this question we performed RNA-seq from wild type and *TAp63*$^{-/-}$ skin and cuSCC lesions. This study revealed significant perturbations in global miRNA and mRNA expression in TAp63-deficient tumors. A human to mouse cross-species analysis of the *TAp63*$^{-/-}$ cuSCC signature with similarly sequenced human cuSCC lesions identified miR-30c-2* and miR-497 as significantly underexpressed in both human and mouse tumors. Transfection of cuSCC cell lines with miR-497 mimics caused a dramatic decrease in proliferation. Conversely, introduction of miR-30c-2* mimics in cuSCC cell lines induced significant apoptosis. Proteomic profiling of cuSCC cell lines transfected with miR-30c-2* and miR-497 mimics and subsequent validation experiments led to the discovery of novel direct targets of miR-30c-2* and miR-497. A cross-platform comparison of the RNA-seq and proteomics signatures identified 7 downregulated proteins, whose corresponding mRNAs were also overexpressed in both mouse and human cuSCC. The most relevant of these proteins exhibited pro-oncogenic functions, including roles in cell cycle and mitotic progression.

Inhibition of the miRNA targets including AURKA, KIF18B, PKMYT1, and ORC1 in cuSCC cell lines suppressed tumor cell proliferation and induced cell death. Interestingly, the expression of miR-497 and AURKA showed a significant negative correlation in human cuSCC patient samples. We also found that high expression of miR-497 correlated with improved survival outcomes in patients with HNSCC. Conversely, HNSCC patients with high expression of AURKA showed significantly reduced survival. Taken together these observations suggest that miR-

497-mediated regulation of AURKA is functionally and clinically important in cuSCC and HNSCC.

Notably, AURKA inhibition has not been investigated as a potential treatment option for human cuSCC. My observations suggested that AURKA might be an effective therapeutic target in SCC. I utilized siRNA-mediated knockdown, as well as the FDA-approved AURKA inhibitor alisertib to investigate the effect of AURKA inhibition on cuSCC cell growth and survival. Through these experiments, I found that inhibition of AURKA potently suppressed cuSCC cell growth and induced cell death. Collectively, these observations suggest that AURKA may be an effective targeted therapy in cuSCC.

This study establishes TAp63 as an essential regulator of miRNA expression during skin carcinogenesis and reveals a previously undescribed functional network of miRNAs and targeted mRNAs. These include viable, yet previously unexplored targets for the treatment of human cuSCC.

CHAPTER 4: TAP73 SUPPRESSES LUNG ADENOCARCINOMA DEVELOPMENT AND PROGRESSION

Chapter 4: TAp73 suppresses lung adenocarcinoma development and progression

4.1. Introduction

The p53 family of transcription factors has been implicated in multiple tumor types including lung adenocarcinoma (LUAC). While p53 is mutated or deleted in a very large percentage of LUAC (47%), p63 and p73 are less frequently mutated (6% and 3%, respectively) (68, 71). The role of p73 in lung cancer however has not been fully investigated. While p73 is rarely mutated in human cancers, studies in genetically-engineered mouse models (GEMMs) have found that the depletion of p73 promotes tumor development (184, 185). Notably, 60% of *p73*$^{-/-}$ mice develop LUAC (184). Importantly, p73 is expressed as complex isoforms due to the presence of two alternative promoters (Figure 1). This results in two classes of N-terminal isoforms, which are typically referred to as TAp73 and ΔNp73. TAp73 isoforms contain an N-terminal transactivation domain (TA) that is highly homologous to the TA domain of p53. This domain is important for the transactivation of multiple transcriptional target genes, including canonical p53 targets (1). Moreover, *TAp73*$^{-/-}$ mice are tumor prone, further supporting the hypothesis that TAp73 is a bona fide tumor suppressor (185). Importantly, 32% of these mice develop LUAC, further suggesting that TAp73 functions as a tumor suppressor in the lung.

To investigate the contribution of TAp73 to LUAC development and progression, we generated a novel TAp73 conditional knockout mouse model and combined it with the autochthonous oncogenic *KRAS* lung adenocarcinoma mouse model (Figure 5) (214, 252). This model, as opposed to orthotopic models in

immune-deficient mice, is useful for interrogating the interactions between tumor cells, the immune system, and the tumor microenvironment.

Here we investigated the role of TAp73 during oncogenic Kras-driven lung tumorigenesis using the Cre-inducible *Kras*$^{LSLG12D/+}$ knock-in mouse model (206, 214) and human LUAC cell lines. We found that the genetic deletion of TAp73 isoforms promoted the development of lung adenomas and LUAC. In addition, we also found that loss of TAp73 resulted in higher grade tumors and increased tumor vascularization. Interestingly, we found that TAp73-deleted tumors exhibited reduced CD8+ and CD4+ T cell infiltration. The results from this study show that TAp73 is a potent tumor suppressor in the lung, through both cell-autonomous and non-cell autonomous mechanisms.

4.2. Results

4.2.1 Generating the TAp73 conditional knockout reporter (*TAp73*^{fltd}) mouse

We generated a TAp73 conditional knockout reporter mouse (*TAp73*^{fltd}) using the cre-loxP system (Figure 21A) to enable tissue- and temporal-specific deletion of the TAp73 isoforms without affecting expression of ΔNp73 isoforms. LoxP sites were cloned into the endogenous p73 gene flanking exons 2 and 3, which contains the translational start site for the TAp73 isoforms. The tdTomato gene was inserted upstream of the 5' loxP site in the anti-sense direction, along with a synthetic CAG promoter downstream of the 3' loxP site. Correctly targeted mouse embryonic stem cells (mESCs) were injected into donor blastocysts, which were subsequently implanted into pseudopregnant females. Resulting chimeric mice were intercrossed

with albino C57BL/6J to facilitate the identification of efficient germline transmission, which was subsequently confirmed by genotyping PCR and Southern blot analysis (Figure 21B-D).

To understand the role of TAp73 in development, we generated TAp73 knockout mice (*TAp73*$^{\Delta td/\Delta td}$) by intercrossing *TAp73*$^{fltd/fltd}$ mice with transgenic mice expressing a germline-specific Cre (*Zp3-Cre*) (216). Cre-mediated recombination resulted in the deletion of exons 2 and 3, and strong tdTomato expression (Figure 21B-E). Quantitative RT-PCR on mouse embryonic fibroblasts (MEFs) isolated from *WT* and *TAp73*$^{\Delta td/\Delta td}$ embryos confirmed the depletion of TAp73 mRNA (Figure 21E and Figure 21F) without affecting ΔNp73 expression (data not shown). Taken together, these results indicate that our targeting strategy efficiently, and correctly ablates TAp73 expression without affecting the expression of ΔNp73 isoforms.

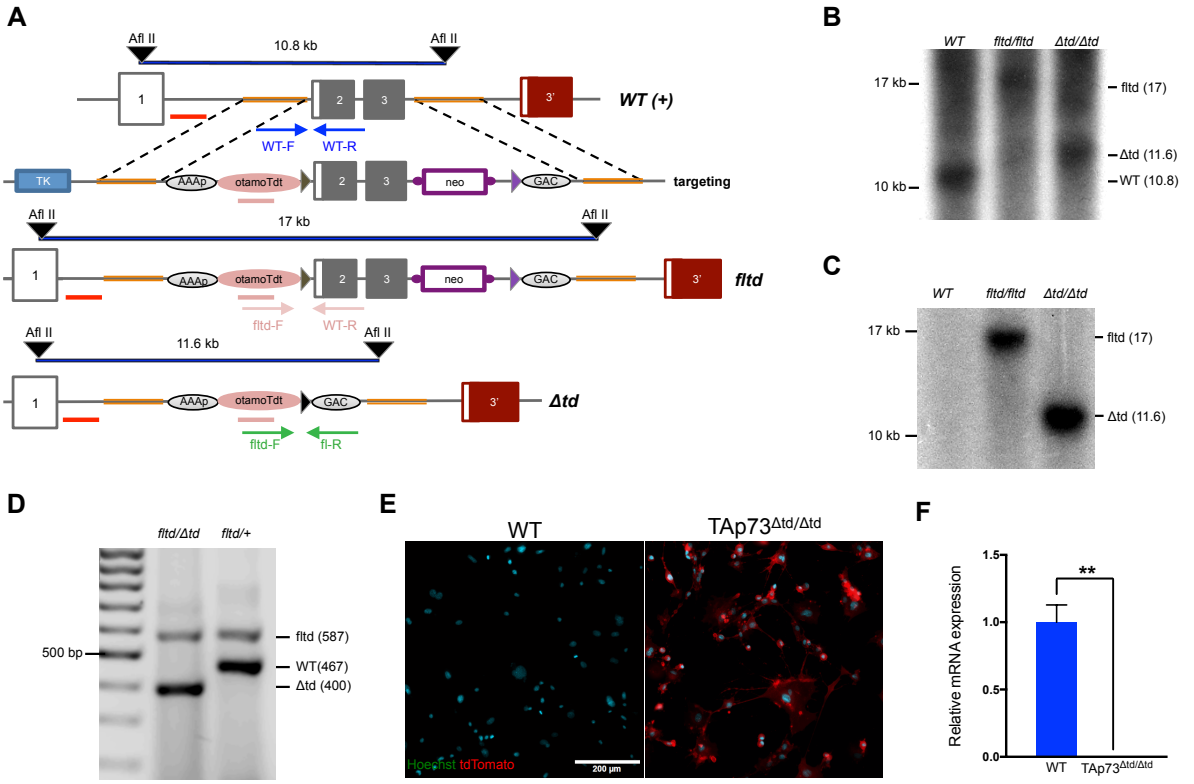

Figure 21: Generating the TAp73 conditional knockout reporter (*TAp73^{fltd}*) mouse. (A) The TAp73 targeting vector was generated by inserting loxP sites (triangles) flanking exon 2 and a neomycin resistance (neo) cassette flanked by frt sites (purple circles) in intron 3. Primers used for genotyping by PCR of wild-type (blue) and TAp73 conditonal knockout reporter (fltd) (pink), and knockout (Δtd) (green) alleles are shown. (B and C) Southern blot analysis of genomic DNA from *WT*, *TAp73$^{fltd/fltd}$*, and *TAp73$^{Δtd/Δtd}$* mice. 5' external probe (B) is shown as a red line at the 3' end of exon 1 in (A). The tdTomato internal probe (C) is depicted as a pink line under the tdTomato coding sequence in (A). (D) Genotyping PCR of gDNA from *TAp73$^{fltd/Δtd}$*, and *TAp73$^{fltd/+}$* mice. (E) Representative merged immunofluorescent micrographs of WT and TAp73$^{Δtd/Δtd}$ mouse embryonic fibroblasts (MEFs). (F)

Taqman qRT-PCR for TAp73 mRNA from *WT* and *TAp73*$^{\Delta td/\Delta td}$ MEFs (n=3 embryos per genotype, ** $p<0.01$).

4.2.2. Loss of TA73 expression promotes lung adenocarcinoma initiation and progression

To study the role of TAp73 deletion in lung tumorigenesis, we intercrossed *TAp73*$^{fltd/fltd}$ mice with the *Kras*$^{LSLG12D/+}$ mouse model (206, 214). This model allowed us to interrogate the effects of TAp73 deletion on oncogenic Kras-driven LUAC. This model faithfully recapitulates many of the histological features of human LUAC. To permanently label cells that undergo Cre-mediated recombination, we utilized a conditional fluorescent reporter allele (*Rosa*$^{mT/mG}$) (213), in which a floxed tdTomato allele is placed upstream of a stop codon and GFP. This allows for the conditional activation of GFP expression upon Cre-mediated recombination. Adenovirus expressing Cre recombinase (Ad-Cre) or empty vector (Ad-Empty) was delivered to *TAp73*$^{fltd/fltd}$*;* *Rosa*$^{mT/mG}$ (*T*), *Kras*$^{LSLG12D/+}$; *Rosa*$^{mT/mG}$ (*K*), and *TAp73*$^{fltd/fltd}$*;* *Kras*$^{LSLG12D/+}$; *Rosa*$^{mT/mG}$ (TK) mice via intratracheal administration. The mouse models were infected with Ad-Cre at 8-10 weeks of age, and euthanized 30 weeks later. As expected, all of the *TK* and *K* mice developed primary lung tumors following infection with Ad-Cre (Figure 22A), whereas none of the mice infected with Ad-empty developed any tumors. At this time point, none of the infected *T* mice showed evidence of lung tumorigenesis (data not shown). These results might be expected, considering the long latency of tumor development in *TAp73*$^{-/-}$ mice developed by the Mak laboratory (185).

To investigate the effects of TAp73 loss, we evaluated the lung tumor phenotypes of K and TK mice. To do so, we imaged H&E stainings taken from the lungs of infected mice and subjected them to image analysis using machine learning

software (Visiopharm v 7.2) (Figure 22B). From this analysis we found that the deletion of TAp73 in the context of oncogenic Kras led to a significant increase in the total number of lung tumors (Figure 22D), as well as the percentage of lung tumor area (Figure 22E). These results suggest that TAp73 may suppress lung tumor initiation.

To determine the effects of TAp73 on tumor progression we set out to quantify the distribution of tumors based on histopathological grade, using a widely used grading system for NSCLC mouse models (208). In this system, grade 1 and grade 2 tumors resemble human pre-malignant lung adenomas, while grade 3 and grade 4 tumors are comparable to fully-malignant human LUAC. Interestingly, manual grading of the lung lesions that were identified in our cohort and subsequent quantification showed that there was a significant increase in the proportion of grade 3 tumors in the infected TK mice, compared to K mice (Figure 22F and Figure 22G). Taken together, these results suggest that TAp73 may inhibit both lung tumor initiation and malignant progression.

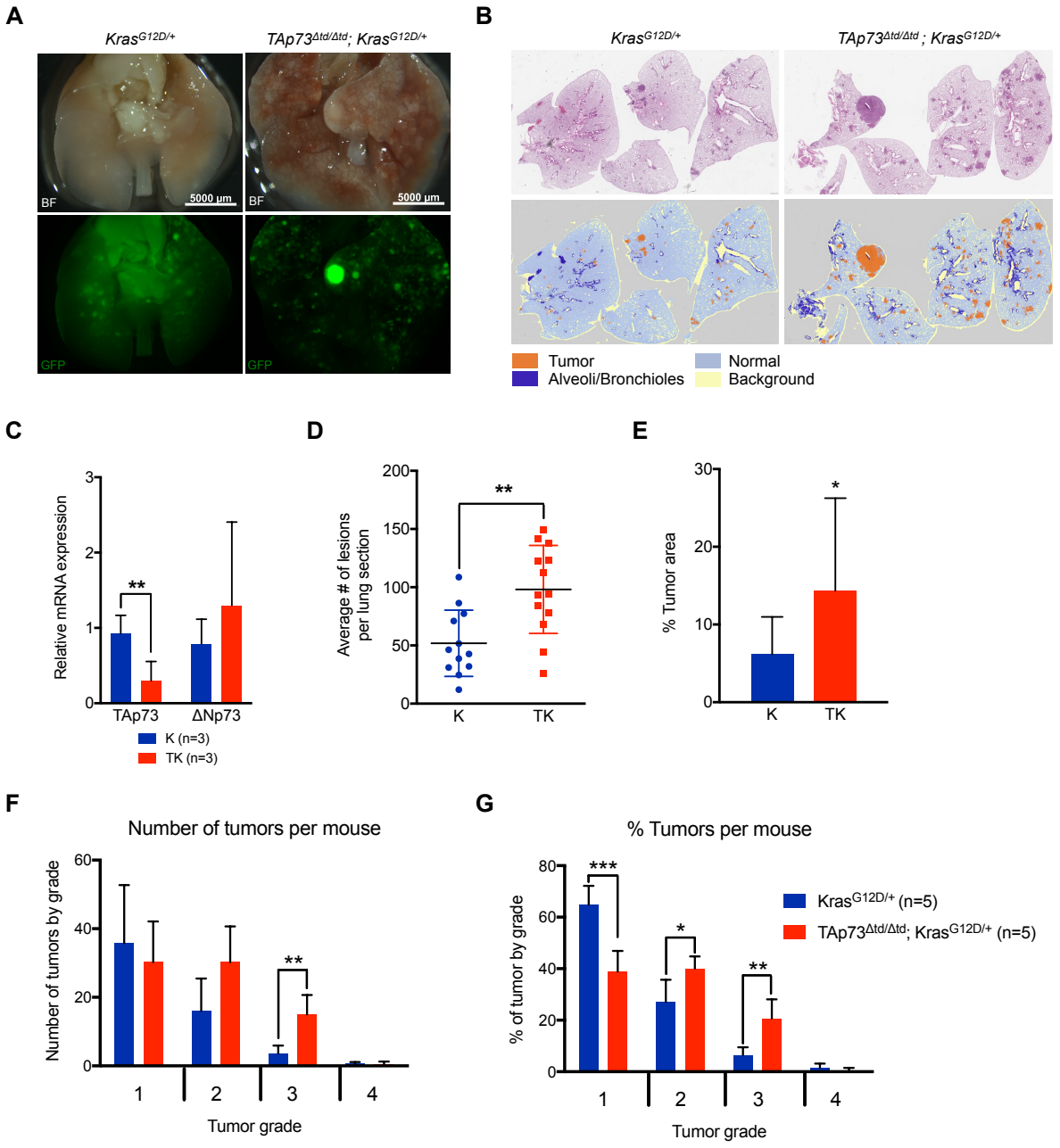

Figure 22: Loss of TA73 expression promotes lung adenocarcinoma initiation and progression. (A) Representative bright field (BF) and GFP imaging of *Kras*$^{LSLG12D/+}$; *Rosa*$^{mT/mG}$ ("K", n=12) and TAp73$^{fltd/fltd}$; *Kras*$^{LSLG12D/+}$; *Rosa*$^{mT/mG}$ ("TK", n=13) mouse lungs 30 weeks after intratracheal adenoviral-Cre administration. Scale bar = 5000µm. (B) Representative H&E stainings and tissue segmentation (orange)

of K and TK mouse lung sections following intratracheal infection with Ad5-CMV-Cre virus. (C) Taqman qRT-PCR for TAp73 and ΔNp73 mRNA from K and TK LUAC tumors (n=3 tumors per genotype, ** $p<0.01$). (D) Average number of tumors per mouse in K (blue) and TK (red) mice 30 weeks after intratracheal adenoviral Cre administration. Each dot corresponds to the average number of lung lesions per section for a single mouse. (E) Average percentage of tumor area in K mice (blue columns) and TK mice (red columns). Columns correspond to percentage of lung area occupied by tumors. (F and G) Number (F) and percentage (G) of lung tumor grades in K (blue columns, n=5) and TK (red columns, n=5) mice. Data shown represent the mean ± SD; * $p<0.05$, ** $p<0.005$, ***$p<0.0001$.

4.2.3. TAp73-deficient tumors exhibit reduced immune cell infiltration

Previous studies have implicated p73 isoforms, including TAp73, in normal immune responses (10, 183, 253). Therefore, we profiled *K* and *TK* lung tumors for various immune markers using immunohistochemical (IHC) staining (Figure 23A). In line with previous observations (254), we found that TK lung adenomas and lung adenocarcinomas exhibited a greater degree of CD31 staining, which is a marker for endothelial cells, indicating increased tumor angiogenesis (Figure 23B). These results support the hypothesis that TAp73 suppresses tumor angiogenesis (253, 254).

Previous studies have implicated p73 isoforms, including TAp73, in immune responses. We also assessed the degree of T cell infiltration in T and TK tumors (Figure 23A-E). Interestingly, there was a significant reduction in the average number of tumor-infiltrating lymphocytes in TK tumors relative to K tumors (Figure 23A and Figure 23C). Specifically, we found reduced infiltration of both $CD4^+$ helper T cells and $CD8^+$ cytotoxic T cells in TK tumors when compared to K tumors (Figure 23D and Figure 23E). PD-L1 and FOXP3 however showed no significant changes between the 2 genotypes (data not shown). Taken together, these results suggest that the loss of TAp73 hinders an adaptive anti-tumor response, which occurs in single mutant K mice.

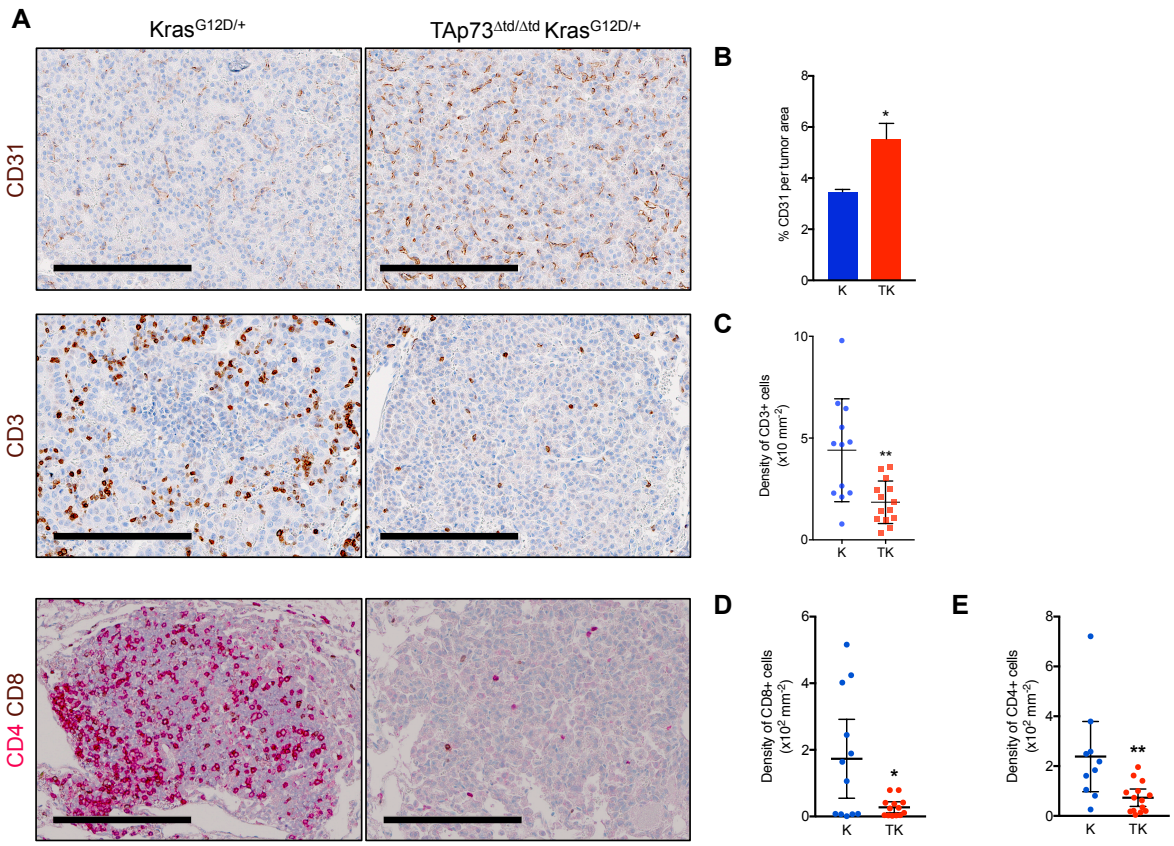

Figure 23: TAp73-deficient tumors exhibit reduced immune cell infiltration. (A) Representative immunohistochemistry on mouse lung sections with the indicated histopathological markers. Scale bars = 200μm. (B) Quantification of the percentage of intratumoral CD31 staining (n=4 and 6 mice). (C-E) Quantification of $CD3^+$ (n=12 and 14 mice) (C), CD8+ (n=12 and 13 mice) (D), and $CD4^+$ (n=10 and 14 mice) (E) cell densities in lung tumors. Data shown represent the mean ± SD; * $p<0.05$, ** $p<0.005$, ***$p<0.0001$; two-tailed Student's t test.

4.2.4. Deletion of TAp73 using CRISPR/Cas9 leads to deregulated cytokine secretion

To establish human cell line model system for mechanistic studies, we utilized a lentiviral-based Crispr-Cas9 strategy to delete TAp73 isoforms in A549 cells. A549 cells-stably expressing Cas9-eGFP were transduced with lentiviruses expressing mCherry and sgRNAs targeting 3 different regions of the TA domain of p73 (lenti-mCherry-sgTAp73). We performed antibiotic selection and subcloned individual A549 cells transduced with each of the lenti-mCherry-sgTAp73 viruses. To verify accurate and efficient targeting of TAp73, we isolated genomic DNA from cells expressing both GFP and mCherry and performed Sanger sequencing of the genomic region flanking the targeted sequences of TAp73. Using this strategy, we screened 16 clones and identified one clone (A549-sgTAp73) that exhibited a 34 bp deletion of exon 2, which encompassed the corresponding targeting region for sgTAp73 #2 (Figure 24A). Importantly, we found that this subclone showed significantly reduced expressed of TAp73β compared to A549-Cas9 cells, as shown by WB (Figure 24B).

To determine if the decreased T cell infiltration observed in the TK tumors was due to dysregulated cytokine expression, we assayed the effect of TAp73-depletion on cytokine secretion using a human cytokine antibody array. Stable A549-Cas9 and A549-sgTAp73 cells were separately serum-starved and cultured in media for 72 hours at which point conditioned media (CM) was collected and incubated with the human cytokine antibody arrays prior to imaging (Figure 24C). From this assay we identified a number of cytokines that were upregulated in the CM from

A549-sgTAp73 cells, including IL-6, VEGF-A, and TGFβ3 (Figure 24CD). Conversely, we identified a number of cytokines that are reduced in the TAp73-deleted cells, including TNFβ, IGFBP-2, EGF, and angiogenin (Figure 24E). We validated the increased amount of IL-6 in the CM of A549-sgTAp73 (Figure 24F), and we are currently in the process of validating the other cytokines using ELISA-based assays. Taken together, these observations suggest that TAp73 may regulate cytokine secretion of LUAC cells.

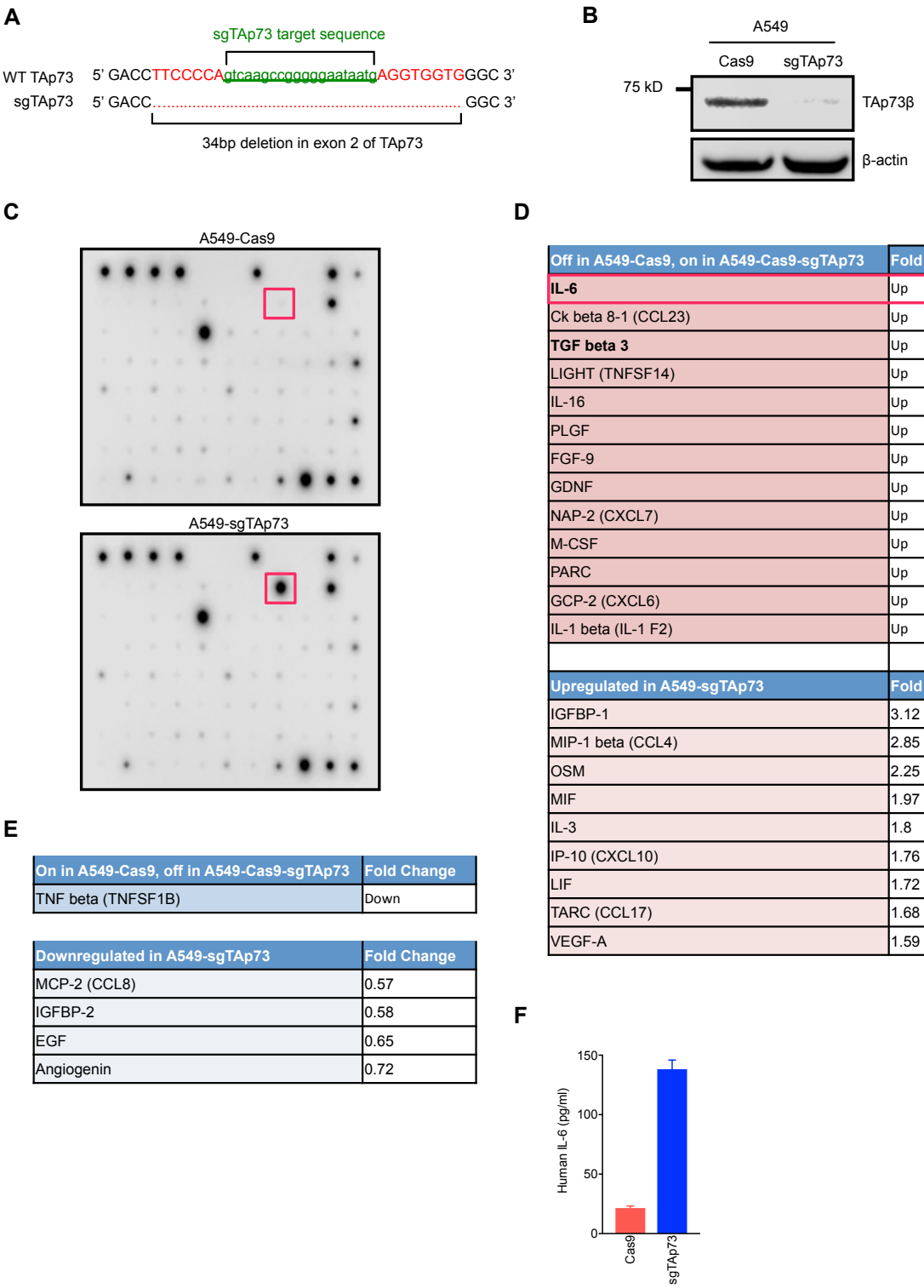

Off in A549-Cas9, on in A549-Cas9-sgTAp73	Fold Change
IL-6	Up
Ck beta 8-1 (CCL23)	Up
TGF beta 3	Up
LIGHT (TNFSF14)	Up
IL-16	Up
PLGF	Up
FGF-9	Up
GDNF	Up
NAP-2 (CXCL7)	Up
M-CSF	Up
PARC	Up
GCP-2 (CXCL6)	Up
IL-1 beta (IL-1 F2)	Up

Upregulated in A549-sgTAp73	Fold Change
IGFBP-1	3.12
MIP-1 beta (CCL4)	2.85
OSM	2.25
MIF	1.97
IL-3	1.8
IP-10 (CXCL10)	1.76
LIF	1.72
TARC (CCL17)	1.68
VEGF-A	1.59

On in A549-Cas9, off in A549-Cas9-sgTAp73	Fold Change
TNF beta (TNFSF1B)	Down

Downregulated in A549-sgTAp73	Fold Change
MCP-2 (CCL8)	0.57
IGFBP-2	0.58
EGF	0.65
Angiogenin	0.72

Figure 24: Deletion of TAp73 using CRISPRi leads to deregulated cytokine secretion. (A) Sequence of human TAp73 and the resulting deletion observed in

cells following transduction with lentivirus expressing Cas9 and a TAp73-specific guide RNA (sgTAp73), followed by antiobiotic selection and subcloning. (B) Western blot analysis of TAp73 inA549 cells transduced with Cas9 or Cas9 plus sgTAp73 as described in (A). (C-E) Cytokine array of A549-Cas9 vs. A549-sgTAp73 cells. List of cytokines that are increased (D) and decreased (E) in A549-sgTAp73 cells (|Fc| > 1.5). Increased secretion of IL-6 is the most dramatic change in the A549-sgTAp73 cells (highlighted in red). (F) Increased secretion of IL-6 in A549-sgTAp73 cells was validated by ELISA. Data shown is from a representative experiment (n=3).

4.2.5. Depletion of TAp73 in human LUSC cell lines enhances tumor cell migration and invasion.

Given the increased proportion of higher-grade lung tumors (e.g. Grade 2 and 3) in TK mice, we examined whether siRNA-mediated knockdown of TAp73 in human LUAC cell lines would enhance the migratory and invasive capacity of A549 cells (Figure 25A). Notably, knockdown of TAp73 resulted in morphological changes that resembled an epithelial-to-mesenchymal transition. (Figure 25B). While untransfected and siControl-transfected A549 cells exhibited an epithelial-like morphology, characterized by colony forming cells with tight cell-cell contacts. TAp73 knockdown cells showed a more mesenchymal phenotype characterized by elongated spindle-like cells, and exhibiting fewer cell-cell contacts. These observations were accompanied by significant increases in the migratory (Figure 25C) and invasive (Figure 25D) abilities of A549 cells following knockdown of TAp73.

Similar to TAp73-knockdown cells, we found that A549-sgTAp73 cells showed enhanced migratory capacity (Figure 25E). However, these cells did not show enhanced invasion, nor did they exhibit the same dramatic EMT-like phenotype of TAp73-knockdown cells (data not shown). In addition, we found that these cells exhibited increased cell growth and proliferation (Figure 25saF). Taken together, these results indicate that the depletion of TAp73 isoforms may enhance the migratory capacity of human LUAC cells.

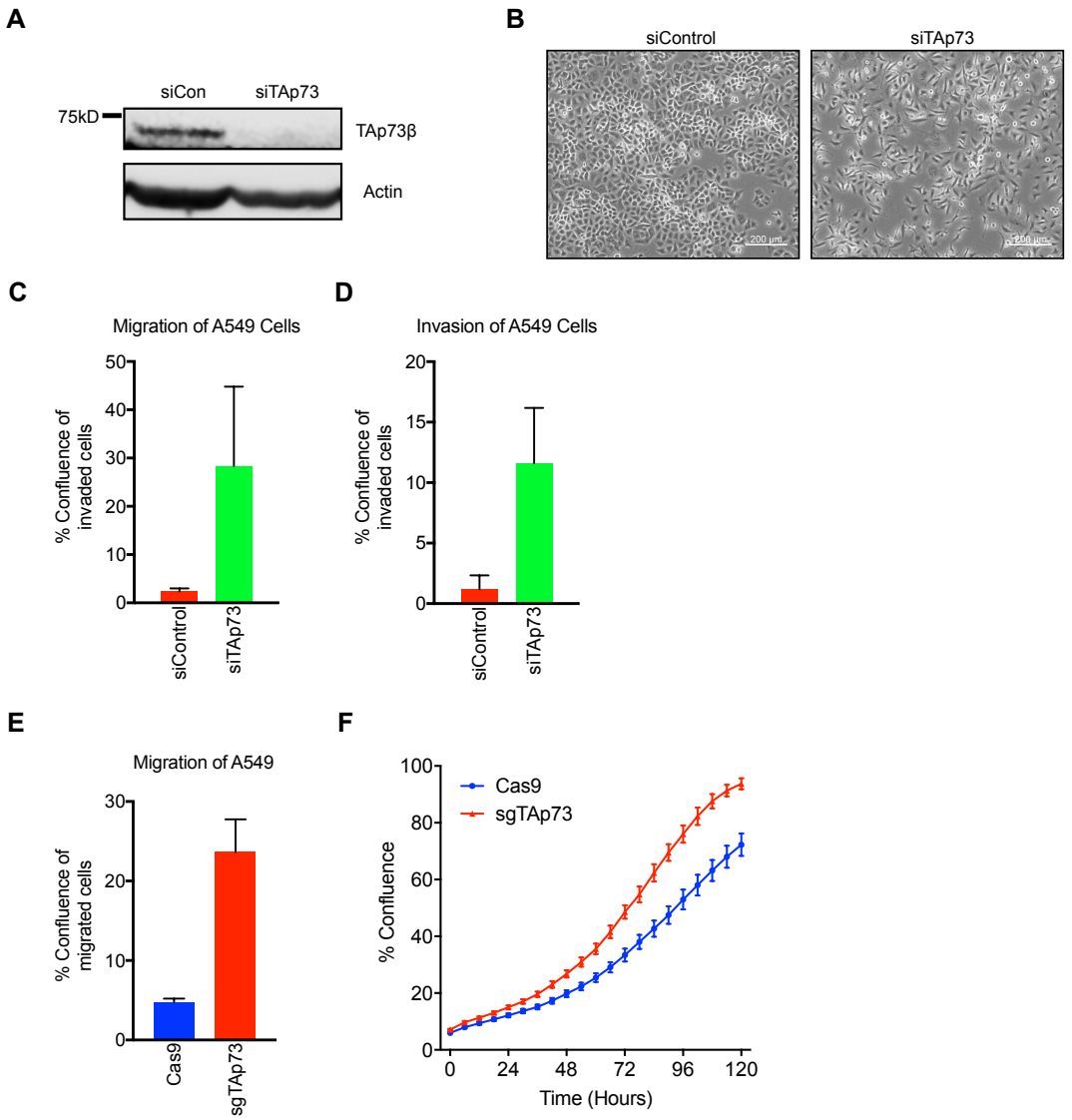

Figure 25: Depletion of TAp73 in human LUSC cell lines enhances tumor cell migration and invasion. (A) Western blot analysis showing successful siRNA-mediated knockdown of TAp73 in the A549 human lung adenocarcinoma (LUAC) cell line. (B) Phase contrast imagesof A549 cells transfected with the indicated siRNAs. (C and D) Migration (C) and invasion (D) assays of A549 cells transfected with the indicated siRNAs (n=2). (E and F) Migration (E) and cell growth curve (F) of A549-Cas9 and A549-sgTAp73 cells.

4.2.6. DISCUSSION

In this study, I have utilized an in vivo lung tumorigenesis model to test the effect of TAp73 deletion on lung tumor formation. This system leverages a conditional oncogenic Kras mutant mouse (*Kras*$^{LSLG12D/+}$) (214) that, upon intratracheal adenoviral Cre infection, develops lung adenocarcinomas with high frequency as early as 16 weeks post infection (208). Supporting the notion that TAp73 functions as a tumor suppressor, we found that the deletion of TAp73 in the context of oncogenic Kras results in a significant increase in tumor development and progression compared to oncogenic Kras activation alone. These results indicate that TAp73 may inhibit both tumor initiation and progression in this context.

Interestingly, we found that the loss of TAp73 promotes tumor angiogenesis, and a pro-tumorigenic immune environment. Immunohistochemical profiling showed that TAp73-deficient tumors exhibit increased tumor vascularization, as demonstrated by increased CD31 staining. These observations support previous studies that suggest that TAp73 is a suppressor of tumor angiogenesis (253, 254). In addition, we found that the deletion of TAp73 in tumors resulted in reduced T cell infiltration, as demonstrated by significant reductions in intratumoral $CD3^+$, $CD4^+$ and $CD8^+$ T cells. Taken together, these results suggest that TAp73-deficient tumors are able to evade adaptive anti-tumor immune responses, through an as of yet unidentified mechanism.

To identify the mechanism through which TAp73-deficient tumor cells evade anti-tumor immunity, we employed a lentiviral based Crispr/Cas9 strategy to delete TAp73 in the A549 human LUAC cell line. We then profiled the secretion of

chemokines and cytokines from these cells and compared them to TAp73-expressing A549 cells. The most significant changes include increased secretion of IL-6 and TGFβ3 by TAp73-deleted A549 cells.

In addition, the depletion of TAp73 in human LUAC cell lines enhances tumor cell proliferation. Inhibition of TAp73 also led to increases in cell migration and invasion. Together, these observations suggest that TAp73 may mediate tumor suppression through both cell- and non-cell-autonomous mechanisms.

Chapter 5: DISCUSSION AND FUTURE DIRECTIONS

Chapter 5: Discussion and Future Directions

5.1. Summary

TP63 and TP73 (which encode p63 and p73, respectively) are highly conserved transcription factors with important roles in epidermal development, stratification, and tissue homeostasis (23, 55, 183, 255). Similar to their homolog, p53, both p63 and p73 have been shown to mediate tumor suppression in multiple tissue types (3, 147, 185, 256). Interestingly, however, both genes are expressed as multiple isoforms, which appear to have different, and, in many cases, antagonistic functions. Through the use of isoform-specific null alleles of p63 and p73, our lab and others have shown that the full-length N-terminal isoforms of p63 and p73 (referred to as TAp63 and TAp73, respectively) exhibit distinct functions in development, metabolism and tumor suppression (5-7, 14, 147). The goal of my thesis research has been focused on understanding the specific functions of TAp63 and TAp73 isoforms in tumorigenesis. To do so, I have developed and employed novel conditional knockout mouse models to investigate the tumor suppresive functions of TAp63 and TAp73 in cutaneous squamous cell carcinoma (cuSCC) and lung adenocarcinoma (LUAC), respectively.

First my research revealed important tumor suppressive functions of TAp63 in cuSCC. Using a UVR-induced model of cuSCC, I found that TAp63-null (*TAp63*$^{-/-}$) mice exhibit increased susceptibility to cuSCC. Previously, our lab has previously shown that TAp63 positively regulates miRNA processing, through direct transcriptional activation of *Dicer,* as well as through the transcriptional activation of individual pre-miRNA transcripts. In an effort to identify miRNAs regulated by TAp63

that predict cuSCC susceptibility, we performed RNA-seq from wild type and *TAp63*$^{-/-}$ skin and cuSCC lesions. Our data revealed significant perturbations in global miRNA and mRNA expression in TAp63-deficient tumors. A human to mouse cross-species analysis of the *TAp63*$^{-/-}$ cuSCC signature with similarly sequenced human cuSCC lesions identified miR-30c-2* and miR-497 as significantly underexpressed in both human and mouse tumors. Transfection of cuSCC cell lines with miR-497 mimics caused a dramatic decrease in proliferation. Conversely, introduction of miR-30c-2* mimics in cuSCC cell lines induced significant apoptosis. We hypothesize that TAp63 mediates tumor suppression in the skin, in part, through the anti-proliferative and pro-apoptotic functions of miR-497 and miR-30c-2*, respectively**.** Through the use of quantitative proteomics, we have identified and validated 7 direct targets of either miRNA, 2 of which are targeted by both miRs. Ongoing experiments are aimed at identifying the therapeutic potential of inhibiting the downstream targets of both miRNAs.

In addition to regulating miRNA expression, our lab and others have discovered essential roles for p63 isoforms in the regulation of multiple stem cell types in the skin and other tissues. While ΔNp63 isoforms appear to be critical for maintaining basal keratinocytes (173, 257), our lab has also found that TAp63 isoforms are necessary for maintaining the replicative potential of skin-derived precursors (SKPs), which are a type of stem cell present in the hair follicles of mice and humans (14). SOX2, a transcription factor with established roles in stem cells including SKPs (14, 258), is frequently overexpressed in human SCCs of the skin, lung, head and neck, and others (73, 259). Interestingly, recent studies have found

that SOX2 functions as regulator of cancer initiation and stemness in cutaneous SCC (232, 233). Given their regulation by TAp63 and SOX2, I hypothesize that SKP cells may serve as a potential cell of origin in cutaneous SCC. To test this hypothesis, I have developed a novel lineage-tracing model to evaluate the tumor initiating abilities of SOX2+ SKP cells *in vivo*. This system allows us to fluorescently label SKP cells, as well as their descendants *in vivo*, thus allowing us to determine if they can serve as a potential cell of origin. We are currently in the process of finishing this experiment and are actively analyzing the data.

Along with TAp63-mediated tumor suppression in the skin, I have also found that TAp73 functions as a tumor suppressor in the lung epithelium. To do so, I have developed a novel TAp73 conditional knockout reporter mouse (*TAp73*^{fltd}), which effectively allows one to identify TAp73-deleted cells *in situ*. To investigate the role of TAp73 in lung cancer, I crossed the *TAp73*^{fltd} mice to a well-characterized mouse model of Kras-driven LUAC. Using this model, I have found that the loss of TAp73 accelerates the initiation and progression of oncogenic Kras-driven LUAC. In line with previous observations, TAp73 loss promotes tumor angiogenesis. Our data also suggest that TAp73 may be necessary for tumor immune responses, as TAp73-deficient lesions exhibit reduced T-cell infiltration. In addition, Crispr/Cas9 targeted deletion of TAp73 in human lung adenocarcinoma cell lines resulted in aberrant cytokine secretion, which may be the causative mechanism that drives the decreased immune infiltration of *TK* tumors. Moreover, TAp73-deficient tumor cells showed increased invasion and migration, indicative of an epithelial-to-mesenchymal transition. Taken together these results suggest that TAp73 functions as a tumor

suppressor in the lung, through both cell-autonomous, as well as non-cell-autonomous mechanisms.

5.2. TAp63-regulated miRNA expression mediates tumor suppression in cuSCC

Mechanistic studies have shown that TAp63 exhibits tumor suppressive functions through transcriptional activation of genes involved in nucleotide excision repair (5), cell death (260, 261), and metabolism (7). Recent studies have also implicated TAp63 in the inhibition of metastasis through the activation of miRNA expression and biogenesis (147, 262). In line with previous observations, this study demonstrates that TAp63 may be a critical tumor suppressor of UVR-induced cuSCC. Specifically, we see that mice lacking TAp63 are more susceptible to UVR-induced SCC, and that these mice have significantly altered miRNA and mRNA expression profiles compared to strain-matched *WT* mice. Interestingly, we found that many of the differentially expressed miRNAs and mRNAs in *TAp63*$^{-/-}$ cuSCC were similarly deregulated in a previously published human cuSCC RNA-seq dataset (72). Through the use of miRNA-mRNA functional pair analysis, we identified a complex network miRNAs and mRNAs that are differentially expressed and exhibit negative correlations in their expression, in both mouse and human cuSCC. Subsequent validation showed the downregulation of miR-30c-2* and miR-497 in both mouse *TAp63*$^{-/-}$ cuSCC and human cuSCC. Moreover, we found that both miR-30c-2* and miR-497 expression is directly regulated by TAp63, and that this regulation is Dicer-dependent (147).

Through the use of miRNA mimics we were able to establish tumor suppressive functions of miR-30c-2* and miR-497 in human cuSCC. Notably, miR-30c-2* reduced cell proliferation and induced significant apoptosis in multiple cell lines. Alternatively, we found that miR-497 overexpression did not induce cell death but rather appeared to induce a striking G1/S cell cycle arrest and significantly reduced cell proliferation. We further showed that re-introduction of miR-30c-2* and miR-497 into tumor xenografts resulted in significantly reduced tumor growth, further demonstrating the therapeutic potential of reintroducing these miRNAs and inhibiting their targets.

miR-30c-2* is the passenger (miR*) strand of pri-miR-30c-2. Despite being considered a passenger strand, the seed sequence of miR-30c-2* UGGGAGA is highly conserved across mammals and reptiles, indicating the likelihood that it is a functional miRNA. Both correlation and functional studies support the notion that miR-30c-2* functions as a tumor suppressor in human cancers. For example, miR-30c-2* has been shown to inhibit cell proliferation and angiogenesis through the direct inhibition of HIF2α (263). miR-30c-2* was also found to inhibit NF-κB and cell cycle progression in breast cancer cells via direct inhibition of TRADD and CCNE1 expression, respectively (264). Here, we show that miR-30c-2* overexpression causes reduced cell proliferation, similar to previous observations. In addition, we found that miR-30c-2* expression led to a highly significant induction of cell death, which is a previously unobserved phenotype of miR-30c-2*. These results indicate that miR-30c-2* is a tumor suppressive miRNA.

miR-497 is the guide strand of pri-miR-497, which is encoded by the first intron of the MIR497HG gene. It belongs to a larger family of miRNAs, referred to as the miR-15/107 family, including miRs-15, 16, 103, 107, 195, 424 and 497, each of which harbor the same seed sequence AGCAGC. Several of the miRNAs in this family, including miR-497, are frequently underexpressed in human cancers (150, 265-267). Recent transcriptional profiling of human cuSCC tumors found that miR-497 is consistently underexpressed in cuSCC and normal skin (72, 150). Interestingly, both of these studies found that miR-497 expression is also significantly reduced in actinic keratosis, which is a common pre-malignant lesion that frequently progresses into fully malignant cuSCC. These results suggest that loss of miR-497 expression may be an important event in the early stages of cuSCC development. Functional studies support the notion that miR-497 functions as a tumor suppressor, through its ability to regulate cell proliferation (242, 268-272), apoptosis (273, 274), migration and invasion (275), and angiogenesis (276). In line with previous studies, we found that miR-497 significantly suppresses cuSCC cell growth, but it does not however induce apoptosis. This may be due to the differences in the specific pathways that are regulated by miR-497 in cuSCC compared to other tumor types. It may also be due to the differences in the level of miR-497 overexpression that was achieved in the various studies. Regardless, our data supports the general hypothesis that miR-497 is a tumor suppressive miRNA.

5.3 Targets of miR-30c-2* and miR-497 as therapeutic targets

Multiple research groups have successfully delivered miRNA mimics in vivo to treat preclinical models of human cancer (277). In fact, there are multiple companies with patented technologies for delivering miRNA mimics that are currently in clinical trials. Perhaps the most advanced compound is mRX34, a miR-34 mimic encapsulated in a lipid carrier, which is currently being marketed by Mirna Therapeutics (278, 279). In this study, we were unable to effectively treat xenograft lesions using synthetic delivery of miR-30c-2* nor miR-497. In previous studies in vivo JETPEI had been successfully used to deliver oligos, including miRNA mimics, to xenograft tumors. The effectiveness of this treatment appears to be limited due to the limited delivery of the mimics to the tumor tissues, and significant accumulation in the liver. We therefore focused our attention on identifying downstream targets of miR-30c-2* and mR-497 as an alternative means for identifying potential therapeutic interventions.

We utilized an unbiased proteomics approach to identify pathways that are targeted by miR-30c-2* and miR-497 in cuSCC cells, which may mediate the observed biological effects. In addition, global proteomic profiling is a more direct high throughput method for identifying bona fide miRNA targets (280). Through these experiments we found that miR-30c-2* inhibited the activity of multiple pathways, including pathways related to ErbB signaling. The ErbB family of receptor tyrosine receptors has been implicated in the pathogenesis of SCC, most notably EGFR (68), which is mutated or amplified in a large percentage of different SCC subtypes, including cuSCC (281). Following miR-497 overexpression, we found significant enrichment for pathways related to the regulation of mitotic progression,

including Mitotic Roles of Polo-like kinase and Cell Cycle: G2/M DNA Damage Checkpoint Regulation. These proteomic changes are in accordance with the observed phenotypes of cells transfected with the corresponding miRNA mimic.

Interestingly, the only previously published targets of either miRNA that were detected in these experiments included the miR-497 targets ANLN and CDK6 (243, 244). One potential mechanistic explanation for the dearth of previously published targets of miR-30c-2* and miR-497 in the proteomics datasets may be differential 3' UTR isoform usage (282). Additionally, the fraction of downregulated proteins in both proteomics experiments were not enriched for MREs of miR-30c-2* or miR-497. Remarkably, miRNA target prediction algorithms found that approximately equal percentages of proteins in the underexpressed and overexpressed fractions of each experimental condition were predicted to be targeted by the corresponding miRNA. This may be due to the inaccurate nature of the prediction algorithms, which may be explained by the fact that we, as a field, still have a limited understanding of the mechanisms that fully govern miRNA-mediated repression (223). Our results prove that prediction algorithms alone are insufficient for identifying bona fide miRNA targets, and highlight the requirement for experimental validation.

Despite these limitations, the prediction software afforded an initial starting point for target identification of either miRNA. We focused our search on relevant targets of miR-30c-2* and miR-497 by comparing the list of underexpressed proteins against the list of overexpressed mRNAs in the mouse TAp63$^{-/-}$ cuSCC and human cuSCC RNAseq signatures. From this analysis, we identified five targets of miR-30c-2* (FAT2, ITGA6, KIF18B, and PKMYT1) and four targets of miR-497 (AURKA,

CDK6, PKMYT1, and KIF18B). We validated the direct targeting of 4/5 targets of miR-30c-2* and all 4 targets of miR-497, through the use Western blotting and miRNA pull-down assays. Interestingly, both miR-30c-2* and miR-497 are predicted to target KIF18B, a kinesin that regulates microtubule dynamics at the plus end of microtubules (283, 284), and PKMYT1 (aka Myt1), a protein kinase that inhibits cyclin B-CDK1 activity via phosphorylation of CDK1 at T14 (285, 286).

Through the use of siRNA-mediated knockdown, we found that the inhibition of the AURKA, KIF18B, PKMYT1, and ORC1 all resembled the phenotypes of the overexpression of the corresponding miRNA. These results suggest that the observed phenotypes of miR-30c-2* and miR-497 may be at least partially mediated through the inhibition of these targets. CDK6, a serine/threonine kinase involved in cell cycle progression had been previously shown to be a direct target of miR-497 in hepatocellular carcinoma cells (241), indicating that this might be an important target of miR-497 in different cancer types. Interestingly, inhibition of CDK6 had no effect on cell growth or cell survival. This may be due to incomplete knockdown of CDK6, or compensation from other CDKs, such as CDK2 and CDK4 (287, 288). Most notably, we found that inhibition of AURKA using both siRNAs and alisertib, an FDA-approved AURKA-specific kinase inhibitor was most effective in suppressing tumor cell proliferation and inducing apoptosis in both cell lines tested.

AURKA is a member of the Aurora family of serine/threonine kinases, which play important functions in cell cycle regulation and mitotic progression. AURKA phosphorylates a number of targets, and is required for recruiting CDK1-cyclin B1 to the centrosome, where it phosphorylates CDC25B and contributes to the G2/M

transition (289). AURKA is required for proper centrosome maturation and duplication and bipolar spindle assembly (290). AURKA can also phosphorylate p53, thereby inhibiting its transcriptional activity and reducing its protein stability (291, 292). Interestingly, AURKA overexpression has also been shown to inhibit the transcriptional activity of TAp73 and p53, thereby suppressing their capacity to induce apoptosis in response to DNA damage (293). Conversely, inhibition of AURKA in cancer cell lines leads to the re-activation of TAp73 and p53-dependent apoptosis. More recent mechanistic studies have revealed that AURKA directly interacts with and phosphorylates p73 at serine 235, which inhibits the DNA-binding and transcriptional activity of p73 (294). In turn, AURKA-dependent phosphorylation of p73-S235 mediates resistance to DNA damage-induced cell death.

In this study, we found that that inhibition of AURKA resulted in a phenotype that was reminiscent of mitotic catastrophe, similar to previously reported phenotypes observed in other cancer cell types (295). These include reduced proliferation and defects in spindle pole assembly and chromosome condensation (296). This in turn results in defective chromosome segregation, ultimately causing mitotic cell death (297, 298).

We also found that AURKA is frequently overexpressed in cuSCC, and that its expression shows a significant negative correlation with miR-497. Previous studies have shown that AURKA is frequently amplified and/or overexpressed in multiple human tumor types (299, 300), and that high expression levels of AURKA correlate with late clinical stage and metastasis in HNSCC (301). Likewise, we found that high AURKA expression or decreased miR-497 expression correlates with poor

survival. Given its oncogenic role, multiple AURKA inhibitors have been entered into clinical trials (302). Perhaps the most efficacious of these inhibitors is alisertib, which is an AURKA-specific inhibitor. Likewise, we found that inhibiting AURKA with alisertib was highly effective in suppressing cuSCC cell growth and inducing cell death. These results are notable, as targeting AURKA using alisertib, or any other small molecule, has yet to have been pursued as a possible treatment option for human cuSCC. Given the lack of FDA approved targeted therapies for advanced cuSCC, this study may command further preclinical testing of AURKA inhibition in the treatment of human cuSCC.

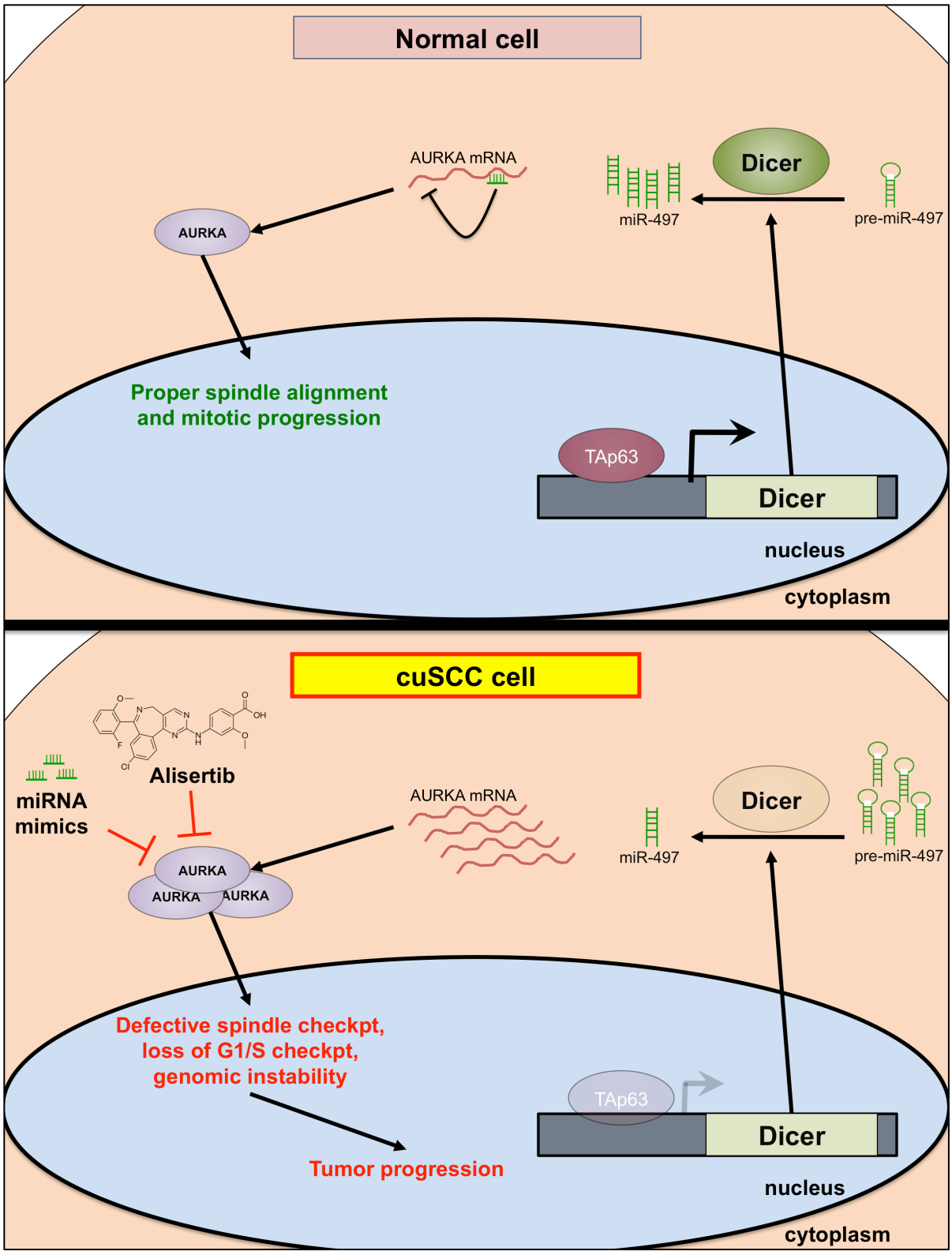

Figure 26: Final Model. In normal cells, TAp63 promotes Dicer expression via direct transactivation. Dicer, in turn, facilitates the maturation of miRNAs, including

miR-497. These miRNAs can then inhibit the translation of select mRNAs, many of which exhibit oncogenic functions. In this study, I found that miR-497 maintains proper AURKA expression levels, which is necessary for proper centrosome maturation, spindle alignment, and chromosome segregation during mitosis. In cuSCC, however, TAp63 and Dicer expression is significantly reduced. As a result, the maturation of tumor suppressive miRNAs, including miR-497 is compromised. This leads to the de-repression of mRNAs, such as AURKA. Overexpression of these targets may promote pro-oncogenic processes, such as inappropriate proliferation and aneuploidy. Through this study, I have shown that the re-introduction of miR-30c-2* or miR-497 can suppress cuSCC survival and proliferation. Additionally, inhibition of the miR-497 target AURKA was found to suppress cuSCC growth and induce mitotic cell death. Together, the results of this study suggest that this regulatory axis may present a novel avenue for therapeutic intervention for the treatment of SCC.

5.4. Investigating the putative cell of origin for cuSCC

In addition to regulating miRNA expression, our lab and others have discovered essential roles for p63 isoforms in the regulation of multiple stem cell types in the skin and other tissues. While ΔNp63 isoforms appear to be critical for maintaining basal keratinocytes (173, 257), our laboratory has previously shown that TAp63 is critical for maintaining the replicative potential of hair follicle stem cells within the skin (14). These observations are of particular interest, given that multiple studies suggest that hair follicle stem cells could serve as the cancer cell of origin for cuSCC (234, 235, 303, 304). SOX2, a transcription factor with established roles in stem cells including SKPs (14, 258), is frequently overexpressed in human SCCs of the skin, lung, head and neck, and others (73, 259). Recent studies have also shown that SOX2 functions as regulator of cancer initiation and stemness in cuSCC (232, 233). Given their regulation by TAp63 and SOX2, I hypothesized that SKP cells may serve be a potential cell of origin in cutaneous SCC. In addition, I hypothesized that TAp63 may prevent the transformation of SKP cells, and thereby prevent cuSCC initiation. To test these hypotheses, I developed a novel lineage-tracing model to evaluate the tumor initiating abilities of $SOX2^+$ SKP cells in vivo. As of the date of this publication, we have only analyzed tumor development in a subset of our cohort, which developed a small number of papillomas and cuSCC. In vivo imaging and immunohistochemical staining demonstrated however, that the majority of developed tumors were GFP-negative. These results suggest that the tumors generated in this study originated in a SOX2-negative precursor, suggesting that SOX2-positive SKP cells may not be cell of origin for cuSCC. The technical limitations of these studies

however preclude one from drawing a definitive conclusion about the tumor initiating potential of this stem cell compartment. Moreover, it is difficult to know precisely how efficiently the endogenous SKP cells underwent Cre-mediated recombination. It is also unclear if the SKP cells that successfully undergo recombination are preserved long enough to experience sufficient oncogenic changes (e.g. mutations), as a result of UVR-treatment. While we did detect GFP positive hair follicles in mice after as much as 44 weeks 4OHT treatment, it is uncertain if these cells are exposed to sufficiently mutagenic UVR. Moreover, we have only analyzed a small proportion of the UVR-treated cohort. We are currently irradiating more mice and are in the process of fully characterizing the histopathological characteristics of the resulting tumors that arise.

5.5. TAp73 suppresses lung adenocarcinoma development and progression

Similar to TAp63, TAp73 has been show to play a very important role in tumor suppression. Previous studies found that germline deletion of TAp73 in mice leads to the development of lung adenocarcinomas and lymphoma (185). Given these observations, I have utilized an in vivo lung tumorigenesis model to test the effect of TAp73 deletion on lung tumor formation. To do so, I generated cohorts of mice bearing the following genotypes: 1) $TAp73^{fltd/fltd}$ 2) $Kras^{LSLG12D/+}$ and 3) $TAp73^{fltd/fltd}$; $Kras^{LSLG12D/+}$. These mice were treated with intratracheal delivery of adenovirus expressing Cre (Ad-Cre) or empty vector (Ad-Empty). Thirty weeks after intratracheal delivery of adenovirus, the mice were euthanized, necropsied, and analyzed for the presence of lung tumors. Supporting the notion that TAp73 functions as a tumor suppressor, we found that the Ad-Cre infected $TAp73^{fltd/fltd}$;

Kras$^{LSLG12D/+}$ mice showed a significant increase in tumor burden compared to the *Kras*$^{LSLG12D/+}$ mice. Upon closer histopathological examination, I found that there was a significant increase in the proportion of high grade tumors (e.g. grade 3 and 4) in *TAp73*$^{fltd/fltd}$*; Kras*$^{LSLG12D/+}$ mice compared to *Kras*$^{LSLG12D/+}$ mice (208). These results indicate that TAp73 may prevent the initiation and progression of Kras-driven LUAC.

5.6. Digital pathology and deep learning in preclinical models of LUAC

Manual grading of murine lung tumors and subsequent quantification showed that there was a significant increase in the proportion of high-grade tumors (e.g. Grade 3 and Grade 4) (208) in tumors that developed in *TAp73*$^{fltd/fltd}$*; Kras*$^{LSLG12D/+}$ mice compared to *Kras*$^{LSLG12D/+}$. This quantification step, however, is laborious, and prone to inaccuracies and possibly low reproducibility. Attempts to automate the grading of these tumors using commercial software however were unsuccessful. Therefore, in collaboration with the Analytical Microscopy and IRAT cores at Moffitt Cancer Center, we aim to develop a Deep learning algorithm for digital pathology image analysis of mouse lung tumor images. Such a system would allow us to automate tissue and tumor segmentation.

An initial cohort of mice will be utilized as a training set for the development of the tumor segmentation and grading algorithms. We have infected a larger validation cohort of mice (each genotype consisting of more than 10 mice). These mice will be euthanized at the 30-week post-infection time point and processed as described above. Tumor sections will be stained using H&E and various immunohistochemical stainings. Slides will be imaged in collaboration with the Analytical Microscopy core,

and subsequently quantified using the newly developed algorithms. Parameters that we are interested in quantifying include the number of tumors per tissue area, percentage of tumor area, distribution of tumor grades, percentage stained cells, staining intensity, etc. By utilizing serial sections of FFPE tissues, we aim to quantify multiple parameters for individual tumors. This would allow for the correlation of histopathological, molecular, and immunological characteristics of hundreds of individual tumors, and provide massive amounts of statistical power to preclinical studies.

This would improve the accuracy of image analysis, reduce observer bias, and save researcher time. The conditional lung tumor model employed in this project is widely used in preclinical studies of NSCLC (206, 208, 209, 211, 214, 231, 252, 305). Identification of lung micrometastases is also frequently scored in other studies examining the underlying biology of tumor metastasis. Therefore, other research labs would stand to benefit from automated digital pathology that is tailored to mouse lung tissue segmentation.

5.7. TAp73 as a putative regulator of adaptive anti-tumor immune responses

Early studies in mice suggested that p73 may play a role in normal immune cell functions. These observations were most clearly demonstrated in *Trp73*$^{-/-}$ mice, which frequently die from infections just a few weeks after birth (183). Subsequent studies demonstrated these functions may be isoform-specific. For example, *TAp73*$^{-/-}$ mice are significantly more sensitive to lipopolysaccharide challenge, showing higher levels of proinflammatory cytokines in the blood and greater mortality

compared to wild-type mice (10). In addition, *TAp73*$^{-/-}$ macrophages were found to secrete higher levels of TNFα, IL-6, and macrophage inflammatory protein-2. These observations suggest that the loss of TAp73 favors the M1 effector phenotype, as opposed to the M2 phenotype. In turn, the normal progression of the inflammatory response is dysregulated.

To determine if the loss of TAp73 facilitates a pro-tumorigenic immune environment, we utilized immunohistochemical (IHC) stainings to profile various immune markers in the lungs of Ad-Cre infected mice. Through these studies we found that TAp73-deficient lesions exhibited significant increases in CD31 staining, indicating increased angiogenesis in these tumors. Interestingly, there are conflicting studies relating to the function of TAp73 in the regulation of cellular responses to hypoxia, including angiogenesis (253, 254, 306). Our results are in accordance with previous studies, which have shown that TAp73 inhibits angiogenesis in tumors (253, 254). Specifically, Amelio et al. suggest that TAp73 inhibits tumor angiogenesis through the degradation of HIF1α, which is in line with our data. Liekwise, Stantic et al found that the loss of TAp73 leads to highly vascularized tumors, and that the inhibition of TAp73 leads to increased HIF1α and HIF1α target genes. Loss of ΔNp73, on the other hand caused a reduction in tumor vascularization. Conversely, Dulloo et al. suggests that TAp73 is induced by hypoxia and, in turn, regulates the transcription of pro-angiogenic genes, including *vegf-A* (306). Nevertheless, our data highlights the anti-angiogenic functions of TAp73, particularly in the context of autochthonous lung tumors.

In addition to increased tumor angiogenesis, we also found that TAp73-deficient tumors exhibit reduced T cell infiltration, as demonstrated by significant reductions in intratumoral CD3+, CD4+ and CD8+ cells. The expression of intratumoral PD-L1 and FOXP3, however, showed no significant changes between either genotype. These observations suggest that the observed decrease in the infiltration of T cells was not due to the dysregulation of these immune checkpoint signals. Taken together, these results suggest that TAp73-deficient tumors are able to evade adaptive anti-tumor immune responses, through an as of yet unidentified mechanism.

To ascertain the mechanism through which TAp73-deficient tumor cells evade anti-tumor immunity, we employed a lentiviral based Crispr/Cas9 strategy to delete TAp73 in the A549 human LUAC cell line. Using this strategy, we were able to generate a single A549 cell line that exhibited a deletion in exon 2 of TAp73 (*A549-sgTAp73*), resulting in a frameshift mutation and a near total loss of TAp73 expression. We then profiled conditioned media from A549-sgTAp73 and A549-Cas9 for the secretion of a large proportion of the known human cytokines. Using this strategy, we found that the secretion of a subset of cytokines is significantly affected in the A549-sgTAp73 cells. The most significantly affected change we found was increased IL-6 secretion in TAp73-deficient cells. We are currently collaborating with an immunologist to better characterize the putative mechanisms through which these deregulated cytokines may impact T cell infiltration and anti-tumor responses.

5.8. Conclusions and future directions

The p53 family of transcription factors regulates a vast transcriptional network, which is important for normal development and tumor suppression. These processes include, but are not limited to, cell cycle arrest, senescence, apoptosis, and metabolic regulation. The presence of multiple, complex isoforms of p53, p63 and p73, however, have made it difficult to understand the specific functions of these genes in various contexts. While p53, TAp63, and TAp73 can transactivate the expression of genes involved in tumor suppressive pathways, the N-terminally truncated isoforms, ΔNp63 and ΔNp73, can suppress this transcriptional activation. In line with these observations, I have been able to demonstrate that the full-length TAp63 and TAp73 isoforms function as tumor suppressors in cuSCC and LUAC.

First, I have found that TAp63 functions as a tumor suppressor in cuSCC through the regulation of miRNAs. Identified miR-30c-2* and miR-497 as being positively regulated by TAp63 through Dicer-dependent processing. These two miRNAs may present novel therapeutic targets in human cuSCC. Moreover, through the integration of next generation RNA sequencing and quantitative proteomics, I have identified multiple, novel direct targets of these miRNAs. In turn, I have found that these targets may be functionally relevant to the initiation and progression of cuSCC. Among these targets are several kinases, for which there are FDA-approved small molecule inhibitors. My results suggest that among these targets, the serine/threonine kinase AURKA may be the most promising target for therapeutic intervention. Alisertib, which is an FDA-approved AURKA inhibitor, is currently being

investigated as a targeted therapy in multiple solid tumor types, however it has not been tested in human cuSCC.

Likewise, I have shown that TAp73 functions as a tumor suppressor in the lung epithelium. Through the use of a well-characterized mouse model of LUAC, I have found that the loss of TAp73 accelerates the initiation and progression of oncogenic Kras-driven LUAC. Further characterization of the resulting tumors suggests TAp73 may mediate tumor suppression through cell- and non-cell-autonomous mechanisms. Interestingly, the loss of TAp73 in oncogenic Kras-driven LUAC appears to inactivate anti-tumor adaptive immune responses, which may account for the increased tumor burden in these mice. In addition, inhibition of TAp73 expression in human LUAC cell lines resulted in increased invasion and migration. Together, these observations suggest that TAp73 may regulate multiple pathways that prevent the initiation and progression of LUAC.

Altogether, my thesis research has uncovered novel functions of TAp63 and TAp73, highlighting the important roles these genes play in tumor suppression. Future research should focus on understanding the molecular mechanisms that regulate the isoform-specific functions of p63 and p73 in different cellular contexts and disease states. Current work in our laboratory aims to uncover the molecular biology that regulates the functions of the p53 family in human cancer. These studies, in addition my thesis research, reveal new avenues for investigating novel targeted therapies and diagnostic biomarkers.

Appendix 1: Genetically engineered mouse models harboring mutations in the p53 family members.

Genotype*:	Phenotypes: Development:	Tumorigenesis:	References:
Trp53$^{-/-}$ (tm1Tyj)	Perinatal lethality	Lymphoma, testicular teratoma, sarcomas	(307)
Trp53$^{+/-}$ (tm1Tyj)	Intestinal polyps	Lymphoma, carcinomas, sarcomas	(307)
Trp63$^{-/-}$ (tm1Fmc)	Incomplete limb development, craniofacial malformations, near complete lack of epidermis*	unknown	(55)
Trp63$^{-/-}$ (tm1Brd)	Incomplete limb development, craniofacial malformations, complete lack of epidermis*	unknown	(23)
Trp63$^{+/-}$ (tm1Fmc)	Premature aging	Lung adenoma, squamous cell carcinoma, hystiocytic sarcoma	(184)
Trp63$^{+/-}$ (tm1Brd)	Premature aging	Epithelial hyperplasia	(308)
Trp73$^{+/-}$ (tm1Fmc)	Developmentally normal	Lymphoma, lung adenocarcinoma, hemangiosarcoma	(184)
Trp73$^{-/-}$ (tm1Fmc)	Postnatal lethality, decreased body size, chronic inflammation, rhinitis, intracranial hemorrhage, hydrocephaly, hipoocampal dysgenesis	Lung adenocarcinoma	(183)
Trp63$^{+/-}$ (tm1Fmc); Trp73$^{+/-}$ (tm1Fmc)	Premature aging, partial paralysis	Metastatic sarcomas and carcinomas, osteosarcoma, rhabdomyosarcoma, hemangiosarcoma, mammary adenocarcinoma, lung adenocarcinoma, salivary adenoma, squamous cell carcinoma, leukemia, lymphoma	(184)
Trp53$^{+/-}$ (tm1Tyj); Trp63$^{+/-}$ (tm1Fmc)	Premature aging	Metastatic sarcomas and carcinomas, osteosarcoma, rhabdomyosarcoma, mammary adenocarcinoma, squamous cell carcinoma, leukemia, transitional cell carcinoma	(184)
Trp53$^{+/-}$ (tm1Tyj); Trp73$^{+/-}$ (tm1Fmc)	Premature aging	Metastatic sarcomas and carcinomas, osteosarcoma, hemangiosarcoma, lung adenocarcinoma, pancreatic adenocarcinoma, hepatocellular carcinoma, lymphoma	(184)

Appendix 2: Genetically engineered mouse models harboring isoform-specific deletions of p63 and p73

Genotype*:	Phenotypes: Development:	Tumorigenesis:	References:
TAp63$^{-/-}$ (tm1.1Elrf)	Fertility defects, skin blistering, wound-healing defects, decreased hair follicle morphogenesis, premature aging, diabetes and obesity	Metastatic sarcomas and carcinomas, osteosarcoma, histocytic sarcoma, rhabdomyosarcoma, angiosarcoma, lung adenocarcinoma, hepatocellular carcinoma, mammary adenocarcinoma, squamous cell carcinoma, transitional cell carcinoma, lymphoma	(7, 14, 147)
TAp63$^{+/-}$ (tm1.1Elrf)	unknown	Metastatic sarcomas and carcinomas, osteosarcoma, histocytic sarcoma, rhabdomyosarcoma, angiosarcoma, lung adenocarcinoma, mammary adenocarcinoma, squamous cell carcinoma, lymphoma	(147)
TAp63$^{-/-}$ (tm2Fmc)	Oocytes are resistant to DNA damage	unknown	(309)
TAp63$^{-/-}$ (tm2.1Aam)	No overt phenotypes	unknown	(3)
TAp63$^{-/-}$ (tm1.1Elrf); Trp53$^{+/-}$ (tm1Tyj)	unknown	Metastatic sarcomas and carcinomas, osteosarcoma, rhabdomyosarcoma, lung adenocarcinoma, mammary adenocarcinoma, squamous cell carcinoma, transitional cell carcinoma, thyroid carcinoma, lymphoma	(147)
TAp63$^{+/-}$ (tm1.1Elrf); Trp53$^{+/-}$ (tm1Tyj)	unknown	Metastatic sarcomas and carcinomas, osteosarcoma, histocytic sarcoma, rhabdomyosarcoma, angiosarcoma, lung adenocarcinoma, mammary adenocarcinoma, squamous cell carcinoma, transitional cell carcinoma, lymphoma	(147)
TAp63$^{+/-}$ (tm1.1Elrf); Trp53$^{-/-}$ (tm1Tyj)	unknown	Metastatic sarcomas and carcinomas, osteosarcoma, histocytic sarcoma, rhabdomyosarcoma, angiosarcoma, mammary adenocarcinoma, squamous cell carcinoma, lymphoma, CML	(147)
TAp63$^{-/-}$ (tm1.1Elrf); Trp53$^{-/-}$ (tm1Tyj)	unknown	Metastatic sarcomas and carcinomas, osteosarcoma, histocytic sarcoma, rhabdomyosarcoma, angiosarcoma, lung adenocarcinoma, mammary adenocarcinoma, squamous cell carcinoma, intestinal carcinoma, salivary carcinoma, lymphoma	(147)
TAp73$^{-/-}$ (tm1Mak)	Infertility; prenatal lethality, hippocampal dysgenesis	Lung adenocarcinoma, lymphoma, colon carcinoma	(185)
TAp73$^{+/-}$ (tm1Mak)	unknown	Lung adenocarcinoma, thymic lymphoma, colon carcinoma, hemangiosarcoma	(185)

Appendix 3: Differentially expressed miRNAs in both mouse TAp63$^{-/-}$ cuSCC and human cuSCC.

	Mouse miRNA:	Expression fold change: *TAp63*$^{-/-}$ mouse SCC vs. skin	Human miRNA:	Fold change: Human SCC vs. skin
1	mmu-mir-338-5p	0.167679401	hsa-mir-338-5p	0.432580953
2	mmu-mir-30c-2-3p	0.352337693	hsa-mir-30c-2-3p	0.52321724
3	mmu-mir-146b-5p	0.453765561	hsa-mir-146b-5p	0.564316928
4	mmu-mir-145a-5p	0.578539783	hsa-mir-145-5p	0.245186413
5	mmu-mir-497-5p	0.581987169	hsa-mir-497-5p	0.562252492
6	mmu-mir-27b-3p	1.593852492	hsa-mir-27b-3p	1.814517203
7	mmu-mir-151-3p	1.972782325	hsa-mir-151a-3p	2.076184467
8	mmu-mir-27b-5p	2.075598463	hsa-mir-27b-5p	1.814517203
9	mmu-mir-15b-3p	2.388412156	hsa-mir-15b-3p	2.253178485
10	mmu-mir-17-3p	2.815433075	hsa-mir-17-3p	1.996950466
11	mmu-mir-106b-5p	2.891542541	hsa-mir-106b-5p	1.97486852
12	mmu-mir-93-5p	3.06542905	hsa-mir-93-5p	1.575598665
13	mmu-mir-17-5p	3.473403521	hsa-mir-17-5p	1.996950466

VITA

Andrew John Davis was born in New Britain, CT, the son of Margie Davis and Gary Michael Davis. After graduating from New Britain High School, New Britain, Connecticut in 2006, he entered Fairfield University in Fairfield, Connecticut. He received the degree of Bachelor of Science with a major in Biology from Fairfield University in May, 2010. The following year he worked as a laboratory technician at Unilever Home & Personal Care in Trumbull, Connecticut. From May 2011 until June 2012 he worked as a research assistant in the laboratory of Bing Hao, Ph.D at the University of Connecticut Health Center in Farmington, Connecticut. In August of 2012 he entered The University of Texas MD Anderson Cancer Center UTHealth Graduate School of Biomedical Sciences in Houston, Texas. In November of 2016, he and his laboratory moved to Moffitt Cancer Center in Tampa, Florida.

Permanent address:

Andrew J. Davis

15501 Bruce B. Downs Blvd.

Unit 1011

Tampa, FL 33647

REFERENCES

1. Su, X., D. Chakravarti, and E. R. Flores. 2013. p63 steps into the limelight: crucial roles in the suppression of tumorigenesis and metastasis. *Nature reviews. Cancer* 13: 136-143.

2. Beretta, C., A. Chiarelli, B. Testoni, R. Mantovani, and L. Guerrini. 2005. Regulation of the cyclin-dependent kinase inhibitor p57Kip2 expression by p63. *Cell cycle* 4: 1625-1631.

3. Guo, X., W. M. Keyes, C. Papazoglu, J. Zuber, W. Li, S. W. Lowe, H. Vogel, and A. A. Mills. 2009. TAp63 induces senescence and suppresses tumorigenesis in vivo. *Nature cell biology* 11: 1451-1457.

4. Lin, Y. L., S. Sengupta, K. Gurdziel, G. W. Bell, T. Jacks, and E. R. Flores. 2009. p63 and p73 transcriptionally regulate genes involved in DNA repair. *PLoS Genet* 5: e1000680.

5. Liu, J., M. Lin, C. Zhang, D. Wang, Z. Feng, and W. Hu. 2012. TAp63gamma enhances nucleotide excision repair through transcriptional regulation of DNA repair genes. *DNA repair* 11: 167-176.

6. Venkatanarayan, A., P. Raulji, W. Norton, D. Chakravarti, C. Coarfa, X. Su, S. K. Sandur, M. S. Ramirez, J. Lee, C. V. Kingsley, E. F. Sananikone, K. Rajapakshe, K. Naff, J. Parker-Thornburg, J. A. Bankson, K. Y. Tsai, P. H. Gunaratne, and E. R. Flores. 2014. IAPP-driven metabolic reprogramming induces regression of p53-deficient tumours in vivo. *Nature*.

7. Su, X., Y. J. Gi, D. Chakravarti, I. L. Chan, A. Zhang, X. Xia, K. Y. Tsai, and E. R. Flores. 2012. TAp63 is a master transcriptional regulator of lipid and glucose metabolism. *Cell metabolism* 16: 511-525.

8. Agostini, M., M. Annicchiarico-Petruzzelli, G. Melino, and A. Rufini. 2016. Metabolic pathways regulated by TAp73 in response to oxidative stress. *Oncotarget*.

9. Du, W., P. Jiang, A. Mancuso, A. Stonestrom, M. D. Brewer, A. J. Minn, T. W. Mak, M. Wu, and X. Yang. 2013. TAp73 enhances the pentose phosphate pathway and supports cell proliferation. *Nature cell biology* 15: 991-1000.

10. Tomasini, R., V. Secq, L. Pouyet, A. K. Thakur, M. Wilhelm, J. Nigri, S. Vasseur, P. Berthezene, E. Calvo, G. Melino, T. W. Mak, and J. L. Iovanna. 2013. TAp73 is required for macrophage-mediated innate immunity and the resolution of inflammatory responses. *Cell death and differentiation* 20: 293-301.

11. Vikhreva, P., V. Petrova, T. Gokbulut, I. Pestlikis, M. Mancini, N. Di Daniele, R. A. Knight, G. Melino, and I. Amelio. 2017. TAp73 upregulates IL-1beta in cancer cells: Potential biomarker in lung and breast cancer? *Biochemical and biophysical research communications* 482: 498-505.

12. Kakuki, T., M. Kurose, K. I. Takano, A. Kondoh, K. Obata, K. Nomura, R. Miyata, Y. Kaneko, T. Konno, S. Takahashi, T. Hatakeyama, T. Kohno, T. Himi, and T. Kojima. 2016. Dysregulation of junctional adhesion molecule-A via p63/GATA-3 in head and neck squamous cell carcinoma. *Oncotarget*.

13. Carroll, D. K., J. S. Carroll, C. O. Leong, F. Cheng, M. Brown, A. A. Mills, J. S. Brugge, and L. W. Ellisen. 2006. p63 regulates an adhesion programme and cell survival in epithelial cells. *Nature cell biology* 8: 551-561.

14. Su, X., M. Paris, Y. J. Gi, K. Y. Tsai, M. S. Cho, Y. L. Lin, J. A. Biernaskie, S. Sinha, C. Prives, L. H. Pevny, F. D. Miller, and E. R. Flores. 2009. TAp63 prevents premature aging by promoting adult stem cell maintenance. *Cell stem cell* 5: 64-75.

15. De Laurenzi, V., A. Rossi, A. Terrinoni, D. Barcaroli, M. Levrero, A. Costanzo, R. A. Knight, P. Guerrieri, and G. Melino. 2000. p63 and p73 transactivate differentiation gene promoters in human keratinocytes. *Biochemical and biophysical research communications* 273: 342-346.

16. Truong, A. B., M. Kretz, T. W. Ridky, R. Kimmel, and P. A. Khavari. 2006. p63 regulates proliferation and differentiation of developmentally mature keratinocytes. *Genes & development* 20: 3185-3197.

17. Borrelli, S., E. Candi, B. Hu, D. Dolfini, M. Ravo, O. M. Grober, A. Weisz, G. P. Dotto, G. Melino, M. A. Vigano, and R. Mantovani. 2010. The p63 target HBP1 is required for skin differentiation and stratification. *Cell death and differentiation* 17: 1896-1907.

18. Yi, R., M. N. Poy, M. Stoffel, and E. Fuchs. 2008. A skin microRNA promotes differentiation by repressing 'stemness'. *Nature* 452: 225-229.

19. Deyoung, M. P., and L. W. Ellisen. 2007. p63 and p73 in human cancer: defining the network. *Oncogene* 26: 5169-5183.

20. Rufini, A., M. Agostini, F. Grespi, R. Tomasini, B. S. Sayan, M. V. Niklison-Chirou, F. Conforti, T. Velletri, A. Mastino, T. W. Mak, G. Melino, and R. A. Knight. 2011. p73 in Cancer. *Genes & cancer* 2: 491-502.

21. Yang, A., M. Kaghad, Y. Wang, E. Gillett, M. D. Fleming, V. Dotsch, N. C. Andrews, D. Caput, and F. McKeon. 1998. p63, a p53 homolog at 3q27-29, encodes

multiple products with transactivating, death-inducing, and dominant-negative activities. *Molecular cell* 2: 305-316.

22. Liefer, K. M., M. I. Koster, X. J. Wang, A. Yang, F. McKeon, and D. R. Roop. 2000. Down-regulation of p63 is required for epidermal UV-B-induced apoptosis. *Cancer research* 60: 4016-4020.

23. Mills, A. A., B. Zheng, X. J. Wang, H. Vogel, D. R. Roop, and A. Bradley. 1999. p63 is a p53 homologue required for limb and epidermal morphogenesis. *Nature* 398: 708-713.

24. Flores, E. R., K. Y. Tsai, D. Crowley, S. Sengupta, A. Yang, F. McKeon, and T. Jacks. 2002. p63 and p73 are required for p53-dependent apoptosis in response to DNA damage. *Nature* 416: 560-564.

25. Belloni, L., F. Moretti, P. Merlo, A. Damalas, A. Costanzo, G. Blandino, and M. Levrero. 2006. DNp73alpha protects myogenic cells from apoptosis. *Oncogene* 25: 3606-3612.

26. Jost, C. A., M. C. Marin, and W. G. Kaelin, Jr. 1997. p73 is a simian [correction of human] p53-related protein that can induce apoptosis. *Nature* 389: 191-194.

27. Ghioni, P., F. Bolognese, P. H. Duijf, H. Van Bokhoven, R. Mantovani, and L. Guerrini. 2002. Complex transcriptional effects of p63 isoforms: identification of novel activation and repression domains. *Molecular and cellular biology* 22: 8659-8668.

28. King, K. E., R. M. Ponnamperuma, T. Yamashita, T. Tokino, L. A. Lee, M. F. Young, and W. C. Weinberg. 2003. deltaNp63alpha functions as both a positive and

a negative transcriptional regulator and blocks in vitro differentiation of murine keratinocytes. *Oncogene* 22: 3635-3644.

29. Chakravarti, D., X. Su, M. S. Cho, N. H. Bui, C. Coarfa, A. Venkatanarayan, A. L. Benham, R. E. Flores Gonzalez, J. Alana, W. Xiao, M. L. Leung, H. Vin, I. L. Chan, A. Aquino, N. Muller, H. Wang, A. J. Cooney, J. Parker-Thornburg, K. Y. Tsai, P. H. Gunaratne, and E. R. Flores. 2014. Induced multipotency in adult keratinocytes through down-regulation of DeltaNp63 or DGCR8. *Proceedings of the National Academy of Sciences of the United States of America* 111: E572-581.

30. Keyes, W. M., M. Pecoraro, V. Aranda, E. Vernersson-Lindahl, W. Li, H. Vogel, X. Guo, E. L. Garcia, T. V. Michurina, G. Enikolopov, S. K. Muthuswamy, and A. A. Mills. 2011. DeltaNp63alpha is an oncogene that targets chromatin remodeler Lsh to drive skin stem cell proliferation and tumorigenesis. *Cell stem cell* 8: 164-176.

31. Rocco, J. W., C. O. Leong, N. Kuperwasser, M. P. DeYoung, and L. W. Ellisen. 2006. p63 mediates survival in squamous cell carcinoma by suppression of p73-dependent apoptosis. *Cancer cell* 9: 45-56.

32. Westfall, M. D., D. J. Mays, J. C. Sniezek, and J. A. Pietenpol. 2003. The Delta Np63 alpha phosphoprotein binds the p21 and 14-3-3 sigma promoters in vivo and has transcriptional repressor activity that is reduced by Hay-Wells syndrome-derived mutations. *Molecular and cellular biology* 23: 2264-2276.

33. Napoli, M., A. Venkatanarayan, P. Raulji, B. A. Meyers, W. Norton, L. S. Mangala, A. K. Sood, C. Rodriguez-Aguayo, G. Lopez-Berestein, H. Vin, M. Duvic, M. B. Tetzlaff, J. L. Curry, A. H. Rook, H. A. Abbas, C. Coarfa, P. H. Gunaratne, K.

Y. Tsai, and E. R. Flores. 2016. DeltaNp63/DGCR8-Dependent MicroRNAs Mediate Therapeutic Efficacy of HDAC Inhibitors in Cancer. *Cancer cell* 29: 874-888.

34. Venkatanarayan, A., P. Raulji, W. Norton, and E. R. Flores. 2015. Novel therapeutic interventions for p53-altered tumors through manipulation of its family members, p63 and p73. *Cell cycle*: 0.

35. Chuong, C. M., and A. Noveen. 1999. Phenotypic determination of epithelial appendages: genes, developmental pathways, and evolution. *The journal of investigative dermatology. Symposium proceedings / the Society for Investigative Dermatology, Inc. [and] European Society for Dermatological Research* 4: 307-311.

36. Hsu, Y. C., L. Li, and E. Fuchs. 2014. Emerging interactions between skin stem cells and their niches. *Nature medicine* 20: 847-856.

37. Moll, R., W. W. Franke, D. L. Schiller, B. Geiger, and R. Krepler. 1982. The catalog of human cytokeratins: patterns of expression in normal epithelia, tumors and cultured cells. *Cell* 31: 11-24.

38. Bickenbach, J. R., J. M. Greer, D. S. Bundman, J. A. Rothnagel, and D. R. Roop. 1995. Loricrin expression is coordinated with other epidermal proteins and the appearance of lipid lamellar granules in development. *The Journal of investigative dermatology* 104: 405-410.

39. Blanpain, C., W. E. Lowry, A. Geoghegan, L. Polak, and E. Fuchs. 2004. Self-renewal, multipotency, and the existence of two cell populations within an epithelial stem cell niche. *Cell* 118: 635-648.

40. Horsley, V., D. O'Carroll, R. Tooze, Y. Ohinata, M. Saitou, T. Obukhanych, M. Nussenzweig, A. Tarakhovsky, and E. Fuchs. 2006. Blimp1 defines a progenitor population that governs cellular input to the sebaceous gland. *Cell* 126: 597-609.

41. Jensen, K. B., C. A. Collins, E. Nascimento, D. W. Tan, M. Frye, S. Itami, and F. M. Watt. 2009. Lrig1 expression defines a distinct multipotent stem cell population in mammalian epidermis. *Cell stem cell* 4: 427-439.

42. Lu, C. P., L. Polak, A. S. Rocha, H. A. Pasolli, S. C. Chen, N. Sharma, C. Blanpain, and E. Fuchs. 2012. Identification of stem cell populations in sweat glands and ducts reveals roles in homeostasis and wound repair. *Cell* 150: 136-150.

43. Watt, F. M., and P. H. Jones. 1993. Expression and function of the keratinocyte integrins. *Dev Suppl*: 185-192.

44. Green, K. J., S. Getsios, S. Troyanovsky, and L. M. Godsel. 2010. Intercellular junction assembly, dynamics, and homeostasis. *Cold Spring Harbor perspectives in biology* 2: a000125.

45. Lechler, T., and E. Fuchs. 2005. Asymmetric cell divisions promote stratification and differentiation of mammalian skin. *Nature* 437: 275-280.

46. Watt, F. M., and H. Green. 1982. Stratification and terminal differentiation of cultured epidermal cells. *Nature* 295: 434-436.

47. Gonzales, K. A. U., and E. Fuchs. 2017. Skin and Its Regenerative Powers: An Alliance between Stem Cells and Their Niche. *Developmental cell* 43: 387-401.

48. Alonso, L., and E. Fuchs. 2006. The hair cycle. *Journal of cell science* 119: 391-393.

49. Greco, V., T. Chen, M. Rendl, M. Schober, H. A. Pasolli, N. Stokes, J. Dela Cruz-Racelis, and E. Fuchs. 2009. A two-step mechanism for stem cell activation during hair regeneration. *Cell stem cell* 4: 155-169.

50. Hsu, Y. C., H. A. Pasolli, and E. Fuchs. 2011. Dynamics between stem cells, niche, and progeny in the hair follicle. *Cell* 144: 92-105.

51. Sennett, R., Z. Wang, A. Rezza, L. Grisanti, N. Roitershtein, C. Sicchio, K. W. Mok, N. J. Heitman, C. Clavel, A. Ma'ayan, and M. Rendl. 2015. An Integrated Transcriptome Atlas of Embryonic Hair Follicle Progenitors, Their Niche, and the Developing Skin. *Developmental cell* 34: 577-591.

52. Jahoda, C. A., K. A. Horne, and R. F. Oliver. 1984. Induction of hair growth by implantation of cultured dermal papilla cells. *Nature* 311: 560-562.

53. Fernandes, K. J., I. A. McKenzie, P. Mill, K. M. Smith, M. Akhavan, F. Barnabe-Heider, J. Biernaskie, A. Junek, N. R. Kobayashi, J. G. Toma, D. R. Kaplan, P. A. Labosky, V. Rafuse, C. C. Hui, and F. D. Miller. 2004. A dermal niche for multipotent adult skin-derived precursor cells. *Nature cell biology* 6: 1082-1093.

54. Toma, J. G., M. Akhavan, K. J. Fernandes, F. Barnabe-Heider, A. Sadikot, D. R. Kaplan, and F. D. Miller. 2001. Isolation of multipotent adult stem cells from the dermis of mammalian skin. *Nature cell biology* 3: 778-784.

55. Yang, A., R. Schweitzer, D. Sun, M. Kaghad, N. Walker, R. T. Bronson, C. Tabin, A. Sharpe, D. Caput, C. Crum, and F. McKeon. 1999. p63 is essential for regenerative proliferation in limb, craniofacial and epithelial development. *Nature* 398: 714-718.

56. Rinne, T., H. G. Brunner, and H. van Bokhoven. 2007. p63-associated disorders. *Cell cycle* 6: 262-268.

57. Candi, E., R. Cipollone, P. Rivetti di Val Cervo, S. Gonfloni, G. Melino, and R. Knight. 2008. p63 in epithelial development. *Cell Mol Life Sci* 65: 3126-3133.

58. Mikkola, M. L. 2007. p63 in skin appendage development. *Cell cycle* 6: 285-290.

59. Koster, M. I., D. Dai, and D. R. Roop. 2007. Conflicting roles for p63 in skin development and carcinogenesis. *Cell cycle* 6: 269-273.

60. Lena, A. M., R. Cipollone, I. Amelio, M. V. Catani, S. Ramadan, G. Browne, G. Melino, and E. Candi. 2010. Skn-1a/Oct-11 and DeltaNp63alpha exert antagonizing effects on human keratin expression. *Biochemical and biophysical research communications* 401: 568-573.

61. Ihrie, R. A., M. R. Marques, B. T. Nguyen, J. S. Horner, C. Papazoglu, R. T. Bronson, A. A. Mills, and L. D. Attardi. 2005. Perp is a p63-regulated gene essential for epithelial integrity. *Cell* 120: 843-856.

62. Koster, M. I., S. Kim, A. A. Mills, F. J. DeMayo, and D. R. Roop. 2004. p63 is the molecular switch for initiation of an epithelial stratification program. *Genes & development* 18: 126-131.

63. Nylander, K., B. Vojtesek, R. Nenutil, B. Lindgren, G. Roos, W. Zhanxiang, B. Sjostrom, A. Dahlqvist, and P. J. Coates. 2002. Differential expression of p63 isoforms in normal tissues and neoplastic cells. *The Journal of pathology* 198: 417-427.

64. Candi, E., A. Rufini, A. Terrinoni, D. Dinsdale, M. Ranalli, A. Paradisi, V. De Laurenzi, L. G. Spagnoli, M. V. Catani, S. Ramadan, R. A. Knight, and G. Melino. 2006. Differential roles of p63 isoforms in epidermal development: selective genetic complementation in p63 null mice. *Cell death and differentiation* 13: 1037-1047.

65. Romano, R. A., K. Smalley, C. Magraw, V. A. Serna, T. Kurita, S. Raghavan, and S. Sinha. 2012. DeltaNp63 knockout mice reveal its indispensable role as a master regulator of epithelial development and differentiation. *Development* 139: 772-782.

66. Nguyen, B. C., K. Lefort, A. Mandinova, D. Antonini, V. Devgan, G. Della Gatta, M. I. Koster, Z. Zhang, J. Wang, A. Tommasi di Vignano, J. Kitajewski, G. Chiorino, D. R. Roop, C. Missero, and G. P. Dotto. 2006. Cross-regulation between Notch and p63 in keratinocyte commitment to differentiation. *Genes & development* 20: 1028-1042.

67. Iso, T., L. Kedes, and Y. Hamamori. 2003. HES and HERP families: multiple effectors of the Notch signaling pathway. *J Cell Physiol* 194: 237-255.

68. Campbell, J. D., C. Yau, R. Bowlby, Y. Liu, K. Brennan, H. Fan, A. M. Taylor, C. Wang, V. Walter, R. Akbani, L. A. Byers, C. J. Creighton, C. Coarfa, J. Shih, A. D. Cherniack, O. Gevaert, M. Prunello, H. Shen, P. Anur, J. Chen, H. Cheng, D. N. Hayes, S. Bullman, C. S. Pedamallu, A. I. Ojesina, S. Sadeghi, K. L. Mungall, A. G. Robertson, C. Benz, A. Schultz, R. S. Kanchi, C. M. Gay, A. Hegde, L. Diao, J. Wang, W. Ma, P. Sumazin, H. S. Chiu, T. W. Chen, P. Gunaratne, L. Donehower, J. S. Rader, R. Zuna, H. Al-Ahmadie, A. J. Lazar, E. R. Flores, K. Y. Tsai, J. H. Zhou, A. K. Rustgi, E. Drill, R. Shen, C. K. Wong, N. Cancer Genome Atlas Research, J.

M. Stuart, P. W. Laird, K. A. Hoadley, J. N. Weinstein, M. Peto, C. R. Pickering, Z. Chen, and C. Van Waes. 2018. Genomic, Pathway Network, and Immunologic Features Distinguishing Squamous Carcinomas. *Cell reports* 23: 194-212 e196.

69. Cancer Genome Atlas Research, N., U. Analysis Working Group: Asan, B. C. C. Agency, Brigham, H. Women's, I. Broad, U. Brown, U. Case Western Reserve, I. Dana-Farber Cancer, U. Duke, C. Greater Poland Cancer, S. Harvard Medical, B. Institute for Systems, K. U. Leuven, C. Mayo, C. Memorial Sloan Kettering Cancer, I. National Cancer, H. Nationwide Children's, U. Stanford, A. University of, M. University of, C. University of North, P. University of, R. University of, C. University of Southern, M. D. A. C. C. University of Texas, W. University of, I. Van Andel Research, U. Vanderbilt, U. Washington, I. Genome Sequencing Center: Broad, L. Washington University in St, B. C. C. A. Genome Characterization Centers, I. Broad, S. Harvard Medical, U. Sidney Kimmel Comprehensive Cancer Center at Johns Hopkins, C. University of North, C. University of Southern California Epigenome, M. D. A. C. C. University of Texas, I. Van Andel Research, I. Genome Data Analysis Centers: Broad, U. Brown, S. Harvard Medical, B. Institute for Systems, C. Memorial Sloan Kettering Cancer, C. University of California Santa, M. D. A. C. C. University of Texas, C. Biospecimen Core Resource: International Genomics, H. Research Institute at Nationwide Children's, S. Tissue Source Sites: Analytic Biologic, C. Asan Medical, B. Asterand, H. Barretos Cancer, BioreclamationIvt, C. Botkin Municipal, S. Chonnam National University Medical, S. Christiana Care Health, Cureline, U. Duke, U. Emory, U. Erasmus, M. Indiana University School of, M. Institute of Oncology of, C. International Genomics, Invidumed, H. Israelitisches Krankenhaus, M. Keimyung

University School of, C. Memorial Sloan Kettering Cancer, G. National Cancer Center, B. Ontario Tumour, C. Peter MacCallum Cancer, S. Pusan National University Medical, S. Ribeirao Preto Medical, H. St. Joseph's, C. Medical, U. St. Petersburg Academic, B. Tayside Tissue, D. University of, C. University of Kansas Medical, M. University of, H. University of North Carolina at Chapel, M. University of Pittsburgh School of, M. D. A. C. C. University of Texas, U. Disease Working Group: Duke, C. Memorial Sloan Kettering Cancer, I. National Cancer, M. D. A. C. C. University of Texas, M. Yonsei University College of, C. I. Data Coordination Center, and H. Project Team: National Institutes of. 2017. Integrated genomic characterization of oesophageal carcinoma. *Nature*.

70. Cancer Genome Atlas, N. 2015. Comprehensive genomic characterization of head and neck squamous cell carcinomas. *Nature* 517: 576-582.

71. Cancer Genome Atlas Research, N. 2012. Comprehensive genomic characterization of squamous cell lung cancers. *Nature* 489: 519-525.

72. Chitsazzadeh, V., C. Coarfa, J. A. Drummond, T. Nguyen, A. Joseph, S. Chilukuri, E. Charpiot, C. H. Adelmann, G. Ching, T. N. Nguyen, C. Nicholas, V. D. Thomas, M. Migden, D. MacFarlane, E. Thompson, J. Shen, Y. Takata, K. McNiece, M. A. Polansky, H. A. Abbas, K. Rajapakshe, A. Gower, A. Spira, K. R. Covington, W. Xiao, P. Gunaratne, C. Pickering, M. Frederick, J. N. Myers, L. Shen, H. Yao, X. Su, R. P. Rapini, D. A. Wheeler, E. T. Hawk, E. R. Flores, and K. Y. Tsai. 2016. Cross-species identification of genomic drivers of squamous cell carcinoma development across preneoplastic intermediates. *Nature communications* 7: 12601.

73. Hoadley, K. A., C. Yau, D. M. Wolf, A. D. Cherniack, D. Tamborero, S. Ng, M. D. Leiserson, B. Niu, M. D. McLellan, V. Uzunangelov, J. Zhang, C. Kandoth, R. Akbani, H. Shen, L. Omberg, A. Chu, A. A. Margolin, L. J. Van't Veer, N. Lopez-Bigas, P. W. Laird, B. J. Raphael, L. Ding, A. G. Robertson, L. A. Byers, G. B. Mills, J. N. Weinstein, C. Van Waes, Z. Chen, E. A. Collisson, N. Cancer Genome Atlas Research, C. C. Benz, C. M. Perou, and J. M. Stuart. 2014. Multiplatform Analysis of 12 Cancer Types Reveals Molecular Classification within and across Tissues of Origin. *Cell* 158: 929-944.

74. Schwaederle, M., S. K. Elkin, B. N. Tomson, J. L. Carter, and R. Kurzrock. 2015. Squamousness: Next-generation sequencing reveals shared molecular features across squamous tumor types. *Cell cycle* 14: 2355-2361.

75. Miller, D. L., and M. A. Weinstock. 1994. Nonmelanoma skin cancer in the United States: incidence. *Journal of the American Academy of Dermatology* 30: 774-778.

76. Rogers, H. W., M. A. Weinstock, A. R. Harris, M. R. Hinckley, S. R. Feldman, A. B. Fleischer, and B. M. Coldiron. 2010. Incidence estimate of nonmelanoma skin cancer in the United States, 2006. *Archives of dermatology* 146: 283-287.

77. Rowe, D. E., R. J. Carroll, and C. L. Day, Jr. 1992. Prognostic factors for local recurrence, metastasis, and survival rates in squamous cell carcinoma of the skin, ear, and lip. Implications for treatment modality selection. *Journal of the American Academy of Dermatology* 26: 976-990.

78. Liu, L. S., and O. R. Colegio. 2013. Molecularly targeted therapies for nonmelanoma skin cancers. *Int J Dermatol* 52: 654-665.

79. Housman, T. S., S. R. Feldman, P. M. Williford, A. B. Fleischer, Jr., N. D. Goldman, J. M. Acostamadiedo, and G. J. Chen. 2003. Skin cancer is among the most costly of all cancers to treat for the Medicare population. *Journal of the American Academy of Dermatology* 48: 425-429.

80. Koh, H. K., A. C. Geller, D. R. Miller, T. A. Grossbart, and R. A. Lew. 1996. Prevention and early detection strategies for melanoma and skin cancer. Current status. *Archives of dermatology* 132: 436-443.

81. Agrawal, N., M. J. Frederick, C. R. Pickering, C. Bettegowda, K. Chang, R. J. Li, C. Fakhry, T. X. Xie, J. Zhang, J. Wang, N. Zhang, A. K. El-Naggar, S. A. Jasser, J. N. Weinstein, L. Trevino, J. A. Drummond, D. M. Muzny, Y. Wu, L. D. Wood, R. H. Hruban, W. H. Westra, W. M. Koch, J. A. Califano, R. A. Gibbs, D. Sidransky, B. Vogelstein, V. E. Velculescu, N. Papadopoulos, D. A. Wheeler, K. W. Kinzler, and J. N. Myers. 2011. Exome sequencing of head and neck squamous cell carcinoma reveals inactivating mutations in NOTCH1. *Science* 333: 1154-1157.

82. Stransky, N., A. M. Egloff, A. D. Tward, A. D. Kostic, K. Cibulskis, A. Sivachenko, G. V. Kryukov, M. S. Lawrence, C. Sougnez, A. McKenna, E. Shefler, A. H. Ramos, P. Stojanov, S. L. Carter, D. Voet, M. L. Cortes, D. Auclair, M. F. Berger, G. Saksena, C. Guiducci, R. C. Onofrio, M. Parkin, M. Romkes, J. L. Weissfeld, R. R. Seethala, L. Wang, C. Rangel-Escareno, J. C. Fernandez-Lopez, A. Hidalgo-Miranda, J. Melendez-Zajgla, W. Winckler, K. Ardlie, S. B. Gabriel, M. Meyerson, E. S. Lander, G. Getz, T. R. Golub, L. A. Garraway, and J. R. Grandis. 2011. The mutational landscape of head and neck squamous cell carcinoma. *Science* 333: 1157-1160.

83. Welsh, M. M., M. R. Karagas, K. M. Applebaum, S. K. Spencer, A. E. Perry, and H. H. Nelson. 2008. A role for ultraviolet radiation immunosuppression in non-melanoma skin cancer as evidenced by gene-environment interactions. *Carcinogenesis* 29: 1950-1954.

84. Brantsch, K. D., C. Meisner, B. Schonfisch, B. Trilling, J. Wehner-Caroli, M. Rocken, and H. Breuninger. 2008. Analysis of risk factors determining prognosis of cutaneous squamous-cell carcinoma: a prospective study. *The lancet oncology* 9: 713-720.

85. Martorell-Calatayud, A., O. Sanmartin Jimenez, J. Cruz Mojarrieta, and C. Guillen Barona. 2013. Cutaneous squamous cell carcinoma: defining the high-risk variant. *Actas Dermosifiliogr* 104: 367-379.

86. Cassarino, D. S., D. P. Derienzo, and R. J. Barr. 2006. Cutaneous squamous cell carcinoma: a comprehensive clinicopathologic classification--part two. *Journal of cutaneous pathology* 33: 261-279.

87. Cassarino, D. S., D. P. Derienzo, and R. J. Barr. 2006. Cutaneous squamous cell carcinoma: a comprehensive clinicopathologic classification. Part one. *Journal of cutaneous pathology* 33: 191-206.

88. Gallagher, R. P., G. B. Hill, C. D. Bajdik, A. J. Coldman, S. Fincham, D. I. McLean, and W. J. Threlfall. 1995. Sunlight exposure, pigmentation factors, and risk of nonmelanocytic skin cancer. II. Squamous cell carcinoma. *Archives of dermatology* 131: 164-169.

89. Sober, A. J., and J. M. Burstein. 1995. Precursors to skin cancer. *Cancer* 75: 645-650.

90. Anwar, J., D. A. Wrone, A. Kimyai-Asadi, and M. Alam. 2004. The development of actinic keratosis into invasive squamous cell carcinoma: evidence and evolving classification schemes. *Clin Dermatol* 22: 189-196.

91. Yanofsky, V. R., S. E. Mercer, and R. G. Phelps. 2011. Histopathological variants of cutaneous squamous cell carcinoma: a review. *Journal of skin cancer* 2011: 210813.

92. Criscione, V. D., M. A. Weinstock, M. F. Naylor, C. Luque, M. J. Eide, S. F. Bingham, and G. Department of Veteran Affairs Topical Tretinoin Chemoprevention Trial. 2009. Actinic keratoses: Natural history and risk of malignant transformation in the Veterans Affairs Topical Tretinoin Chemoprevention Trial. *Cancer* 115: 2523-2530.

93. Rossi, R., M. Mori, and T. Lotti. 2007. Actinic keratosis. *Int J Dermatol* 46: 895-904.

94. Mittelbronn, M. A., D. L. Mullins, F. A. Ramos-Caro, and F. P. Flowers. 1998. Frequency of pre-existing actinic keratosis in cutaneous squamous cell carcinoma. *Int J Dermatol* 37: 677-681.

95. Kovacs, A., K. Yonemoto, K. Katsuoka, S. Nishiyama, and I. Harhai. 1996. Bowen's disease: statistical study of a 10 year period. *J Dermatol* 23: 267-274.

96. Lee, M. M., and M. M. Wick. 1990. Bowen's disease. *CA: a cancer journal for clinicians* 40: 237-242.

97. Saxena, A., D. A. Kasper, C. D. Campanelli, J. B. Lee, T. R. Humphreys, and G. F. Webster. 2006. Pigmented Bowen's disease clinically mimicking melanoma of the nail. *Dermatol Surg* 32: 1522-1525.

98. Cox, N. H., D. J. Eedy, C. A. Morton, G. Therapy, and B. A. o. D. Audit Subcommittee. 2007. Guidelines for management of Bowen's disease: 2006 update. *The British journal of dermatology* 156: 11-21.

99. Freeman, R. G. 1984. History of the American Society of Dermatopathology. *Am J Dermatopathol* 6: 25-33.

100. Lohmann, C. M., and A. R. Solomon. 2001. Clinicopathologic variants of cutaneous squamous cell carcinoma. *Adv Anat Pathol* 8: 27-36.

101. Ulrich, M., E. Stockfleth, J. Roewert-Huber, and S. Astner. 2007. Noninvasive diagnostic tools for nonmelanoma skin cancer. *The British journal of dermatology* 157 Suppl 2: 56-58.

102. Karia, P. S., A. Jambusaria-Pahlajani, D. P. Harrington, G. F. Murphy, A. A. Qureshi, and C. D. Schmults. 2014. Evaluation of American Joint Committee on Cancer, International Union Against Cancer, and Brigham and Women's Hospital tumor staging for cutaneous squamous cell carcinoma. *Journal of clinical oncology : official journal of the American Society of Clinical Oncology* 32: 327-334.

103. Dinehart, S. M., and S. V. Pollack. 1989. Metastases from squamous cell carcinoma of the skin and lip. An analysis of twenty-seven cases. *Journal of the American Academy of Dermatology* 21: 241-248.

104. O'Bryan, K., W. Sherman, G. W. Niedt, B. Taback, S. Manolidis, A. Wang, and D. Ratner. 2013. An evolving paradigm for the workup and management of high-risk cutaneous squamous cell carcinoma. *Journal of the American Academy of Dermatology* 69: 595-602 e591.

105. Schmitt, A. R., J. D. Brewer, J. S. Bordeaux, and C. L. Baum. 2014. Staging for cutaneous squamous cell carcinoma as a predictor of sentinel lymph node biopsy results: meta-analysis of American Joint Committee on Cancer criteria and a proposed alternative system. *JAMA Dermatol* 150: 19-24.

106. Karia, P. S., J. Han, and C. D. Schmults. 2013. Cutaneous squamous cell carcinoma: estimated incidence of disease, nodal metastasis, and deaths from disease in the United States, 2012. *Journal of the American Academy of Dermatology* 68: 957-966.

107. Clayman, G. L., J. J. Lee, F. C. Holsinger, X. Zhou, M. Duvic, A. K. El-Naggar, V. G. Prieto, E. Altamirano, S. L. Tucker, S. S. Strom, M. L. Kripke, and S. M. Lippman. 2005. Mortality risk from squamous cell skin cancer. *Journal of clinical oncology : official journal of the American Society of Clinical Oncology* 23: 759-765.

108. Ross, A. S., F. M. Whalen, R. Elenitsas, X. Xu, A. B. Troxel, and C. D. Schmults. 2009. Diameter of involved nerves predicts outcomes in cutaneous squamous cell carcinoma with perineural invasion: an investigator-blinded retrospective cohort study. *Dermatol Surg* 35: 1859-1866.

109. Breuninger, H., B. Black, and G. Rassner. 1990. Microstaging of squamous cell carcinomas. *Am J Clin Pathol* 94: 624-627.

110. Ulrich, C., J. Kanitakis, E. Stockfleth, and S. Euvrard. 2008. Skin cancer in organ transplant recipients--where do we stand today? *Am J Transplant* 8: 2192-2198.

111. Silverberg, M. J., W. Leyden, E. M. Warton, C. P. Quesenberry, Jr., E. A. Engels, and M. M. Asgari. 2013. HIV infection status, immunodeficiency, and the

incidence of non-melanoma skin cancer. *Journal of the National Cancer Institute* 105: 350-360.

112. Smith, K. J., S. Hamza, and H. Skelton. 2004. Histologic features in primary cutaneous squamous cell carcinomas in immunocompromised patients focusing on organ transplant patients. *Dermatol Surg* 30: 634-641.

113. Swanson, N. A., R. C. Grekin, and S. R. Baker. 1983. Mohs surgery: techniques, indications, and applications in head and neck surgery. *Head Neck Surg* 6: 683-692.

114. Miller, S. J. 2010. Defining, treating, and studying very high-risk cutaneous squamous cell carcinomas. *Archives of dermatology* 146: 1292-1295.

115. Brodland, D. G., and J. A. Zitelli. 1992. Surgical margins for excision of primary cutaneous squamous cell carcinoma. *Journal of the American Academy of Dermatology* 27: 241-248.

116. Leibovitch, I., S. C. Huilgol, D. Selva, D. Hill, S. Richards, and R. Paver. 2005. Cutaneous squamous cell carcinoma treated with Mohs micrographic surgery in Australia I. Experience over 10 years. *Journal of the American Academy of Dermatology* 53: 253-260.

117. Veness, M., and S. Richards. 2003. Role of modern radiotherapy in treating skin cancer. *Australas J Dermatol* 44: 159-166; quiz 167-158.

118. Al-Othman, M. O., W. M. Mendenhall, and R. J. Amdur. 2001. Radiotherapy alone for clinical T4 skin carcinoma of the head and neck with surgery reserved for salvage. *Am J Otolaryngol* 22: 387-390.

119. Parikh, S. A., V. A. Patel, and D. Ratner. 2014. Advances in the management of cutaneous squamous cell carcinoma. *F1000Prime Rep* 6: 70.

120. Jambusaria-Pahlajani, A., S. D. Hess, K. A. Katz, D. Berg, and C. D. Schmults. 2010. Uncertainty in the perioperative management of high-risk cutaneous squamous cell carcinoma among Mohs surgeons. *Archives of dermatology* 146: 1225-1231.

121. Uribe, P., and S. Gonzalez. 2011. Epidermal growth factor receptor (EGFR) and squamous cell carcinoma of the skin: molecular bases for EGFR-targeted therapy. *Pathol Res Pract* 207: 337-342.

122. Ozanne, B., C. S. Richards, F. Hendler, D. Burns, and B. Gusterson. 1986. Over-expression of the EGF receptor is a hallmark of squamous cell carcinomas. *The Journal of pathology* 149: 9-14.

123. Gaffney, D. C., H. P. Soyer, and F. Simpson. 2014. The epidermal growth factor receptor in squamous cell carcinoma: An emerging drug target. *Australas J Dermatol* 55: 24-34.

124. Maubec, E., P. Petrow, I. Scheer-Senyarich, P. Duvillard, L. Lacroix, J. Gelly, A. Certain, X. Duval, B. Crickx, V. Buffard, N. Basset-Seguin, P. Saez, A. B. Duval-Modeste, H. Adamski, S. Mansard, F. Grange, A. Dompmartin, S. Faivre, F. Mentre, and M. F. Avril. 2011. Phase II study of cetuximab as first-line single-drug therapy in patients with unresectable squamous cell carcinoma of the skin. *Journal of clinical oncology : official journal of the American Society of Clinical Oncology* 29: 3419-3426.

125. Lewis, C. M., B. S. Glisson, L. Feng, F. Wan, X. Tang, Wistuba, II, A. K. El-Naggar, D. I. Rosenthal, M. S. Chambers, R. A. Lustig, and R. S. Weber. 2012. A phase II study of gefitinib for aggressive cutaneous squamous cell carcinoma of the head and neck. *Clinical cancer research : an official journal of the American Association for Cancer Research* 18: 1435-1446.

126. Braathen, L. R., C. A. Morton, N. Basset-Seguin, R. Bissonnette, M. J. Gerritsen, Y. Gilaberte, P. Calzavara-Pinton, A. Sidoroff, H. C. Wulf, and R. M. Szeimies. 2012. Photodynamic therapy for skin field cancerization: an international consensus. International Society for Photodynamic Therapy in Dermatology. *J Eur Acad Dermatol Venereol* 26: 1063-1066.

127. Torezan, L. A., and C. Festa-Neto. 2013. Cutaneous field cancerization: clinical, histopathological and therapeutic aspects. *An Bras Dermatol* 88: 775-786.

128. Lebwohl, M., N. Swanson, L. L. Anderson, A. Melgaard, Z. Xu, and B. Berman. 2012. Ingenol mebutate gel for actinic keratosis. *The New England journal of medicine* 366: 1010-1019.

129. Gupta, A. K., M. Paquet, E. Villanueva, and W. Brintnell. 2012. Interventions for actinic keratoses. *Cochrane Database Syst Rev* 12: CD004415.

130. Lin, D. C., J. J. Hao, Y. Nagata, L. Xu, L. Shang, X. Meng, Y. Sato, Y. Okuno, A. M. Varela, L. W. Ding, M. Garg, L. Z. Liu, H. Yang, D. Yin, Z. Z. Shi, Y. Y. Jiang, W. Y. Gu, T. Gong, Y. Zhang, X. Xu, O. Kalid, S. Shacham, S. Ogawa, M. R. Wang, and H. P. Koeffler. 2014. Genomic and molecular characterization of esophageal squamous cell carcinoma. *Nature genetics* 46: 467-473.

131. Pickering, C. R., J. H. Zhou, J. J. Lee, J. A. Drummond, S. A. Peng, R. E. Saade, K. Y. Tsai, J. L. Curry, M. T. Tetzlaff, S. Y. Lai, J. Yu, D. M. Muzny, H. Doddapaneni, E. Shinbrot, K. R. Covington, J. Zhang, S. Seth, C. Caulin, G. L. Clayman, A. K. El-Naggar, R. A. Gibbs, R. S. Weber, J. N. Myers, D. A. Wheeler, and M. J. Frederick. 2014. Mutational landscape of aggressive cutaneous squamous cell carcinoma. *Clinical cancer research : an official journal of the American Association for Cancer Research* 20: 6582-6592.

132. Ojesina, A. I., L. Lichtenstein, S. S. Freeman, C. S. Pedamallu, I. Imaz-Rosshandler, T. J. Pugh, A. D. Cherniack, L. Ambrogio, K. Cibulskis, B. Bertelsen, S. Romero-Cordoba, V. Trevino, K. Vazquez-Santillan, A. S. Guadarrama, A. A. Wright, M. W. Rosenberg, F. Duke, B. Kaplan, R. Wang, E. Nickerson, H. M. Walline, M. S. Lawrence, C. Stewart, S. L. Carter, A. McKenna, I. P. Rodriguez-Sanchez, M. Espinosa-Castilla, K. Woie, L. Bjorge, E. Wik, M. K. Halle, E. A. Hoivik, C. Krakstad, N. B. Gabino, G. S. Gomez-Macias, L. D. Valdez-Chapa, M. L. Garza-Rodriguez, G. Maytorena, J. Vazquez, C. Rodea, A. Cravioto, M. L. Cortes, H. Greulich, C. P. Crum, D. S. Neuberg, A. Hidalgo-Miranda, C. R. Escareno, L. A. Akslen, T. E. Carey, O. K. Vintermyr, S. B. Gabriel, H. A. Barrera-Saldana, J. Melendez-Zajgla, G. Getz, H. B. Salvesen, and M. Meyerson. 2014. Landscape of genomic alterations in cervical carcinomas. *Nature* 506: 371-375.

133. Kandoth, C., M. D. McLellan, F. Vandin, K. Ye, B. Niu, C. Lu, M. Xie, Q. Zhang, J. F. McMichael, M. A. Wyczalkowski, M. D. Leiserson, C. A. Miller, J. S. Welch, M. J. Walter, M. C. Wendl, T. J. Ley, R. K. Wilson, B. J. Raphael, and L.

Ding. 2013. Mutational landscape and significance across 12 major cancer types. *Nature* 502: 333-339.

134. Durinck, S., C. Ho, N. J. Wang, W. Liao, L. R. Jakkula, E. A. Collisson, J. Pons, S. W. Chan, E. T. Lam, C. Chu, K. Park, S. W. Hong, J. S. Hur, N. Huh, I. M. Neuhaus, S. S. Yu, R. C. Grekin, T. M. Mauro, J. E. Cleaver, P. Y. Kwok, P. E. LeBoit, G. Getz, K. Cibulskis, J. C. Aster, H. Huang, E. Purdom, J. Li, L. Bolund, S. T. Arron, J. W. Gray, P. T. Spellman, and R. J. Cho. 2011. Temporal dissection of tumorigenesis in primary cancers. *Cancer Discov* 1: 137-143.

135. Forbes, S. A., G. Tang, N. Bindal, S. Bamford, E. Dawson, C. Cole, C. Y. Kok, M. Jia, R. Ewing, A. Menzies, J. W. Teague, M. R. Stratton, and P. A. Futreal. 2010. COSMIC (the Catalogue of Somatic Mutations in Cancer): a resource to investigate acquired mutations in human cancer. *Nucleic acids research* 38: D652-657.

136. Pacifico, A., L. H. Goldberg, K. Peris, S. Chimenti, G. Leone, and H. N. Ananthaswamy. 2008. Loss of CDKN2A and p14ARF expression occurs frequently in human nonmelanoma skin cancers. *The British journal of dermatology* 158: 291-297.

137. Wang, N. J., Z. Sanborn, K. L. Arnett, L. J. Bayston, W. Liao, C. M. Proby, I. M. Leigh, E. A. Collisson, P. B. Gordon, L. Jakkula, S. Pennypacker, Y. Zou, M. Sharma, J. P. North, S. S. Vemula, T. M. Mauro, I. M. Neuhaus, P. E. Leboit, J. S. Hur, K. Park, N. Huh, P. Y. Kwok, S. T. Arron, P. P. Massion, A. E. Bale, D. Haussler, J. E. Cleaver, J. W. Gray, P. T. Spellman, A. P. South, J. C. Aster, S. C. Blacklow, and R. J. Cho. 2011. Loss-of-function mutations in Notch receptors in

cutaneous and lung squamous cell carcinoma. *Proceedings of the National Academy of Sciences of the United States of America* 108: 17761-17766.

138. Su, F., A. Viros, C. Milagre, K. Trunzer, G. Bollag, O. Spleiss, J. S. Reis-Filho, X. Kong, R. C. Koya, K. T. Flaherty, P. B. Chapman, M. J. Kim, R. Hayward, M. Martin, H. Yang, Q. Wang, H. Hilton, J. S. Hang, J. Noe, M. Lambros, F. Geyer, N. Dhomen, I. Niculescu-Duvaz, A. Zambon, D. Niculescu-Duvaz, N. Preece, L. Robert, N. J. Otte, S. Mok, D. Kee, Y. Ma, C. Zhang, G. Habets, E. A. Burton, B. Wong, H. Nguyen, M. Kockx, L. Andries, B. Lestini, K. B. Nolop, R. J. Lee, A. K. Joe, J. L. Troy, R. Gonzalez, T. E. Hutson, I. Puzanov, B. Chmielowski, C. J. Springer, G. A. McArthur, J. A. Sosman, R. S. Lo, A. Ribas, and R. Marais. 2012. RAS mutations in cutaneous squamous-cell carcinomas in patients treated with BRAF inhibitors. *The New England journal of medicine* 366: 207-215.

139. Ratushny, V., M. D. Gober, R. Hick, T. W. Ridky, and J. T. Seykora. 2012. From keratinocyte to cancer: the pathogenesis and modeling of cutaneous squamous cell carcinoma. *The Journal of clinical investigation* 122: 464-472.

140. Brash, D. E., J. A. Rudolph, J. A. Simon, A. Lin, G. J. McKenna, H. P. Baden, A. J. Halperin, and J. Ponten. 1991. A role for sunlight in skin cancer: UV-induced p53 mutations in squamous cell carcinoma. *Proceedings of the National Academy of Sciences of the United States of America* 88: 10124-10128.

141. Eckert, R. L., G. Adhikary, C. A. Young, R. Jans, J. F. Crish, W. Xu, and E. A. Rorke. 2013. AP1 transcription factors in epidermal differentiation and skin cancer. *Journal of skin cancer* 2013: 537028.

142. South, A. P., K. J. Purdie, S. A. Watt, S. Haldenby, N. Y. den Breems, M. Dimon, S. T. Arron, M. J. Kluk, J. C. Aster, A. McHugh, D. J. Xue, J. H. Dayal, K. S. Robinson, S. M. Rizvi, C. M. Proby, C. A. Harwood, and I. M. Leigh. 2014. NOTCH1 mutations occur early during cutaneous squamous cell carcinogenesis. *The Journal of investigative dermatology* 134: 2630-2638.

143. Li, Y. Y., G. J. Hanna, A. C. Laga, R. I. Haddad, J. H. Lorch, and P. S. Hammerman. 2015. Genomic analysis of metastatic cutaneous squamous cell carcinoma. *Clinical cancer research : an official journal of the American Association for Cancer Research* 21: 1447-1456.

144. Yuan, T. L., and L. C. Cantley. 2008. PI3K pathway alterations in cancer: variations on a theme. *Oncogene* 27: 5497-5510.

145. Liu, K., B. Lin, M. Zhao, X. Yang, M. Chen, A. Gao, F. Liu, J. Que, and X. Lan. 2013. The multiple roles for Sox2 in stem cell maintenance and tumorigenesis. *Cell Signal* 25: 1264-1271.

146. Ramsey, M. R., C. Wilson, B. Ory, S. M. Rothenberg, W. Faquin, A. A. Mills, and L. W. Ellisen. 2013. FGFR2 signaling underlies p63 oncogenic function in squamous cell carcinoma. *The Journal of clinical investigation* 123: 3525-3538.

147. Su, X., D. Chakravarti, M. S. Cho, L. Liu, Y. J. Gi, Y. L. Lin, M. L. Leung, A. El-Naggar, C. J. Creighton, M. B. Suraokar, I. Wistuba, and E. R. Flores. 2010. TAp63 suppresses metastasis through coordinate regulation of Dicer and miRNAs. *Nature* 467: 986-990.

148. Calin, G. A., and C. M. Croce. 2006. MicroRNA signatures in human cancers. *Nature reviews. Cancer* 6: 857-866.

149. Ma, L., and R. A. Weinberg. 2008. MicroRNAs in malignant progression. *Cell cycle* 7: 570-572.

150. Mizrahi, A., A. Barzilai, D. Gur-Wahnon, I. Z. Ben-Dov, S. Glassberg, T. Meningher, E. Elharar, M. Masalha, J. Jacob-Hirsch, H. Tabibian-Keissar, I. Barshack, J. Roszik, R. Leibowitz-Amit, Y. Sidi, and D. Avni. 2018. Alterations of microRNAs throughout the malignant evolution of cutaneous squamous cell carcinoma: the role of miR-497 in epithelial to mesenchymal transition of keratinocytes. *Oncogene* 37: 218-230.

151. Sand, M., M. Skrygan, D. Georgas, D. Sand, S. A. Hahn, T. Gambichler, P. Altmeyer, and F. G. Bechara. 2012. Microarray analysis of microRNA expression in cutaneous squamous cell carcinoma. *Journal of dermatological science* 68: 119-126.

152. Wang, A., N. X. Landen, F. Meisgen, W. Lohcharoenkal, M. Stahle, E. Sonkoly, and A. Pivarcsi. 2014. MicroRNA-31 Is Overexpressed in Cutaneous Squamous Cell Carcinoma and Regulates Cell Motility and Colony Formation Ability of Tumor Cells. *PloS one* 9: e103206.

153. Ge, Y., L. Zhang, M. Nikolova, B. Reva, and E. Fuchs. 2015. Strand-specific in vivo screen of cancer-associated miRNAs unveils a role for miR-21 in SCC progression. *Nature cell biology*.

154. Ma, X., M. Kumar, S. N. Choudhury, L. E. Becker Buscaglia, J. R. Barker, K. Kanakamedala, M. F. Liu, and Y. Li. 2011. Loss of the miR-21 allele elevates the expression of its target genes and reduces tumorigenesis. *Proceedings of the National Academy of Sciences of the United States of America* 108: 10144-10149.

155. Griffiths-Jones, S., H. K. Saini, S. van Dongen, and A. J. Enright. 2008. miRBase: tools for microRNA genomics. *Nucleic acids research* 36: D154-158.

156. Bartel, D. P. 2009. MicroRNAs: target recognition and regulatory functions. *Cell* 136: 215-233.

157. Cai, X., C. H. Hagedorn, and B. R. Cullen. 2004. Human microRNAs are processed from capped, polyadenylated transcripts that can also function as mRNAs. *Rna* 10: 1957-1966.

158. Denli, A. M., B. B. Tops, R. H. Plasterk, R. F. Ketting, and G. J. Hannon. 2004. Processing of primary microRNAs by the Microprocessor complex. *Nature* 432: 231-235.

159. Gregory, R. I., K. P. Yan, G. Amuthan, T. Chendrimada, B. Doratotaj, N. Cooch, and R. Shiekhattar. 2004. The Microprocessor complex mediates the genesis of microRNAs. *Nature* 432: 235-240.

160. Lee, Y., M. Kim, J. Han, K. H. Yeom, S. Lee, S. H. Baek, and V. N. Kim. 2004. MicroRNA genes are transcribed by RNA polymerase II. *The EMBO journal* 23: 4051-4060.

161. Yi, R., Y. Qin, I. G. Macara, and B. R. Cullen. 2003. Exportin-5 mediates the nuclear export of pre-microRNAs and short hairpin RNAs. *Genes & development* 17: 3011-3016.

162. Bohnsack, M. T., K. Czaplinski, and D. Gorlich. 2004. Exportin 5 is a RanGTP-dependent dsRNA-binding protein that mediates nuclear export of pre-miRNAs. *Rna* 10: 185-191.

163. Bernstein, E., A. A. Caudy, S. M. Hammond, and G. J. Hannon. 2001. Role for a bidentate ribonuclease in the initiation step of RNA interference. *Nature* 409: 363-366.

164. Grishok, A., A. E. Pasquinelli, D. Conte, N. Li, S. Parrish, I. Ha, D. L. Baillie, A. Fire, G. Ruvkun, and C. C. Mello. 2001. Genes and mechanisms related to RNA interference regulate expression of the small temporal RNAs that control C. elegans developmental timing. *Cell* 106: 23-34.

165. Hutvagner, G., J. McLachlan, A. E. Pasquinelli, E. Balint, T. Tuschl, and P. D. Zamore. 2001. A cellular function for the RNA-interference enzyme Dicer in the maturation of the let-7 small temporal RNA. *Science* 293: 834-838.

166. Hammond, S. M., S. Boettcher, A. A. Caudy, R. Kobayashi, and G. J. Hannon. 2001. Argonaute2, a link between genetic and biochemical analyses of RNAi. *Science* 293: 1146-1150.

167. Mourelatos, Z., J. Dostie, S. Paushkin, A. Sharma, B. Charroux, L. Abel, J. Rappsilber, M. Mann, and G. Dreyfuss. 2002. miRNPs: a novel class of ribonucleoproteins containing numerous microRNAs. *Genes & development* 16: 720-728.

168. Khvorova, A., A. Reynolds, and S. D. Jayasena. 2003. Functional siRNAs and miRNAs exhibit strand bias. *Cell* 115: 209-216.

169. Schwarz, D. S., G. Hutvagner, T. Du, Z. Xu, N. Aronin, and P. D. Zamore. 2003. Asymmetry in the assembly of the RNAi enzyme complex. *Cell* 115: 199-208.

170. Chiang, H. R., L. W. Schoenfeld, J. G. Ruby, V. C. Auyeung, N. Spies, D. Baek, W. K. Johnston, C. Russ, S. Luo, J. E. Babiarz, R. Blelloch, G. P. Schroth, C.

Nusbaum, and D. P. Bartel. 2010. Mammalian microRNAs: experimental evaluation of novel and previously annotated genes. *Genes & development* 24: 992-1009.

171. He, L., X. He, L. P. Lim, E. de Stanchina, Z. Xuan, Y. Liang, W. Xue, L. Zender, J. Magnus, D. Ridzon, A. L. Jackson, P. S. Linsley, C. Chen, S. W. Lowe, M. A. Cleary, and G. J. Hannon. 2007. A microRNA component of the p53 tumour suppressor network. *Nature* 447: 1130-1134.

172. Suzuki, H. I., K. Yamagata, K. Sugimoto, T. Iwamoto, S. Kato, and K. Miyazono. 2009. Modulation of microRNA processing by p53. *Nature* 460: 529-533.

173. Lena, A. M., R. Shalom-Feuerstein, P. Rivetti di Val Cervo, D. Aberdam, R. A. Knight, G. Melino, and E. Candi. 2008. miR-203 represses 'stemness' by repressing DeltaNp63. *Cell death and differentiation* 15: 1187-1195.

174. Cordisco, S., R. Maurelli, S. Bondanza, M. Stefanini, G. Zambruno, L. Guerra, and E. Dellambra. 2010. Bmi-1 reduction plays a key role in physiological and premature aging of primary human keratinocytes. *The Journal of investigative dermatology* 130: 1048-1062.

175. Rivetti di Val Cervo, P., A. M. Lena, M. Nicoloso, S. Rossi, M. Mancini, H. Zhou, G. Saintigny, E. Dellambra, T. Odorisio, C. Mahe, G. A. Calin, E. Candi, and G. Melino. 2012. p63-microRNA feedback in keratinocyte senescence. *Proceedings of the National Academy of Sciences of the United States of America* 109: 1133-1138.

176. Lu, J., G. Getz, E. A. Miska, E. Alvarez-Saavedra, J. Lamb, D. Peck, A. Sweet-Cordero, B. L. Ebert, R. H. Mak, A. A. Ferrando, J. R. Downing, T. Jacks, H.

R. Horvitz, and T. R. Golub. 2005. MicroRNA expression profiles classify human cancers. *Nature* 435: 834-838.

177. Thomson, J. M., M. Newman, J. S. Parker, E. M. Morin-Kensicki, T. Wright, and S. M. Hammond. 2006. Extensive post-transcriptional regulation of microRNAs and its implications for cancer. *Genes & development* 20: 2202-2207.

178. Karube, Y., H. Tanaka, H. Osada, S. Tomida, Y. Tatematsu, K. Yanagisawa, Y. Yatabe, J. Takamizawa, S. Miyoshi, T. Mitsudomi, and T. Takahashi. 2005. Reduced expression of Dicer associated with poor prognosis in lung cancer patients. *Cancer Sci* 96: 111-115.

179. Lin, R. J., Y. C. Lin, J. Chen, H. H. Kuo, Y. Y. Chen, M. B. Diccianni, W. B. London, C. H. Chang, and A. L. Yu. 2010. microRNA signature and expression of Dicer and Drosha can predict prognosis and delineate risk groups in neuroblastoma. *Cancer research* 70: 7841-7850.

180. Merritt, W. M., Y. G. Lin, L. Y. Han, A. A. Kamat, W. A. Spannuth, R. Schmandt, D. Urbauer, L. A. Pennacchio, J. F. Cheng, A. M. Nick, M. T. Deavers, A. Mourad-Zeidan, H. Wang, P. Mueller, M. E. Lenburg, J. W. Gray, S. Mok, M. J. Birrer, G. Lopez-Berestein, R. L. Coleman, M. Bar-Eli, and A. K. Sood. 2008. Dicer, Drosha, and outcomes in patients with ovarian cancer. *The New England journal of medicine* 359: 2641-2650.

181. Kaghad, M., H. Bonnet, A. Yang, L. Creancier, J. C. Biscan, A. Valent, A. Minty, P. Chalon, J. M. Lelias, X. Dumont, P. Ferrara, F. McKeon, and D. Caput. 1997. Monoallelically expressed gene related to p53 at 1p36, a region frequently deleted in neuroblastoma and other human cancers. *Cell* 90: 809-819.

182. Ishimoto, O., C. Kawahara, K. Enjo, M. Obinata, T. Nukiwa, and S. Ikawa. 2002. Possible oncogenic potential of DeltaNp73: a newly identified isoform of human p73. *Cancer research* 62: 636-641.

183. Yang, A., N. Walker, R. Bronson, M. Kaghad, M. Oosterwegel, J. Bonnin, C. Vagner, H. Bonnet, P. Dikkes, A. Sharpe, F. McKeon, and D. Caput. 2000. p73-deficient mice have neurological, pheromonal and inflammatory defects but lack spontaneous tumours. *Nature* 404: 99-103.

184. Flores, E. R., S. Sengupta, J. B. Miller, J. J. Newman, R. Bronson, D. Crowley, A. Yang, F. McKeon, and T. Jacks. 2005. Tumor predisposition in mice mutant for p63 and p73: evidence for broader tumor suppressor functions for the p53 family. *Cancer cell* 7: 363-373.

185. Tomasini, R., K. Tsuchihara, M. Wilhelm, M. Fujitani, A. Rufini, C. C. Cheung, F. Khan, A. Itie-Youten, A. Wakeham, M. S. Tsao, J. L. Iovanna, J. Squire, I. Jurisica, D. Kaplan, G. Melino, A. Jurisicova, and T. W. Mak. 2008. TAp73 knockout shows genomic instability with infertility and tumor suppressor functions. *Genes & development* 22: 2677-2691.

186. Rossi, M., A. E. Sayan, A. Terrinoni, G. Melino, and R. A. Knight. 2004. Mechanism of induction of apoptosis by p73 and its relevance to neuroblastoma biology. *Ann N Y Acad Sci* 1028: 143-149.

187. Shimodaira, H., A. Yoshioka-Yamashita, R. D. Kolodner, and J. Y. Wang. 2003. Interaction of mismatch repair protein PMS2 and the p53-related transcription factor p73 in apoptosis response to cisplatin. *Proceedings of the National Academy of Sciences of the United States of America* 100: 2420-2425.

188. Zaika, E., J. Wei, D. Yin, C. Andl, U. Moll, W. El-Rifai, and A. I. Zaika. 2011. p73 protein regulates DNA damage repair. *FASEB J* 25: 4406-4414.

189. Strano, S., O. Monti, N. Pediconi, A. Baccarini, G. Fontemaggi, E. Lapi, F. Mantovani, A. Damalas, G. Citro, A. Sacchi, G. Del Sal, M. Levrero, and G. Blandino. 2005. The transcriptional coactivator Yes-associated protein drives p73 gene-target specificity in response to DNA Damage. *Molecular cell* 18: 447-459.

190. Lee, C. W., and N. B. La Thangue. 1999. Promoter specificity and stability control of the p53-related protein p73. *Oncogene* 18: 4171-4181.

191. Muller, M., T. Schilling, A. E. Sayan, A. Kairat, K. Lorenz, H. Schulze-Bergkamen, M. Oren, A. Koch, A. Tannapfel, W. Stremmel, G. Melino, and P. H. Krammer. 2005. TAp73/Delta Np73 influences apoptotic response, chemosensitivity and prognosis in hepatocellular carcinoma. *Cell death and differentiation* 12: 1564-1577.

192. Melino, G., F. Bernassola, M. Ranalli, K. Yee, W. X. Zong, M. Corazzari, R. A. Knight, D. R. Green, C. Thompson, and K. H. Vousden. 2004. p73 Induces apoptosis via PUMA transactivation and Bax mitochondrial translocation. *The Journal of biological chemistry* 279: 8076-8083.

193. Jemal, A., F. Bray, M. M. Center, J. Ferlay, E. Ward, and D. Forman. 2011. Global cancer statistics. *CA: a cancer journal for clinicians* 61: 69-90.

194. Siegel, R., D. Naishadham, and A. Jemal. 2013. Cancer statistics, 2013. *CA: a cancer journal for clinicians* 63: 11-30.

195. Torre, L. A., F. Bray, R. L. Siegel, J. Ferlay, J. Lortet-Tieulent, and A. Jemal. 2015. Global cancer statistics, 2012. *CA: a cancer journal for clinicians* 65: 87-108.

196. Kwak, E. L., Y. J. Bang, D. R. Camidge, A. T. Shaw, B. Solomon, R. G. Maki, S. H. Ou, B. J. Dezube, P. A. Janne, D. B. Costa, M. Varella-Garcia, W. H. Kim, T. J. Lynch, P. Fidias, H. Stubbs, J. A. Engelman, L. V. Sequist, W. Tan, L. Gandhi, M. Mino-Kenudson, G. C. Wei, S. M. Shreeve, M. J. Ratain, J. Settleman, J. G. Christensen, D. A. Haber, K. Wilner, R. Salgia, G. I. Shapiro, J. W. Clark, and A. J. Iafrate. 2010. Anaplastic lymphoma kinase inhibition in non-small-cell lung cancer. *The New England journal of medicine* 363: 1693-1703.

197. Paez, J. G., P. A. Janne, J. C. Lee, S. Tracy, H. Greulich, S. Gabriel, P. Herman, F. J. Kaye, N. Lindeman, T. J. Boggon, K. Naoki, H. Sasaki, Y. Fujii, M. J. Eck, W. R. Sellers, B. E. Johnson, and M. Meyerson. 2004. EGFR mutations in lung cancer: correlation with clinical response to gefitinib therapy. *Science* 304: 1497-1500.

198. Cancer Genome Atlas Research, N. 2014. Comprehensive molecular profiling of lung adenocarcinoma. *Nature* 511: 543-550.

199. Topalian, S. L., F. S. Hodi, J. R. Brahmer, S. N. Gettinger, D. C. Smith, D. F. McDermott, J. D. Powderly, R. D. Carvajal, J. A. Sosman, M. B. Atkins, P. D. Leming, D. R. Spigel, S. J. Antonia, L. Horn, C. G. Drake, D. M. Pardoll, L. Chen, W. H. Sharfman, R. A. Anders, J. M. Taube, T. L. McMiller, H. Xu, A. J. Korman, M. Jure-Kunkel, S. Agrawal, D. McDonald, G. D. Kollia, A. Gupta, J. M. Wigginton, and M. Sznol. 2012. Safety, activity, and immune correlates of anti-PD-1 antibody in cancer. *The New England journal of medicine* 366: 2443-2454.

200. Topalian, S. L., C. G. Drake, and D. M. Pardoll. 2015. Immune checkpoint blockade: a common denominator approach to cancer therapy. *Cancer cell* 27: 450-461.

201. Gajewski, T. F., H. Schreiber, and Y. X. Fu. 2013. Innate and adaptive immune cells in the tumor microenvironment. *Nat Immunol* 14: 1014-1022.

202. Schreiber, R. D., L. J. Old, and M. J. Smyth. 2011. Cancer immunoediting: integrating immunity's roles in cancer suppression and promotion. *Science* 331: 1565-1570.

203. Garon, E. B., N. A. Rizvi, R. Hui, N. Leighl, A. S. Balmanoukian, J. P. Eder, A. Patnaik, C. Aggarwal, M. Gubens, L. Horn, E. Carcereny, M. J. Ahn, E. Felip, J. S. Lee, M. D. Hellmann, O. Hamid, J. W. Goldman, J. C. Soria, M. Dolled-Filhart, R. Z. Rutledge, J. Zhang, J. K. Lunceford, R. Rangwala, G. M. Lubiniecki, C. Roach, K. Emancipator, L. Gandhi, and K.-. Investigators. 2015. Pembrolizumab for the treatment of non-small-cell lung cancer. *The New England journal of medicine* 372: 2018-2028.

204. Reck, M., D. Rodriguez-Abreu, A. G. Robinson, R. Hui, T. Csoszi, A. Fulop, M. Gottfried, N. Peled, A. Tafreshi, S. Cuffe, M. O'Brien, S. Rao, K. Hotta, M. A. Leiby, G. M. Lubiniecki, Y. Shentu, R. Rangwala, J. R. Brahmer, and K.-. Investigators. 2016. Pembrolizumab versus Chemotherapy for PD-L1-Positive Non-Small-Cell Lung Cancer. *The New England journal of medicine* 375: 1823-1833.

205. Fridman, W. H., F. Pages, C. Sautes-Fridman, and J. Galon. 2012. The immune contexture in human tumours: impact on clinical outcome. *Nature reviews. Cancer* 12: 298-306.

206. Jackson, E. L., N. Willis, K. Mercer, R. T. Bronson, D. Crowley, R. Montoya, T. Jacks, and D. A. Tuveson. 2001. Analysis of lung tumor initiation and progression using conditional expression of oncogenic K-ras. *Genes & development* 15: 3243-3248.

207. Tuveson, D. A., A. T. Shaw, N. A. Willis, D. P. Silver, E. L. Jackson, S. Chang, K. L. Mercer, R. Grochow, H. Hock, D. Crowley, S. R. Hingorani, T. Zaks, C. King, M. A. Jacobetz, L. Wang, R. T. Bronson, S. H. Orkin, R. A. DePinho, and T. Jacks. 2004. Endogenous oncogenic K-ras(G12D) stimulates proliferation and widespread neoplastic and developmental defects. *Cancer cell* 5: 375-387.

208. Jackson, E. L., K. P. Olive, D. A. Tuveson, R. Bronson, D. Crowley, M. Brown, and T. Jacks. 2005. The differential effects of mutant p53 alleles on advanced murine lung cancer. *Cancer research* 65: 10280-10288.

209. DuPage, M., A. L. Dooley, and T. Jacks. 2009. Conditional mouse lung cancer models using adenoviral or lentiviral delivery of Cre recombinase. *Nature protocols* 4: 1064-1072.

210. Feldser, D. M., K. K. Kostova, M. M. Winslow, S. E. Taylor, C. Cashman, C. A. Whittaker, F. J. Sanchez-Rivera, R. Resnick, R. Bronson, M. T. Hemann, and T. Jacks. 2010. Stage-specific sensitivity to p53 restoration during lung cancer progression. *Nature* 468: 572-575.

211. Winslow, M. M., T. L. Dayton, R. G. Verhaak, C. Kim-Kiselak, E. L. Snyder, D. M. Feldser, D. D. Hubbard, M. J. DuPage, C. A. Whittaker, S. Hoersch, S. Yoon, D. Crowley, R. T. Bronson, D. Y. Chiang, M. Meyerson, and T. Jacks. 2011. Suppression of lung adenocarcinoma progression by Nkx2-1. *Nature* 473: 101-104.

212. Arnold, K., A. Sarkar, M. A. Yram, J. M. Polo, R. Bronson, S. Sengupta, M. Seandel, N. Geijsen, and K. Hochedlinger. 2011. Sox2(+) adult stem and progenitor cells are important for tissue regeneration and survival of mice. *Cell stem cell* 9: 317-329.

213. Muzumdar, M. D., B. Tasic, K. Miyamichi, L. Li, and L. Luo. 2007. A global double-fluorescent Cre reporter mouse. *Genesis* 45: 593-605.

214. Johnson, L., K. Mercer, D. Greenbaum, R. T. Bronson, D. Crowley, D. A. Tuveson, and T. Jacks. 2001. Somatic activation of the K-ras oncogene causes early onset lung cancer in mice. *Nature* 410: 1111-1116.

215. Liu, P., N. A. Jenkins, and N. G. Copeland. 2003. A highly efficient recombineering-based method for generating conditional knockout mutations. *Genome research* 13: 476-484.

216. Lewandoski, M., K. M. Wassarman, and G. R. Martin. 1997. Zp3-cre, a transgenic mouse line for the activation or inactivation of loxP-flanked target genes specifically in the female germ line. *Curr Biol* 7: 148-151.

217. Park, Y. W., M. N. Younes, S. A. Jasser, O. G. Yigitbasi, G. Zhou, C. D. Bucana, B. N. Bekele, and J. N. Myers. 2005. AEE788, a dual tyrosine kinase receptor inhibitor, induces endothelial cell apoptosis in human cutaneous squamous cell carcinoma xenografts in nude mice. *Clinical cancer research : an official journal of the American Association for Cancer Research* 11: 1963-1973.

218. Martins, V. L., J. J. Vyas, M. Chen, K. Purdie, C. A. Mein, A. P. South, A. Storey, J. A. McGrath, and E. A. O'Toole. 2009. Increased invasive behaviour in

cutaneous squamous cell carcinoma with loss of basement-membrane type VII collagen. *Journal of cell science* 122: 1788-1799.

219. Purdie, K. J., C. Pourreyron, and A. P. South. 2011. Isolation and culture of squamous cell carcinoma lines. *Methods in molecular biology* 731: 151-159.

220. Kozomara, A., and S. Griffiths-Jones. 2014. miRBase: annotating high confidence microRNAs using deep sequencing data. *Nucleic acids research* 42: D68-73.

221. Johnson, W. E., C. Li, and A. Rabinovic. 2007. Adjusting batch effects in microarray expression data using empirical Bayes methods. *Biostatistics* 8: 118-127.

222. Creighton, C. J., A. K. Nagaraja, S. M. Hanash, M. M. Matzuk, and P. H. Gunaratne. 2008. A bioinformatics tool for linking gene expression profiling results with public databases of microRNA target predictions. *Rna* 14: 2290-2296.

223. Agarwal, V., G. W. Bell, J. W. Nam, and D. P. Bartel. 2015. Predicting effective microRNA target sites in mammalian mRNAs. *eLife* 4.

224. Milan, E., T. Perini, M. Resnati, U. Orfanelli, L. Oliva, A. Raimondi, P. Cascio, A. Bachi, M. Marcatti, F. Ciceri, and S. Cenci. 2015. A plastic SQSTM1/p62-dependent autophagic reserve maintains proteostasis and determines proteasome inhibitor susceptibility in multiple myeloma cells. *Autophagy* 11: 1161-1178.

225. Pruneri, G., S. Fabris, P. Dell'Orto, M. O. Biasi, S. Valentini, B. Del Curto, D. Laszlo, L. Cattaneo, R. Fasani, L. Rossini, M. Manzotti, F. Bertolini, G. Martinelli, A. Neri, and G. Viale. 2005. The transactivating isoforms of p63 are overexpressed in high-grade follicular lymphomas independent of the occurrence of p63 gene amplification. *The Journal of pathology* 206: 337-345.

226. Girardini, J. E., M. Napoli, S. Piazza, A. Rustighi, C. Marotta, E. Radaelli, V. Capaci, L. Jordan, P. Quinlan, A. Thompson, M. Mano, A. Rosato, T. Crook, E. Scanziani, A. R. Means, G. Lozano, C. Schneider, and G. Del Sal. 2011. A Pin1/mutant p53 axis promotes aggressiveness in breast cancer. *Cancer cell* 20: 79-91.

227. Kurien, B. T., and R. H. Scofield. 2015. *Western blotting : methods and protocols*. Humana Press, New York.

228. Cox, J., and M. Mann. 2008. MaxQuant enables high peptide identification rates, individualized p.p.b.-range mass accuracies and proteome-wide protein quantification. *Nat Biotechnol* 26: 1367-1372.

229. Mendell, J. T., and E. N. Olson. 2012. MicroRNAs in stress signaling and human disease. *Cell* 148: 1172-1187.

230. Mukherji, S., M. S. Ebert, G. X. Zheng, J. S. Tsang, P. A. Sharp, and A. van Oudenaarden. 2011. MicroRNAs can generate thresholds in target gene expression. *Nature genetics* 43: 854-859.

231. Ferone, G., J. Y. Song, K. D. Sutherland, R. Bhaskaran, K. Monkhorst, J. P. Lambooij, N. Proost, G. Gargiulo, and A. Berns. 2016. SOX2 Is the Determining Oncogenic Switch in Promoting Lung Squamous Cell Carcinoma from Different Cells of Origin. *Cancer cell* 30: 519-532.

232. Boumahdi, S., G. Driessens, G. Lapouge, S. Rorive, D. Nassar, M. Le Mercier, B. Delatte, A. Caauwe, S. Lenglez, E. Nkusi, S. Brohee, I. Salmon, C. Dubois, V. del Marmol, F. Fuks, B. Beck, and C. Blanpain. 2014. SOX2 controls

tumour initiation and cancer stem-cell functions in squamous-cell carcinoma. *Nature* 511: 246-250.

233. Siegle, J. M., A. Basin, A. Sastre-Perona, Y. Yonekubo, J. Brown, R. Sennett, M. Rendl, A. Tsirigos, J. A. Carucci, and M. Schober. 2014. SOX2 is a cancer-specific regulator of tumour initiating potential in cutaneous squamous cell carcinoma. *Nature communications* 5: 4511.

234. Lapouge, G., B. Beck, D. Nassar, C. Dubois, S. Dekoninck, and C. Blanpain. 2012. Skin squamous cell carcinoma propagating cells increase with tumour progression and invasiveness. *The EMBO journal* 31: 4563-4575.

235. Schober, M., and E. Fuchs. 2011. Tumor-initiating stem cells of squamous cell carcinomas and their control by TGF-beta and integrin/focal adhesion kinase (FAK) signaling. *Proceedings of the National Academy of Sciences of the United States of America* 108: 10544-10549.

236. Gunaratne, P. H., C. Coarfa, B. Soibam, and A. Tandon. 2012. miRNA data analysis: next-gen sequencing. *Methods in molecular biology* 822: 273-288.

237. Hanahan, D., and R. A. Weinberg. 2011. Hallmarks of cancer: the next generation. *Cell* 144: 646-674.

238. Hanahan, D., and R. A. Weinberg. 2000. The hallmarks of cancer. *Cell* 100: 57-70.

239. Bruegger, C., W. Kempf, I. Spoerri, A. W. Arnold, P. H. Itin, and B. Burger. 2013. MicroRNA expression differs in cutaneous squamous cell carcinomas and healthy skin of immunocompetent individuals. *Experimental dermatology* 22: 426-428.

240. Shen, L., J. Li, L. Xu, J. Ma, H. Li, X. Xiao, J. Zhao, and L. Fang. 2012. miR-497 induces apoptosis of breast cancer cells by targeting Bcl-w. *Exp Ther Med* 3: 475-480.

241. Furuta, M., K. Kozaki, K. Tanimoto, S. Tanaka, S. Arii, T. Shimamura, A. Niida, S. Miyano, and J. Inazawa. 2013. The tumor-suppressive miR-497-195 cluster targets multiple cell-cycle regulators in hepatocellular carcinoma. *PloS one* 8: e60155.

242. Li, W., X. Jin, X. Deng, G. Zhang, B. Zhang, and L. Ma. 2014. The putative tumor suppressor microRNA-497 modulates gastric cancer cell proliferation and invasion by repressing eIF4E. *Biochemical and biophysical research communications* 449: 235-240.

243. Wang, S., Y. Mo, K. Midorikawa, Z. Zhang, G. Huang, N. Ma, W. Zhao, Y. Hiraku, S. Oikawa, and M. Murata. 2015. The potent tumor suppressor miR-497 inhibits cancer phenotypes in nasopharyngeal carcinoma by targeting ANLN and HSPA4L. *Oncotarget* 6: 35893-35907.

244. Whisnant, A. W., H. P. Bogerd, O. Flores, P. Ho, J. G. Powers, N. Sharova, M. Stevenson, C. H. Chen, and B. R. Cullen. 2013. In-depth analysis of the interaction of HIV-1 with cellular microRNA biogenesis and effector mechanisms. *MBio* 4: e000193.

245. Dweep, H., and N. Gretz. 2015. miRWalk2.0: a comprehensive atlas of microRNA-target interactions. *Nat Methods* 12: 697.

246. Lewis, B. P., I. H. Shih, M. W. Jones-Rhoades, D. P. Bartel, and C. B. Burge. 2003. Prediction of mammalian microRNA targets. *Cell* 115: 787-798.

247. Miranda, K. C., T. Huynh, Y. Tay, Y. S. Ang, W. L. Tam, A. M. Thomson, B. Lim, and I. Rigoutsos. 2006. A pattern-based method for the identification of MicroRNA binding sites and their corresponding heteroduplexes. *Cell* 126: 1203-1217.

248. Orom, U. A., and A. H. Lund. 2007. Isolation of microRNA targets using biotinylated synthetic microRNAs. *Methods* 43: 162-165.

249. Galluzzi, L., I. Vitale, S. A. Aaronson, J. M. Abrams, D. Adam, P. Agostinis, E. S. Alnemri, L. Altucci, I. Amelio, D. W. Andrews, M. Annicchiarico-Petruzzelli, A. V. Antonov, E. Arama, E. H. Baehrecke, N. A. Barlev, N. G. Bazan, F. Bernassola, M. J. M. Bertrand, K. Bianchi, M. V. Blagosklonny, K. Blomgren, C. Borner, P. Boya, C. Brenner, M. Campanella, E. Candi, D. Carmona-Gutierrez, F. Cecconi, F. K. Chan, N. S. Chandel, E. H. Cheng, J. E. Chipuk, J. A. Cidlowski, A. Ciechanover, G. M. Cohen, M. Conrad, J. R. Cubillos-Ruiz, P. E. Czabotar, V. D'Angiolella, T. M. Dawson, V. L. Dawson, V. De Laurenzi, R. De Maria, K. M. Debatin, R. J. DeBerardinis, M. Deshmukh, N. Di Daniele, F. Di Virgilio, V. M. Dixit, S. J. Dixon, C. S. Duckett, B. D. Dynlacht, W. S. El-Deiry, J. W. Elrod, G. M. Fimia, S. Fulda, A. J. Garcia-Saez, A. D. Garg, C. Garrido, E. Gavathiotis, P. Golstein, E. Gottlieb, D. R. Green, L. A. Greene, H. Gronemeyer, A. Gross, G. Hajnoczky, J. M. Hardwick, I. S. Harris, M. O. Hengartner, C. Hetz, H. Ichijo, M. Jaattela, B. Joseph, P. J. Jost, P. P. Juin, W. J. Kaiser, M. Karin, T. Kaufmann, O. Kepp, A. Kimchi, R. N. Kitsis, D. J. Klionsky, R. A. Knight, S. Kumar, S. W. Lee, J. J. Lemasters, B. Levine, A. Linkermann, S. A. Lipton, R. A. Lockshin, C. Lopez-Otin, S. W. Lowe, T. Luedde, E. Lugli, M. MacFarlane, F. Madeo, M. Malewicz, W. Malorni, G. Manic, J. C. Marine,

S. J. Martin, J. C. Martinou, J. P. Medema, P. Mehlen, P. Meier, S. Melino, E. A. Miao, J. D. Molkentin, U. M. Moll, C. Munoz-Pinedo, S. Nagata, G. Nunez, A. Oberst, M. Oren, M. Overholtzer, M. Pagano, T. Panaretakis, M. Pasparakis, J. M. Penninger, D. M. Pereira, S. Pervaiz, M. E. Peter, M. Piacentini, P. Pinton, J. H. M. Prehn, H. Puthalakath, G. A. Rabinovich, M. Rehm, R. Rizzuto, C. M. P. Rodrigues, D. C. Rubinsztein, T. Rudel, K. M. Ryan, E. Sayan, L. Scorrano, F. Shao, Y. Shi, J. Silke, H. U. Simon, A. Sistigu, B. R. Stockwell, A. Strasser, G. Szabadkai, S. W. G. Tait, D. Tang, N. Tavernarakis, A. Thorburn, Y. Tsujimoto, B. Turk, T. Vanden Berghe, P. Vandenabeele, M. G. Vander Heiden, A. Villunger, H. W. Virgin, K. H. Vousden, D. Vucic, E. F. Wagner, H. Walczak, D. Wallach, Y. Wang, J. A. Wells, W. Wood, J. Yuan, Z. Zakeri, B. Zhivotovsky, L. Zitvogel, G. Melino, and G. Kroemer. 2018. Molecular mechanisms of cell death: recommendations of the Nomenclature Committee on Cell Death 2018. *Cell death and differentiation* 25: 486-541.

250. Chen, F., Y. Zhang, E. Parra, J. Rodriguez, C. Behrens, R. Akbani, Y. Lu, J. M. Kurie, D. L. Gibbons, G. B. Mills, Wistuba, II, and C. J. Creighton. 2016. Multiplatform-based molecular subtypes of non-small-cell lung cancer. *Oncogene*.

251. Park, B. J., S. J. Lee, J. I. Kim, S. J. Lee, C. H. Lee, S. G. Chang, J. H. Park, and S. G. Chi. 2000. Frequent alteration of p63 expression in human primary bladder carcinomas. *Cancer research* 60: 3370-3374.

252. Meuwissen, R., S. C. Linn, M. van der Valk, W. J. Mooi, and A. Berns. 2001. Mouse model for lung tumorigenesis through Cre/lox controlled sporadic activation of the K-Ras oncogene. *Oncogene* 20: 6551-6558.

253. Stantic, M., H. A. Sakil, H. Zirath, T. Fang, G. Sanz, A. Fernandez-Woodbridge, A. Marin, E. Susanto, T. W. Mak, M. Arsenian Henriksson, and M. T. Wilhelm. 2015. TAp73 suppresses tumor angiogenesis through repression of proangiogenic cytokines and HIF-1alpha activity. *Proceedings of the National Academy of Sciences of the United States of America* 112: 220-225.

254. Amelio, I., S. Inoue, E. K. Markert, A. J. Levine, R. A. Knight, T. W. Mak, and G. Melino. 2015. TAp73 opposes tumor angiogenesis by promoting hypoxia-inducible factor 1alpha degradation. *Proceedings of the National Academy of Sciences of the United States of America* 112: 226-231.

255. Inoue, S., R. Tomasini, A. Rufini, A. J. Elia, M. Agostini, I. Amelio, D. Cescon, D. Dinsdale, L. Zhou, I. S. Harris, S. Lac, J. Silvester, W. Y. Li, M. Sasaki, J. Haight, A. Brustle, A. Wakeham, C. McKerlie, A. Jurisicova, G. Melino, and T. W. Mak. 2014. TAp73 is required for spermatogenesis and the maintenance of male fertility. *Proceedings of the National Academy of Sciences of the United States of America* 111: 1843-1848.

256. Flores, E. R. 2007. The roles of p63 in cancer. *Cell cycle* 6: 300-304.

257. Candi, E., I. Amelio, M. Agostini, and G. Melino. 2015. MicroRNAs and p63 in epithelial stemness. *Cell death and differentiation* 22: 12-21.

258. Sarkar, A., and K. Hochedlinger. 2013. The sox family of transcription factors: versatile regulators of stem and progenitor cell fate. *Cell stem cell* 12: 15-30.

259. Maier, S., T. Wilbertz, M. Braun, V. Scheble, M. Reischl, R. Mikut, R. Menon, P. Nikolov, K. Petersen, C. Beschorner, H. Moch, C. Kakies, C. Protzel, J. Bauer, A. Soltermann, F. Fend, A. Staebler, C. Lengerke, and S. Perner. 2011. SOX2

amplification is a common event in squamous cell carcinomas of different organ sites. *Human pathology* 42: 1078-1088.

260. Sen, T., N. Sen, Y. Huang, D. Sinha, Z. G. Luo, E. A. Ratovitski, and D. Sidransky. 2011. Tumor protein p63/nuclear factor kappaB feedback loop in regulation of cell death. *The Journal of biological chemistry* 286: 43204-43213.

261. Celardo, I., F. Grespi, A. Antonov, F. Bernassola, A. V. Garabadgiu, G. Melino, and I. Amelio. 2013. Caspase-1 is a novel target of p63 in tumor suppression. *Cell death & disease* 4: e645.

262. Tucci, P., M. Agostini, F. Grespi, E. K. Markert, A. Terrinoni, K. H. Vousden, P. A. Muller, V. Dotsch, S. Kehrloesser, B. S. Sayan, G. Giaccone, S. W. Lowe, N. Takahashi, P. Vandenabeele, R. A. Knight, A. J. Levine, and G. Melino. 2012. Loss of p63 and its microRNA-205 target results in enhanced cell migration and metastasis in prostate cancer. *Proceedings of the National Academy of Sciences of the United States of America* 109: 15312-15317.

263. Mathew, L. K., S. S. Lee, N. Skuli, S. Rao, B. Keith, K. L. Nathanson, P. Lal, and M. C. Simon. 2014. Restricted expression of miR-30c-2-3p and miR-30a-3p in clear cell renal cell carcinomas enhances HIF2alpha activity. *Cancer Discov* 4: 53-60.

264. Shukla, K., A. K. Sharma, A. Ward, R. Will, T. Hielscher, A. Balwierz, C. Breunig, E. Munstermann, R. Konig, I. Keklikoglou, and S. Wiemann. 2015. MicroRNA-30c-2-3p negatively regulates NF-kappaB signaling and cell cycle progression through downregulation of TRADD and CCNE1 in breast cancer. *Molecular oncology* 9: 1106-1119.

265. Calin, G. A., C. D. Dumitru, M. Shimizu, R. Bichi, S. Zupo, E. Noch, H. Aldler, S. Rattan, M. Keating, K. Rai, L. Rassenti, T. Kipps, M. Negrini, F. Bullrich, and C. M. Croce. 2002. Frequent deletions and down-regulation of micro- RNA genes miR15 and miR16 at 13q14 in chronic lymphocytic leukemia. *Proceedings of the National Academy of Sciences of the United States of America* 99: 15524-15529.

266. Chen, X., K. Shi, Y. Wang, M. Song, W. Zhou, H. Tu, and Z. Lin. 2015. Clinical value of integrated-signature miRNAs in colorectal cancer: miRNA expression profiling analysis and experimental validation. *Oncotarget* 6: 37544-37556.

267. Luo, Q., C. Wei, X. Li, J. Li, L. Chen, Y. Huang, H. Song, D. Li, and L. Fang. 2014. MicroRNA-195-5p is a potential diagnostic and therapeutic target for breast cancer. *Oncol Rep* 31: 1096-1102.

268. Chen, Y., D. Kuang, X. Zhao, D. Chen, X. Wang, Q. Yang, J. Wan, Y. Zhu, Y. Wang, S. Zhang, Y. Wang, Q. Tang, M. Masuzawa, G. Wang, and Y. Duan. 2016. miR-497-5p inhibits cell proliferation and invasion by targeting KCa3.1 in angiosarcoma. *Oncotarget* 7: 58148-58161.

269. Hydbring, P., Y. Wang, A. Fassl, X. Li, V. Matia, T. Otto, Y. J. Choi, K. E. Sweeney, J. M. Suski, H. Yin, R. L. Bogorad, S. Goel, H. Yuzugullu, K. J. Kauffman, J. Yang, C. Jin, Y. Li, D. Floris, R. Swanson, K. Ng, E. Sicinska, L. Anders, J. J. Zhao, K. Polyak, D. G. Anderson, C. Li, and P. Sicinski. 2017. Cell-Cycle-Targeting MicroRNAs as Therapeutic Tools against Refractory Cancers. *Cancer cell* 31: 576-590 e578.

270. Ozata, D. M., S. Caramuta, D. Velazquez-Fernandez, P. Akcakaya, H. Xie, A. Hoog, J. Zedenius, M. Backdahl, C. Larsson, and W. O. Lui. 2011. The role of microRNA deregulation in the pathogenesis of adrenocortical carcinoma. *Endocr Relat Cancer* 18: 643-655.

271. Soriano, A., L. Paris-Coderch, L. Jubierre, A. Martinez, X. Zhou, O. Piskareva, I. Bray, I. Vidal, A. Almazan-Moga, C. Molist, J. Roma, J. R. Bayascas, O. Casanovas, R. L. Stallings, J. Sanchez de Toledo, S. Gallego, and M. F. Segura. 2016. MicroRNA-497 impairs the growth of chemoresistant neuroblastoma cells by targeting cell cycle, survival and vascular permeability genes. *Oncotarget* 7: 9271-9287.

272. Xu, J. W., T. X. Wang, L. You, L. F. Zheng, H. Shu, T. P. Zhang, and Y. P. Zhao. 2014. Insulin-like growth factor 1 receptor (IGF-1R) as a target of MiR-497 and plasma IGF-1R levels associated with TNM stage of pancreatic cancer. *PloS one* 9: e92847.

273. Wang, L., B. Li, L. Li, and T. Wang. 2013. MicroRNA-497 suppresses proliferation and induces apoptosis in prostate cancer cells. *Asian Pac J Cancer Prev* 14: 3499-3502.

274. Wu, R., S. Tang, M. Wang, X. Xu, C. Yao, and S. Wang. 2016. MicroRNA-497 Induces Apoptosis and Suppresses Proliferation via the Bcl-2/Bax-Caspase9-Caspase3 Pathway and Cyclin D2 Protein in HUVECs. *PloS one* 11: e0167052.

275. Wu, Z., X. Li, X. Cai, C. Huang, and M. Zheng. 2016. miR-497 inhibits epithelial mesenchymal transition in breast carcinoma by targeting Slug. *Tumour Biol* 37: 7939-7950.

276. Yan, J. J., Y. N. Zhang, J. Z. Liao, K. P. Ke, Y. Chang, P. Y. Li, M. Wang, J. S. Lin, and X. X. He. 2015. MiR-497 suppresses angiogenesis and metastasis of hepatocellular carcinoma by inhibiting VEGFA and AEG-1. *Oncotarget* 6: 29527-29542.

277. Rupaimoole, R., and F. J. Slack. 2017. MicroRNA therapeutics: towards a new era for the management of cancer and other diseases. *Nat Rev Drug Discov* 16: 203-222.

278. Bader, A. G. 2012. miR-34 - a microRNA replacement therapy is headed to the clinic. *Front Genet* 3: 120.

279. Misso, G., M. T. Di Martino, G. De Rosa, A. A. Farooqi, A. Lombardi, V. Campani, M. R. Zarone, A. Gulla, P. Tagliaferri, P. Tassone, and M. Caraglia. 2014. Mir-34: a new weapon against cancer? *Mol Ther Nucleic Acids* 3: e194.

280. Selbach, M., B. Schwanhausser, N. Thierfelder, Z. Fang, R. Khanin, and N. Rajewsky. 2008. Widespread changes in protein synthesis induced by microRNAs. *Nature* 455: 58-63.

281. Toll, A., R. Salgado, M. Yebenes, G. Martin-Ezquerra, M. Gilaberte, T. Baro, F. Sole, F. Alameda, B. Espinet, and R. M. Pujol. 2010. Epidermal growth factor receptor gene numerical aberrations are frequent events in actinic keratoses and invasive cutaneous squamous cell carcinomas. *Experimental dermatology* 19: 151-153.

282. Nam, J. W., O. S. Rissland, D. Koppstein, C. Abreu-Goodger, C. H. Jan, V. Agarwal, M. A. Yildirim, A. Rodriguez, and D. P. Bartel. 2014. Global analyses of the

effect of different cellular contexts on microRNA targeting. *Molecular cell* 53: 1031-1043.

283. Lee, Y. M., E. Kim, M. Park, E. Moon, S. M. Ahn, W. Kim, K. B. Hwang, Y. K. Kim, W. Choi, and W. Kim. 2010. Cell cycle-regulated expression and subcellular localization of a kinesin-8 member human KIF18B. *Gene* 466: 16-25.

284. Stout, J. R., A. L. Yount, J. A. Powers, C. Leblanc, S. C. Ems-McClung, and C. E. Walczak. 2011. Kif18B interacts with EB1 and controls astral microtubule length during mitosis. *Mol Biol Cell* 22: 3070-3080.

285. Booher, R. N., P. S. Holman, and A. Fattaey. 1997. Human Myt1 is a cell cycle-regulated kinase that inhibits Cdc2 but not Cdk2 activity. *The Journal of biological chemistry* 272: 22300-22306.

286. Liu, F., J. J. Stanton, Z. Wu, and H. Piwnica-Worms. 1997. The human Myt1 kinase preferentially phosphorylates Cdc2 on threonine 14 and localizes to the endoplasmic reticulum and Golgi complex. *Molecular and cellular biology* 17: 571-583.

287. Kozar, K., and P. Sicinski. 2005. Cell cycle progression without cyclin D-CDK4 and cyclin D-CDK6 complexes. *Cell cycle* 4: 388-391.

288. Malumbres, M., R. Sotillo, D. Santamaria, J. Galan, A. Cerezo, S. Ortega, P. Dubus, and M. Barbacid. 2004. Mammalian cells cycle without the D-type cyclin-dependent kinases Cdk4 and Cdk6. *Cell* 118: 493-504.

289. Dutertre, S., M. Cazales, M. Quaranta, C. Froment, V. Trabut, C. Dozier, G. Mirey, J. P. Bouche, N. Theis-Febvre, E. Schmitt, B. Monsarrat, C. Prigent, and B.

Ducommun. 2004. Phosphorylation of CDC25B by Aurora-A at the centrosome contributes to the G2-M transition. *Journal of cell science* 117: 2523-2531.

290. Fu, J., M. Bian, Q. Jiang, and C. Zhang. 2007. Roles of Aurora kinases in mitosis and tumorigenesis. *Molecular cancer research : MCR* 5: 1-10.

291. Katayama, H., K. Sasai, H. Kawai, Z. M. Yuan, J. Bondaruk, F. Suzuki, S. Fujii, R. B. Arlinghaus, B. A. Czerniak, and S. Sen. 2004. Phosphorylation by aurora kinase A induces Mdm2-mediated destabilization and inhibition of p53. *Nature genetics* 36: 55-62.

292. Liu, Q., S. Kaneko, L. Yang, R. I. Feldman, S. V. Nicosia, J. Chen, and J. Q. Cheng. 2004. Aurora-A abrogation of p53 DNA binding and transactivation activity by phosphorylation of serine 215. *The Journal of biological chemistry* 279: 52175-52182.

293. Dar, A. A., A. Belkhiri, J. Ecsedy, A. Zaika, and W. El-Rifai. 2008. Aurora kinase A inhibition leads to p73-dependent apoptosis in p53-deficient cancer cells. *Cancer research* 68: 8998-9004.

294. Katayama, H., J. Wang, W. Treekitkarnmongkol, H. Kawai, K. Sasai, H. Zhang, H. Wang, H. P. Adams, S. Jiang, S. N. Chakraborty, F. Suzuki, R. B. Arlinghaus, J. Liu, J. A. Mobley, W. E. Grizzle, H. Wang, and S. Sen. 2012. Aurora kinase-A inactivates DNA damage-induced apoptosis and spindle assembly checkpoint response functions of p73. *Cancer cell* 21: 196-211.

295. Gautschi, O., J. Heighway, P. C. Mack, P. R. Purnell, P. N. Lara, and D. R. Gandara. 2008. Aurora kinases as anticancer drug targets. *Clinical Cancer Research* 14: 1639-1648.

296. Tanaka, E., Y. Hashimoto, T. Ito, T. Okumura, T. Kan, G. Watanabe, M. Imamura, J. Inazawa, and Y. Shimada. 2005. The clinical significance of Aurora-A/STK15/BTAK expression in human esophageal squamous cell carcinoma. *Clinical cancer research : an official journal of the American Association for Cancer Research* 11: 1827-1834.

297. Hirota, T., N. Kunitoku, T. Sasayama, T. Marumoto, D. Zhang, M. Nitta, K. Hatakeyama, and H. Saya. 2003. Aurora-A and an interacting activator, the LIM protein Ajuba, are required for mitotic commitment in human cells. *Cell* 114: 585-598.

298. Marumoto, T., S. Honda, T. Hara, M. Nitta, T. Hirota, E. Kohmura, and H. Saya. 2003. Aurora-A kinase maintains the fidelity of early and late mitotic events in HeLa cells. *The Journal of biological chemistry* 278: 51786-51795.

299. Ji, H., D. Li, L. Chen, T. Shimamura, S. Kobayashi, K. McNamara, U. Mahmood, A. Mitchell, Y. Sun, R. Al-Hashem, L. R. Chirieac, R. Padera, R. T. Bronson, W. Kim, P. A. Janne, G. I. Shapiro, D. Tenen, B. E. Johnson, R. Weissleder, N. E. Sharpless, and K. K. Wong. 2006. The impact of human EGFR kinase domain mutations on lung tumorigenesis and in vivo sensitivity to EGFR-targeted therapies. *Cancer cell* 9: 485-495.

300. Li, D., J. Zhu, P. F. Firozi, J. L. Abbruzzese, D. B. Evans, K. Cleary, H. Friess, and S. Sen. 2003. Overexpression of oncogenic STK15/BTAK/Aurora A kinase in human pancreatic cancer. *Clinical cancer research : an official journal of the American Association for Cancer Research* 9: 991-997.

301. Reiter, R., P. Gais, U. Jutting, M. K. Steuer-Vogt, A. Pickhard, K. Bink, S. Rauser, S. Lassmann, H. Hofler, M. Werner, and A. Walch. 2006. Aurora kinase A messenger RNA overexpression is correlated with tumor progression and shortened survival in head and neck squamous cell carcinoma. *Clinical cancer research : an official journal of the American Association for Cancer Research* 12: 5136-5141.

302. Tang, A., K. Gao, L. Chu, R. Zhang, J. Yang, and J. Zheng. 2017. Aurora kinases: novel therapy targets in cancers. *Oncotarget* 8: 23937-23954.

303. Malanchi, I., H. Peinado, D. Kassen, T. Hussenet, D. Metzger, P. Chambon, M. Huber, D. Hohl, A. Cano, W. Birchmeier, and J. Huelsken. 2008. Cutaneous cancer stem cell maintenance is dependent on beta-catenin signalling. *Nature* 452: 650-653.

304. Beck, B., G. Driessens, S. Goossens, K. K. Youssef, A. Kuchnio, A. Caauwe, P. A. Sotiropoulou, S. Loges, G. Lapouge, A. Candi, G. Mascre, B. Drogat, S. Dekoninck, J. J. Haigh, P. Carmeliet, and C. Blanpain. 2011. A vascular niche and a VEGF-Nrp1 loop regulate the initiation and stemness of skin tumours. *Nature* 478: 399-403.

305. Nagaraj, A. S., J. Lahtela, A. Hemmes, T. Pellinen, S. Blom, J. R. Devlin, K. Salmenkivi, O. Kallioniemi, M. I. Mayranpaa, K. Narhi, and E. W. Verschuren. 2017. Cell of Origin Links Histotype Spectrum to Immune Microenvironment Diversity in Non-small-Cell Lung Cancer Driven by Mutant Kras and Loss of Lkb1. *Cell reports* 18: 673-684.

306. Dulloo, I., B. H. Phang, R. Othman, S. Y. Tan, A. Vijayaraghavan, L. K. Goh, M. Martin-Lopez, M. M. Marques, C. W. Li, Y. Wang, M. C. Marin, W. Xian, F.

McKeon, and K. Sabapathy. 2015. Hypoxia-inducible TAp73 supports tumorigenesis by regulating the angiogenic transcriptome. *Nature cell biology*.

307. Jacks, T., L. Remington, B. O. Williams, E. M. Schmitt, S. Halachmi, R. T. Bronson, and R. A. Weinberg. 1994. Tumor spectrum analysis in p53-mutant mice. *Curr Biol* 4: 1-7.

308. Keyes, W. M., H. Vogel, M. I. Koster, X. Guo, Y. Qi, K. M. Petherbridge, D. R. Roop, A. Bradley, and A. A. Mills. 2006. p63 heterozygous mutant mice are not prone to spontaneous or chemically induced tumors. *Proceedings of the National Academy of Sciences of the United States of America* 103: 8435-8440.

309. Suh, E. K., A. Yang, A. Kettenbach, C. Bamberger, A. H. Michaelis, Z. Zhu, J. A. Elvin, R. T. Bronson, C. P. Crum, and F. McKeon. 2006. p63 protects the female germ line during meiotic arrest. *Nature* 444: 624-628.